Macro-Structured Carbon Nanofibers Catalysts on Titania extrudate and Cordierite Monolith for Selective Hydrogenation

Jie Zhu

MACRO-STRUCTURED CARBON NANOFIBERS CATALYSTS ON TITANIA EXTRUDATE AND CORDIERITE MONOLITH FOR SELECTIVE HYDROGENATION

Jie Zhu

Promotion committee

Prof. dr. ir. J. W. M. Hilgenkamp	Chairman	University of Twente	The Netherlands
Prof. dr. ir. L. Lefferts	Promoter	University of Twente	The Netherlands
Prof. dr. K. Seshan		University of Twente	The Netherlands
Prof. dr. G. Mul		University of Twente	The Netherlands
Prof. dr. M. Muhler		Ruhr-Universität Bochum	Germany
Dr. J.G. van Ommen		University of Twente	The Netherlands
Prof. dr. ir. J.-J. Zhu		Changzhou University	China
Prof. dr. J. A. Moullijn		Delft University of Technology	The Netherlands

The research described in this thesis was carried out in the *Catalytic Processes and Materials* (CPM) group of the University of Twente, The Netherlands. I acknowledge financial support for my PhD study from *China Scholarship Council* (CSC).

Cover design: Jie Zhu

Motivation: The idea of the cover design was originated from a talk with my friend, Aijie Liu, in which I showed her a picture of carbon nanofibers support (Figure 1.10). She said that the intertwined structure of carbon nanofibers looked like an ant nest in the earth. Hence, I designed the covers by her inspiration. The image in front cover shows the working ants finding the golds easily due to they walking out of the caves, while that in back cover shows they looking for the golds and the way outside toughly due to the long and maze-like tunnels. Two images hint the outstanding advantages of carbon nanofibers support, compared to a conventional porous material. Carbon nanofibers can form agglomerates with high surface areas and pore volumes without any micro porosity. These advantages prevent mass transfer limitations inside CNF agglomerates, improving product selectivity in catalytic reactions.

Publisher: Gilderprint, Enschede, The Netherlands

ISBN: 978-90-365-3942-5 DOI: 10.3990/1.9789036539425

MACRO-STRUCTURED CARBON NANOFIBERS CATALYSTS ON TITANIA EXTRUDATE AND CORDIERITE MONOLITH FOR SELECTIVE HYDROGENATION

DISSERTATION

to obtain
the degree of doctor at the University of Twente,
on the authority of the rector magnificus,
Prof. dr. H. Brinksma
on account of the decision of the graduation committee,
to be publicly defended
on Wednesday September 16th 2015 at 12:45

by

Jie Zhu

Born on December 30th 1977
in Changzhou, Jiangsu Province, China

This dissertation has been approved by the promoter
Prof. dr. ir. L. Lefferts

献给我们的父母
和我爱的小小、昊昊

Dedicated to our parents,
and to my Xiaoxiao, Haohao
with love.

Table of Content

Chapter 1

Introduction

Selective hydrogenation is a key process in production of both fine chemicals and bulk chemicals with important applications in materials, pharmaceutical and cosmetic industries [1-3]. In this introduction, the theory of mass transfer in relevant three-phase catalytic reactors will be described, focusing on the influence of not only activity but also selectivity. The approach followed in this thesis to improve the performance using structured catalysts will be described.

1.1 Mass transfer in three-phase catalytic reactions

Three-phase reactions are generally recognized to proceed according to the following eight steps: (i) Mass transfer of the reacting gas molecules from the gas to liquid (gas-liquid transfer); (ii) Mass transfer of the reacting molecules dissolved in liquid from bulk of the liquid to the outer surface of the catalyst pellet (external diffusion); (iii) Diffusion of the reacting molecules to the pore surface within the catalyst (internal diffusion); (iv) Adsorption of the reacting molecules on the pore surface; (v) Reaction at specific active sites on the catalyst surface; (vi) Desorption of the product molecules from the pore surface; (vii) Diffusion of the product molecules from the pore surface to the outer surface of the catalyst (internal diffusion); (viii) Mass transfer of the product molecules from the outer surface of the catalyst to the bulk fluid (external diffusion).

The above process is schematically represented in Figure 1.1 for the reaction A to B [4]. Since the majority of active sites are on the inner surface of the catalyst, the reactants will diffuse from the bulk fluid to the active sites in catalyst, prior to adsorption and reaction on them. Clearly, the mass transfer of the reactants in this process, including external and internal diffusion, have significant effects on catalytic activity and product selectivity in selective hydrogenations, by influencing concentrations of reactants and products at the active sites.

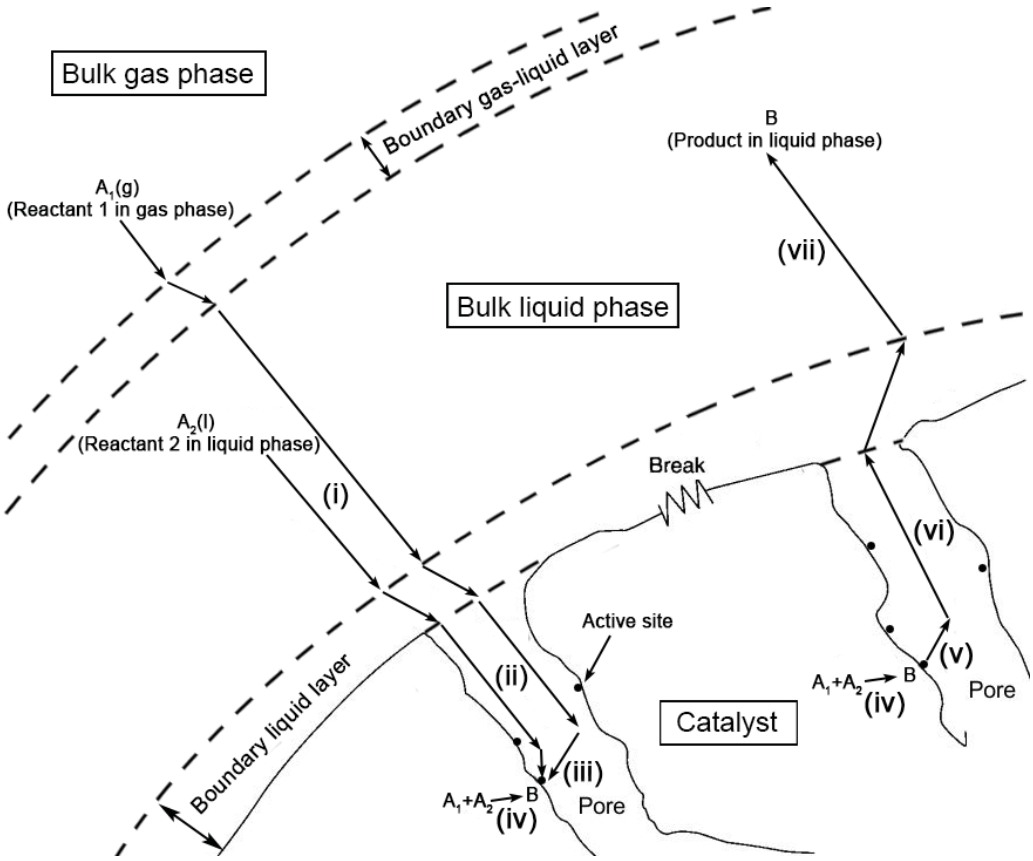

Figure 1.1: Heterogeneous catalytic mechanism for reactants A_1 and A_2 to product B [4]

1.1.1 External diffusion effects

Diffusion is the spontaneous intermingling of atoms or molecules by random thermal motion. It gives rise to the motion of a species relative to the motion of the mixture. In the absence of other gradients (such as temperature, electric potential, or gravitational potential), molecules of a given species within a single phase will always diffuse from the region of higher concentration to the region of lower concentration. For dilute solute concentrations and constant total concentration, this gradient results in a molar flux of the species, i.e., motion, in 3-dimensions of the concentration gradient, which can be described by Fick's law (Equation 1.1) [5].

$$W_A = J_A = -cD_{AB}\nabla y_A \qquad 1.1$$

Where W_A is the molar flux of A; J_A is the diffusional flux of A resulting from a concentration difference; c is the total concentration (mol/dm^3); D_{AB} is the diffusivity of A in B (dm^2/s), and y_A is the mole fraction of A; ∇ is the gradient in three-dimensional coordinates, $\nabla = i\frac{\partial}{\partial x} + j\frac{\partial}{\partial y} + k\frac{\partial}{\partial z}$.

In a three-phase catalytic system, the concentration gradient of reactants on both sides of the interface, including gas-liquid and liquid-solid interface, drives the mass transfer of the reactants. Specifically, gas reactants need to pass through the gas-liquid interface first to arrive at the bulk of the liquid, and then through the liquid-solid interface to the solid catalyst surface, together with reactants dissolved in the liquid. A useful way of modeling mass transfer is to treat any interface as a stagnant film of thickness δ, hypothesizing that all the resistance to mass transfer is found within this film, and that the properties (i.e., concentration, temperature) at the outer edge of the film are identical to those of the bulk gas or liquid phase.

(1) Gas-Liquid mass transfer

Due to continuous gas adsorption, mass transfer of gas reactants from a gas phase to a liquid phase, proceeds via the interfacial area. It leads to the formation of two film resistances in two adjacent phases [6]. It could be described with two-film theory by Equation 1.2, and shown in Figure 1.2.

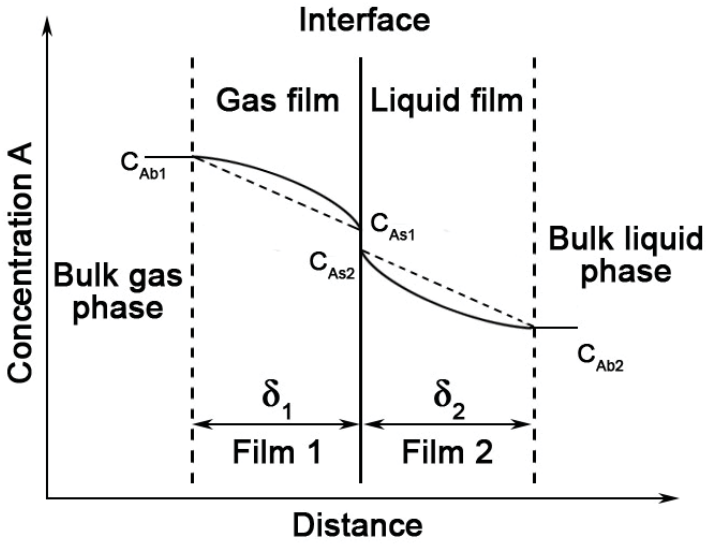

Figure 1.2: Gas-liquid phase mass transfer for reactant A (C_{Ab1} and C_{Ab2}: concentration of A in bulk gas phase and bulk liquid phase, respectively; C_{As1} and C_{As2}: gas phase interfacial concentration of A and liquid phase one, respectively; δ_1 and δ_2: the boundary layer thickness of gas film and liquid film)

$$dC_{Ab2}/dt = K_L a(C_A^* - C_{Ab2}) \quad 1.2$$

where C_{Ab2} is the concentration of dissolved gas reactant in bulk liquid (mol/dm^3); t is time (s); K_L is the mass transfer coefficient (cm/s); a is the gas-liquid interface area per liquid volume (cm^2/cm^3); K_La is volumetric gas-liquid mass transfer coefficient (liquid side, s^{-1}); C_A* is equilibrium solubility of the gas molecule A in the liquid (mol/dm^3).

As described, mass transfer of the gas reactant A first takes place from a high concentration C_{Ab1}, through the film 1 with the thickness of δ_1, to the interface. Here, the gas phase interfacial concentration C_{As1} is in equilibrium with the liquid phase interfacial concentration C_{As2}. Then, mass transfer continues from the interface, through film 2 with thickness of δ_2, to the bulk liquid phase with the concentration of C_{Ab2}. So, the gas-liquid mass transfer resistance occurs in two films [7].

In actual applications, the Carberry number for mass transport (*Ca*) [8] is often calculated to decide on the effects of gas-liquid external diffusion in a reaction. It states that gas-liquid external diffusion resistance is low and can be neglected if the effectiveness factor for gas-liquid external mass diffusion (η_e) in a function of *Ca* number is beyond 0.90, as expressed in Equation 1.3.

$$\eta_e = (1 - Ca_{G-L})^{n_1} > 0.9, \;\; Ca_{G-L} = \frac{r_A}{K_L a C_A^*} \tag{1.3}$$

Where C_A* is equilibrium solubility of the gas molecule A in the liquid (mol/dm^3); n_1 is the reaction order; r_A is observed reaction rate per unit volume of the catalyst (mol/dm^3·s); K_La is volumetric gas-liquid mass transfer coefficient (liquid side, s^{-1}).

Obviously, slow reaction rate, large mass transfer coefficient and high solubility will enhance the gas-liquid mass transfer.

(2) Liquid-Solid mass transfer

The lower concentrations of the reactants on the surface of the catalyst pellet as compared to in the bulk of the liquid, due to the continuous consumption of reactants in the catalytic reaction, drives the transport of reactants from the bulk of the liquid to the surface of the catalyst pellet constantly. A reasonable representation of the concentration profile for a reactant "A" diffusing from the bulk liquid phase to the external surface of a catalyst pellet is shown in Figure 1.3. Like for gas-liquid phase mass transfer, the change in concentration of "A" from C_{Ab2} (in bulk liquid) to C_{As3} (at the outer surface site of the catalyst pellet) takes place in a thin fluid film next to the surface of the sphere. The hydrodynamic boundary layer (Figure 1.3) is usually defined as the distance from a solid object to where the fluid velocity is 99% of the bulk velocity [9]. All the liquid-solid mass transfer resistance is also supposed to be in this layer.

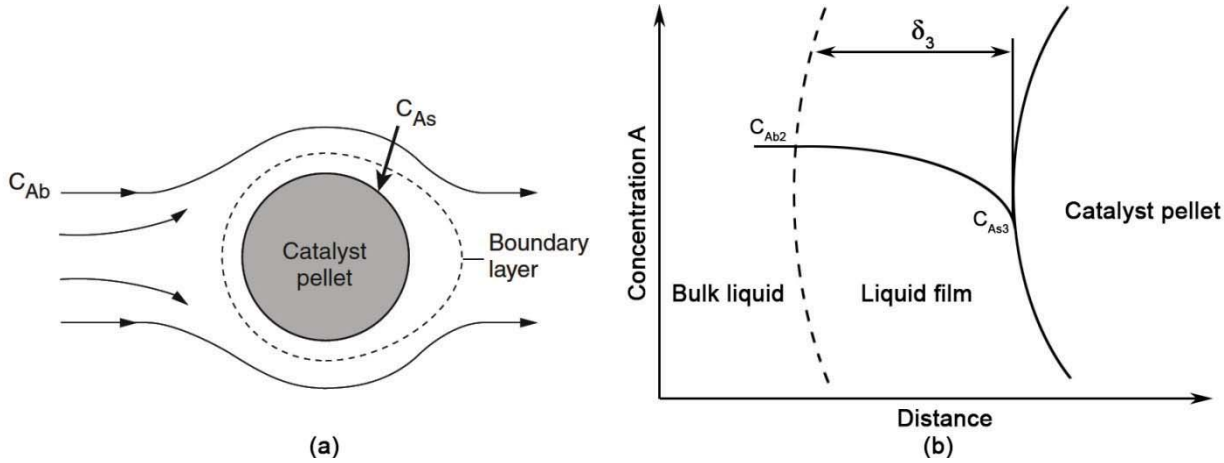

Figure 1.3: External diffusion of the reactant: (a) boundary layer around the surface of a catalyst pellet; (b) profile for a reactant "A" diffusing to the external surface [9] (C_{Ab2}: concentration of "A" in bulk liquid; C_{As3}: concentration of "A" on outer surface site of the catalyst pellet; δ_3: the boundary layer thickness)

If the film thickness is much smaller than the radius of the pellet, curvature effects can be neglected. As a result, only the one-dimensional diffusion equation must be solved. So, in equimolar counter diffusion (EMCD) or dilute concentrations, Equation 1.1 can be deduced to Equation 1.4 [10].

$$W_{Az} = \frac{D_{AB}}{\delta_3} \cdot [C_{Ab2} - C_{As3}] \qquad 1.4$$

Where W_{Az} is the molar flux of A in the z-direction; C_{Ab2} and C_{As3} represent the concentrations of A in the bulk liquid and that on the external surface of the pellet, respectively.

The ratio of the diffusivity D_{AB} to the film thickness δ is the mass transfer coefficient, k_c, that is,

$$k_{L-S} = \frac{D_{AB}}{\delta_3} \qquad 1.5$$

Reasonably, the higher the coefficient ($k_{L\text{-}S}$), the faster the mass transfer of A to B. The resistance to the diffusion of reactants will result in a negative effect on the reaction rate, especially for a fast reaction. Therefore, the improvement of mass transfer or the removal of mass transfer limitation is a desired target in those heterogeneous catalytic reactions which are influenced by mass transfer.

Carberry number can also be used to estimate liquid-solid external diffusion limitation, similar to the gas-liquid case, as shown in Equation 1.6.

$$\eta_e = (1 - Ca_{L-S})^{n_1} > 0.9, \;\; Ca_{L-S} = \frac{r_A}{k_{L-S} a C_{Ab}} \qquad 1.6$$

Where C_{Ab} is the concentration of A in bulk liquid (mol/dm^3); $k_{L\text{-}S}$ is the liquid-solid mass transfer coefficients (cm/s); a is the gas-liquid interface area per liquid volume (cm^2/cm^3); and r_A is the observed reaction rate per unit volume of catalyst (mol/dm^3·s).

Usually in a fixed-bed reactor, both decreasing the particle size (d_p) and increasing the velocity of the fluid flowing along the particle (U) will increase liquid-solid mass transfer coefficient ($k_{L\text{-}S}$). When operating the reaction at sufficiently high velocities or sufficiently small particle sizes, the main controlling factor on the reaction rate will shift from transport to kinetics, indicating the elimination of external diffusion limitation, as shown in Figure 1.4.

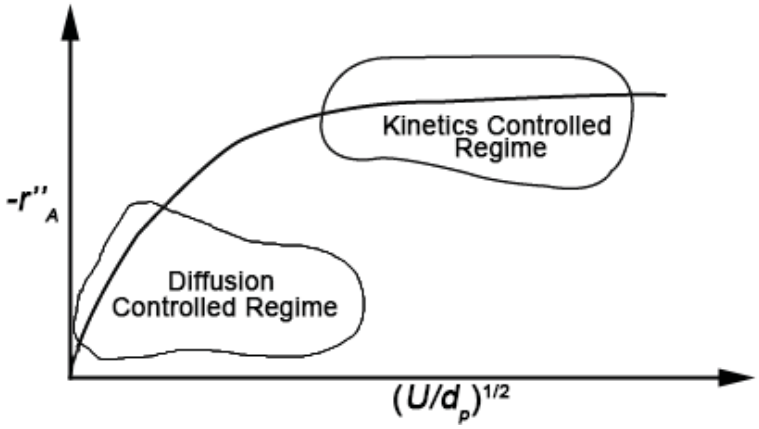

Figure 1.4: Effect of the bulk flow velocity or stirring speed on reaction rate [11]

1.1.2 Internal diffusion effects

A catalyst is often designed with a porous structure, possessing a high surface area in order to increase the surface area of the active phase. So it will improve the intrinsic activity per gram of catalyst. As most of the active sites are located in the internal surface of the catalyst, reactant molecule "A" will need to diffuse through the pores within the pellet to the active sites, where the reaction occurs. The resulting decrease in the reactant concentration in the pores (C_i), as compared to the external surface (C_{As3}), is the driving force for continuous reactant diffusion through the pores, as shown in Figure 1.5.

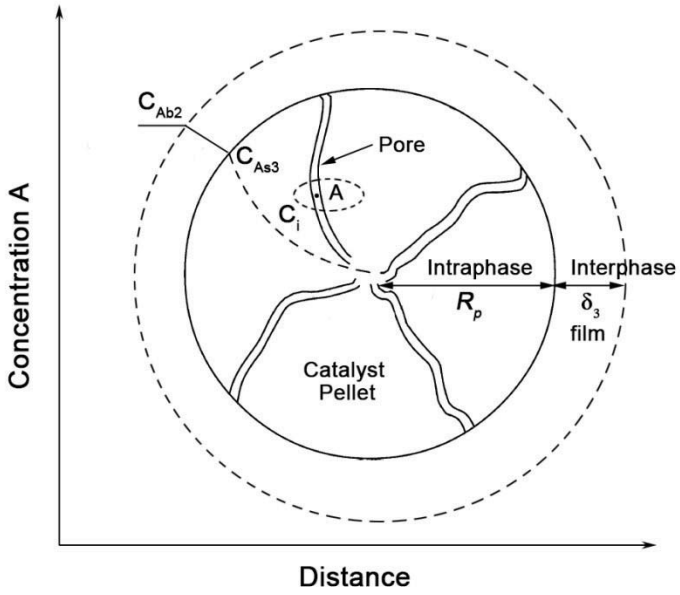

Figure 1.5: Diffusion of the reactant A through the pores (C_{Ab2}: concentration of "A" in bulk liquid; C_{As3}: concentration of "A" on outer surface site of the catalyst pellet; C_i: concentration of "A" in the pores; δ_3: the boundary layer thickness) [12]

For the purpose of describing the effects of internal diffusion on the rate of catalytic reactions, internal effectiveness factor (η), Thiele modulus (ϕ) are introduced to estimate how efficient the reactant diffuses into the pellet before reacting, as shown in Equation 1.7 and 1.8 [13].

$$\phi_n^2 = \frac{k_n R^2 C_{As}^{n-1}}{D_e} = \frac{k_n R C_{As}^n}{D_e[(C_{As}-0)/R]} = \frac{Surface\ reaction\ rate}{Diffusion\ rate} \quad 1.7$$

$$\eta = \frac{Actual\ reaction\ rate}{Reaction\ rate\ assuming\ no\ diffusion\ limitation} = \frac{-r_A}{-r_{As}} = \left(\frac{2}{n+1}\right)^{1/2} \frac{3}{\phi_n} \quad 1.8$$

Where k is intrinsic reaction rate constant ($s^{-1}\cdot(mol/L)^{1-n}$); R is catalyst pellet radius (m); C_{As} is the concentration of reactant A on the external catalyst surface (mol/L); n is the reaction order and D_e is the effective diffusion coefficient (m^2/s). D_e can be calculated using Equation 1.9 [14].

$$D_e = \frac{D_b \theta}{\tau} \quad 1.9$$

Where D_b is the bulk diffusion coefficient (cm^2/s), θ is the internal void fraction of the solid particle, τ is the tortuosity factor of the pores. The typical values for θ are between 0.3 and 0.6, and for τ between 2 and 5.

Clearly, the smaller the Thiele modulus, the higher the internal effectiveness factor, thereafter the lower the internal diffusion limitation, as shown in Figure 1.6. When the calculated $\eta \geqslant 0.95$, the reaction can be considered to have negligible mass transfer limitations.

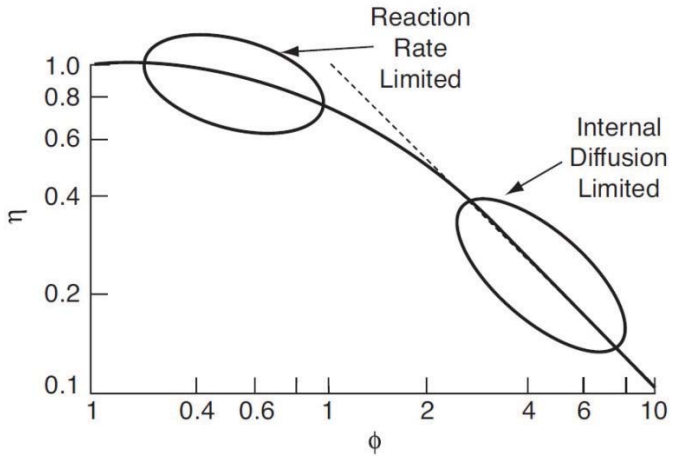

Figure 1.6: Internal effectiveness factor versus Thiele modulus [15]

However, the greatest difficulty with the Thiele modulus is that the intristic rate constant, k_n, and the reaction order are frequently not known. Weisz-Prater number (N_{WP}), another approach to estimate the internal diffusion limitation in heterogeneous catalysis, eliminates this difficulty. It is particularly useful because it provides a dimensionless number containing only observable parameters that can be readily measured or calculated (Equation 1.10). It says that if $N_{WP}<0.3$, rates for all reactions with the reaction order 2 or less should have negligible mass transfer limitations, while a value for $N_{WP}>6$ indicates definite diffusion control. The criteria of η and N_{WP} for different reaction orders are summarized in Table 1.1 [16].

$$N_{WP} = \frac{r_a R^2}{D_e C_{As}} \tag{1.10}$$

Where r_a is the observed rate per catalyst volume (mol/cm^3·s); R is catalyst pellet radius (m); D_e is the effective diffusion coefficient (m^2/s) and C_{As} is the concentration of reactant A on the catalyst surface (mol/L).

Therefore, based on the expression of Weisz-Prater criterion, it can be understood that internal diffusion limitation can be suppressed in three ways: (1) slow down the reaction rate; (2) decrease the radius of catalyst pellet (diffusion length); (3) increase the effective diffusion coefficient by either increasing the internal void fraction or decreasing tortuosity of the pores.

Table 1.1 Weisz-Prater criteria for different reaction orders

Effectiveness factor	Reaction order	Value of N_{WP}
$\eta \geqslant 0.95$	n=0	$N_{WP} \leqslant 6$
$\eta \geqslant 0.95$	n=1	$N_{WP} \leqslant 0.6$
$\eta \geqslant 0.95$	n=2	$N_{WP} \leqslant 0.3$

1.2 Three phase catalytic reactors and structured supports

1.2.1 Three phase catalytic reactors

A three phase catalytic reactor is a system in which gas and liquid phases are contacted with a solid catalyst. Most frequently used are stirred tank slurry reactor and packed bed reactors. The choice of use of a certain reactor type is governed by its advantages and disadvantages.

1.2.1.1 Stirred tank slurry reactor

Stirred tank reactors normally use small catalyst particles (typically 30μm) such as activated carbon and silica supported catalysts. They are suspended in liquid medium through which gas is dispersed. These small catalyst particles have advantages of high external surface area, high rates of liquid to solid mass transfer as well as fast internal diffusion, thanks to the very short diffusion paths, leading to a more efficient utilization of catalyst particle. Thus, this type of reactor is widely used in oxidation and hydrogenation reactions because the transport of oxygen and hydrogen are usually diffusion limited. However, the major disadvantage of the stirred tank reactors is the required separation of product and catalyst, necessitating a filtration step of the fine catalyst particles from the liquid product [17]. The filtration unit usually is rather sensitive to process disturbance, causing downtime. Moreover, attrition of catalyst particles may cause the loss of active metal phase [18].

1.2.1.2 Packed bed reactor

A packed bed reactor, such as the trickle bed reactor, is much more convenient than a slurry reactor, avoiding catalyst separation. It is typically applied for processes involving slow reactions because of their advantage of high catalyst loading and long residence time. Catalyst particle size is relatively large (1-10 mm) to limit the pressure drop through the reactor. However, the large catalyst particles lead to longer diffusion paths and low external surface area, easily causing internal diffusion limitation [17]. In addition, possible liquid

maldistribution and heat removal problem can hamper the conversion and selectivity of the reaction. It is clear that these limitations are unfavorable from the point of view of process economics [19].

1.2.1.3 Stirred basket reactor

Stirred basket reactor, a useful tool in the laboratory, consist of either a stirred reactor with a stationary cage of catalyst or a reactor with a rotating basket of catalyst. They combined some advantages of fixed-bed reactors and slurry reactors. For example, the catalyst separation is easy, which is conducive to the continuous operation; the possibility of sedimentation of heavier particles is eliminated, and the attrition of catalyst particles is minimal, which ensures that the catalyst particle size remains constant throughout the experiments. Therefore, stirred basket reactors are often applied for to determine intrinsic kinetics to enhance development and understanding of the process.

1.2.2 Structured supports for three phase catalytic reactors

Some preformed supports, including monolith (Figure 1.7a) [20-22], metal foam (Figure 1.7b) [23-25] and carbon felt (Figure 1.7c) [26, 27], are often used to prepare structured catalysts.

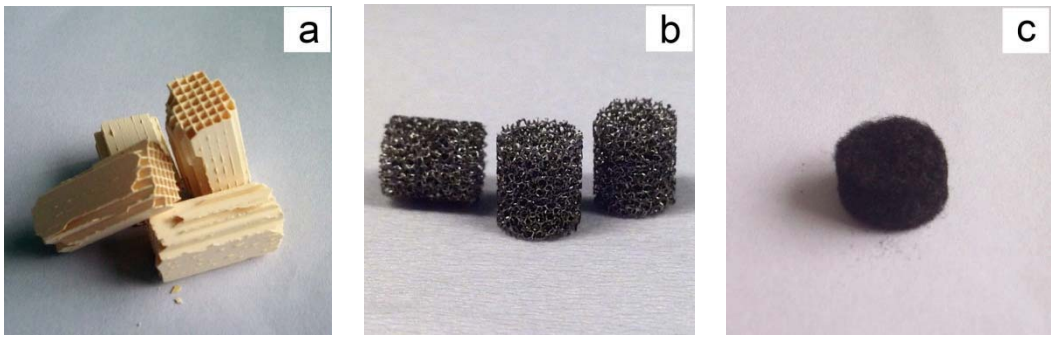

Figure 1.7: Some formed supports: (a) cordierite monolith; (b) nickel foam; (c) carbon felt

For example, monoliths are ceramic or metallic blocks containing parallel, straight channels. Ceramic monoliths have been used extensively in gas-solid applications such as the automotive exhaust converter and deNO_x reactors [17]. Increasingly, they are also considered as an interesting alternative for liquid-solid and gas-liquid-solid applications in fixed-bed or slurry reactors because of: (1) the short diffusional distance in the catalytically active layer; (2) the excellent mass transfer that can be achieved for two-phase flow in capillaries; (3) the low energy requirements due to the low pressure drop and (4) the absence of a catalyst separation step. It is noted that, at sufficient superficial velocities, a two-phase flow pattern called Taylor

flow is observed in capillaries. The gas and liquid move through the channel as separate slugs. The gas bubble filled up the whole space of the channel and only a thin liquid film separates the gas from the catalyst. This film layer remains at the wall when the liquid slug passes by. Inside the liquid slug itself, a recirculation pattern is observed. This recirculation enhances gas-solid mass transfer [20, 21].

Like two sides of a coin, the low specific surface area of structured supports, especially for monolith and metal foam (~1 m^2/g), is not sufficient to host enough catalytically active metal particles. Therefore, a layer of coating with high specific surface area is usually synthesized to cover the surface to increase its effective surface area. Usually, these thin washcoated layers can be made by depositing an oxide layer (alumina, silica, etc) with similar texture and porosity as compared to traditional catalyst support particles. Some early works [28-30] have already shown that high surface area γ-alumina washcoats can be achieved especially on monoliths and foams. These washcoated layers can be adjusted to different parameters such as, thickness of layer which governs the diffusion lengths and porosity of the layer. Such a structured support would effectively combine the advantages of both slurry phase operation, offering short diffusion path, and fixed bed operation, avoiding catalyst separation and attrition. This would allow independent optimization of intrinsic reaction kinetics, transport phenomena and hydrodynamics [31].

However, the porous washcoated layers generally suffer from relatively low pore volume and high tortuosity. They are unfavorable for reactions that are seriously influenced by internal diffusion limitations. Therefore, alternative thin layers such as entangled carbon nanofibers (CNFs) or nanotubes (CNTs) are designed to improve the structure (high pore volume, high surface area and low tortuosity), aiming to suppress internal diffusion limitation.

1.2.3 Structured carbon nanofibers supports

Carbon nanotube (CNT) and nanofiber (CNF), a new group of carbonaceous materials, are produced catalytically by decomposing carbon source gases (typically methane, carbon monoxide, synthesis gas, ethylene and ethane), on supported metal catalysts, such as Ni, Fe and Co containing catalysts, in the temperature range 425-925 ^oC [32]. Based on De Jong and Geus [33], the mechanism for CNF growth involves three steps. The hydrocarbon gas first decomposes on the exposed surface of metal nanoparticles, then carbon diffuses through the particle and finally, it precipitates to form CNF at the other end of the particle. This is schematically shown in Figure 1.8. Furthermore, there is still debate about the driving force for the carbon to dissolve on the one side of the metal particle and to segregate at the other

side. Hoogenraad et al. [34] proposed a specific mechanism to explain the initiation of CNF formation: diffusion of carbon into the metal particle leads to formation of metal carbide, which then decomposes to regenerate metal and precipitate graphite enveloping the metal particle. The metal particle is squeezed out of graphitic carbon due to pressure buildup during the formation of graphite layers.

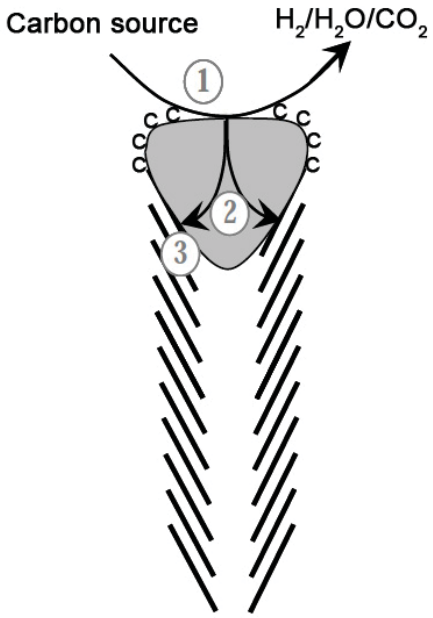

Figure 1.8: Schematic representation of the catalytic growth of a CNF using a carbon source gas. ① Decomposition of carbon source gases on the metal surface; ② Carbon atoms dissolve in and diffuse through the bulk of the metal; ③ Precipitation of carbon in the form of a CNF consisting of graphite [33].

CNFs possess a number of exceptional physical and chemical characteristics that make them promising materials as catalyst supports. They are resistant to strong acids and bases, have high mechanical flexibility and strength, as well as improved carbon-metal interactions that have been found to enhance catalytic performance [35, 36]. In addition, they can form agglomerates with high surface areas (100-200 m^2/g) and pore volumes (0.5-2.0 cm^3/g) without any micro porosity (Figure 1.9) [37], which mimics the inverse structure of a conventional porous support material, as shown in Figure 1.10 [38]. These advantages prevent mass transfer limitations inside CNF agglomerates, improving product selectivity in catalytic reactions. For example, C. Pham-Huu et.al [39] reported a higher selectivity to hydrocinnamaldehyde in cinnamaldehyde hydrogenation by using Pd catalyst supported on CNFs as compared to Pd supported on activated charcoal, which is attributed to the suppression of diffusion limitations.

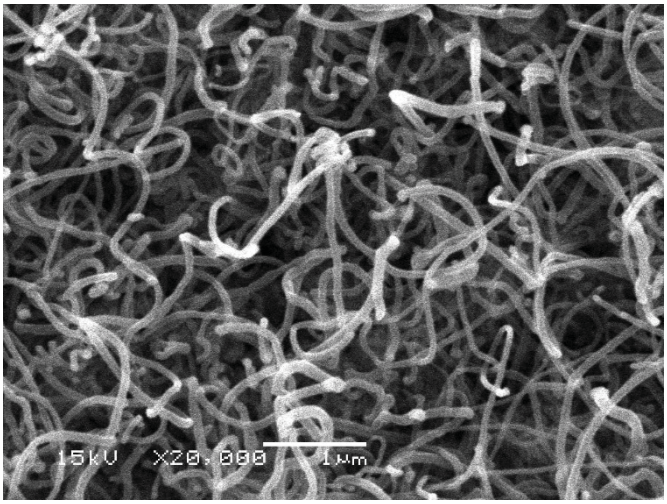

Figure 1.9: Scanning electron micrograph of porous carbon nanofiber matrix grown on Ni particles at 600°C using methane as a carbon source [37].

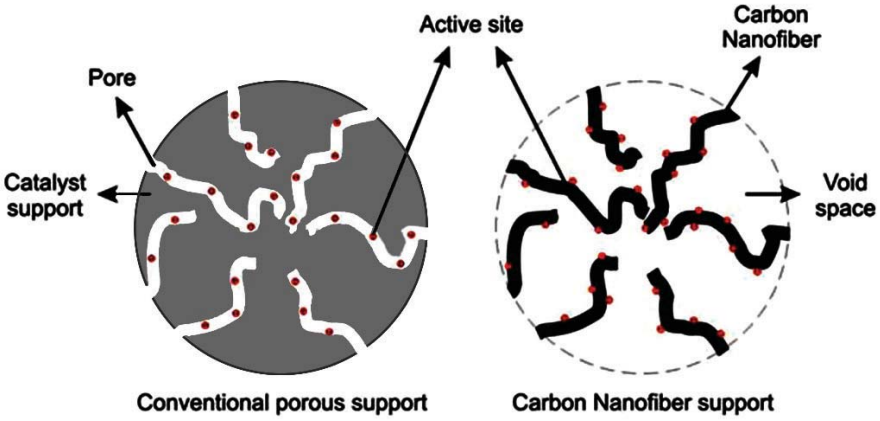

Figure 1.10: CNFs mimicking the inverse structure of conventional porous structured material [38]

However, most studies have focused on developing nanoscopic CNFs, which suffer from tedious separation of the agglomerates in slurry reactors, or high pressure drop in trickle bed reactors. These disadvantages also limited the applications of CNF in catalysis. One way to overcome these disadvantages is to immobilize CNF layers on structured materials, including monoliths [30, 40, 41], foams [42, 43], glass fibers [44], carbon cloth [45] and activated carbon fibers [46]. Chinthaginjala et al. [43] developed a structured Pd catalyst, by depositing Pd nanoparticles on a thin CNF layer previously grown on a Ni foam. It showed fast mass transfer in nitrite hydrogenation. Thakur et al. [47] also reported enhanced mass transfer in bromate reduction in water for Ru nanoparticles deposited on a CNF layer on a homemade Teflon (PTFE) chip. In this thesis, TiO_2 extrudates and cordierite monolith are used to prepare structured CNF(T) materials for application in some selective hydrogenation reactions.

1.3 Selective hydrogenation of unsaturated aldehydes

1.3.1 Selective hydrogenation of citral, cinnamaldehyde and 4-carboxybenzaldehyde

With the ever increasing demand for special chemicals, selective hydrogenation of unsaturated aldehydes become one of the current challenges to be tackled both from the fundamental and from the industrial standpoint [48-50]. For example, citral and cinnamaldehyde, two typical α,β-unsaturated aldehydes, have a pair of conjugated functional groups that can be hydrogenated: a carbonyl group (C=O) and a conjugate double bond (C=C). In addition, citral possesses another isolated double bond (C=C). Since palladium catalyst is more active in the hydrogenation of the C=C bond than the conjugated C=O bond [51], citral can be hydrogenated to citronellal with reasonable selectivity. However, deep hydrogenation to citronellol and finally to 3,7-dimethyloctan-1-ol also occurs. Cinnamaldehyde (CAL) can undergo a similar hydrogenation process as citral, producing hydrocinnamic aldehyde (HCAL) first, followed by deep hydrogenation to hydrocinnamic alcohol (HCOL), even 1-Propylbenzene (1-PB). Consecutive reaction routes for citral and cinnamaldehyde hydrogenation are shown as Figure 1.11 and 1.12, respectively.

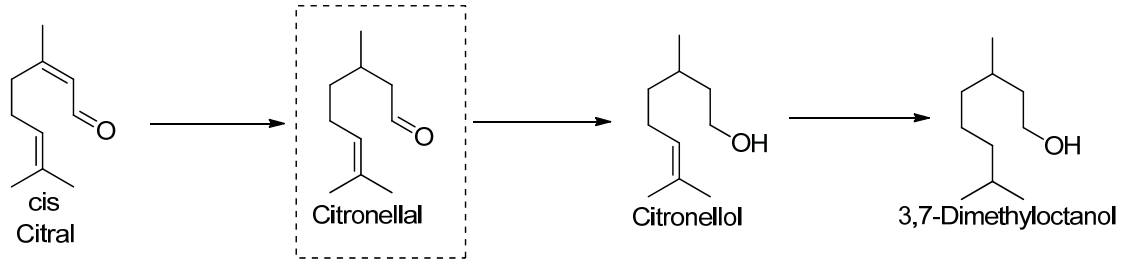

Figure 1.11: Consecutive reaction route for citral hydrogenation

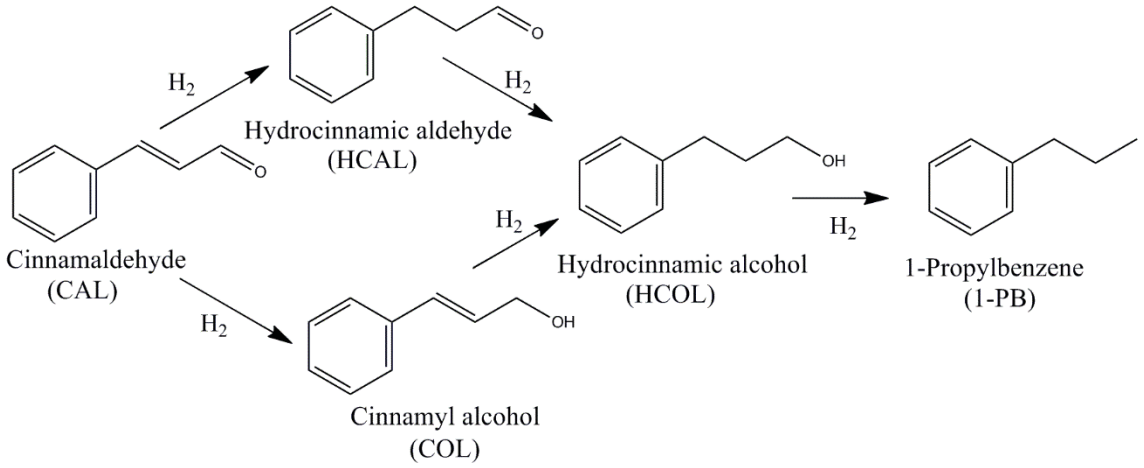

Figure 1.12: Consecutive reaction route for cinnamaldehyde hydrogenation

Besides citral and CAL hydrogenation, in this thesis also 4-carboxybenzaldehyde (4-CBA) hydrogenation is used as a model reaction to determine the properties of structured CNF(T) catalysts. 4-CBA, the main impurity in crude terephthalic acid (CTA), needs to be removed for obtaining purified terephthalic acid (PTA). The latter is an important industrial raw material used for the manufacture of polyethylene terephthalate (PET), polybutylene terephthalate (PBT) and polytrimethylene terephthalate (PTT), which are mainly applied in the production of fibers, resins, films and fabrics [52, 53]. The main upgrading step in refining CTA to PTA is catalytic hydrogenation of 4-CBA to 4-(hydroxymethyl) benzoic acid (4-HMBA) and further to *p*-toluic acid (*p*-TA) in water (Figure.1.13) [54, 55]. 4-HMBA and *p*-TA are more soluble than 4-CBA and are thus much easier removed during PTA-crystallization, staying behind in the liquid.

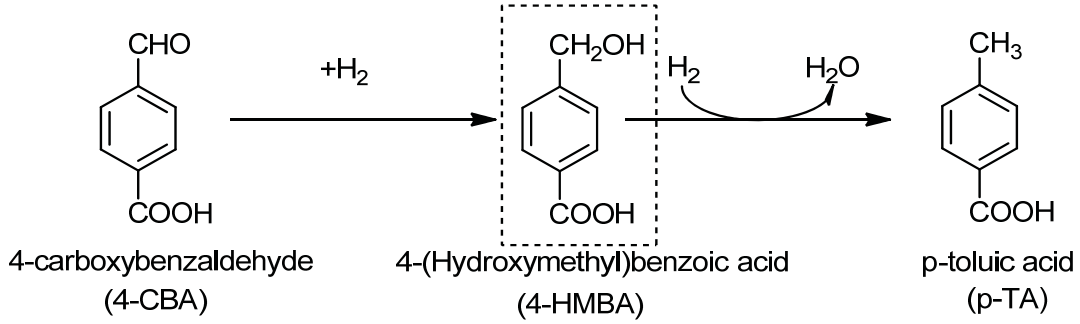

Figure 1.13: Consecutive reaction route for 4-carboxybenzaldehyde hydrogenation

In this thesis, the intermediate products of three reactions, including citronellal, HCAL and 4-HMBA, were the desired products (molecules in dash frames in Figure 1.11-1.13), while avoiding the formation of deep hydrogenated products, such as citronellol, 3,7-dimethyloctan-1-ol, HCOL and *p*-TA, as much as possible. The product distributions in such consecutive reactions depend on the internal diffusion limitations of the reactants in the catalyst.

1.3.2 Effects of internal diffusion limitations on catalytic properties

Internal diffusion limitation induces negative effects on both the reaction rate and the selectivity to the intermediate product, which is critical in selective catalytic reactions. Its negative effect on the intermediate selectivity is caused by the fact that the internal diffusion of the molecules competes with the reaction [16, 56-58], and it usually depends on the structure properties of the catalyst, including porosity, tortuosity and diffusion length, as discussed in the section 1.1.2. Internal diffusion limitation decreases the selectivity to the intermediate product because of slow removal of the intermediate product, out of the catalyst

particle. The resulting increase of the intermediate product in the catalyst particles is responsible for decreasing selectivity.

H.R. Yue et al. [59], for example, studied selective hydrogenation of dimethyl oxalate (DMO) to ethylene glycol (EG) using Cu/SiO_2 based monolithic catalyst. Compared with the low EG selectivity (83.4%) over the packed bed Cu/SiO_2 catalyst, EG selectivity over monolith is significantly enhanced (95.3%). However, the selectivity to ethanol, the deeply hydrogenated product of EG, and 1,2-butanediol (1,2-BDO), the consecutive reaction product of ethanol and EG, were approximately 6% of total over packed bed catalyst, which is more than 3 times (2%) of the same products higher as compared to the monolith. It is primarily due to the relatively short diffusive pathway of the thin wash-coat layer ($\leqslant$ 40 μm) in the monolithic catalyst, which leads to a more efficient use of the active phase.

Additionally, T.A. Nijhuis et al. [58] studied the effects of particle size on selective hydrogenation of 3-methyl-1-pentyn-3-ol to 3-methyl-1-pentene-3-ol over Pd/SiO_2 catalyst in slurry reactors. In experiments, the smaller the catalyst particle size, the higher the activity and alkene selectivity. In contrast, the selectivity to 3-methyl-3-pentanol, the deeply hydrogenated product of 3-methyl-1-pentene-3-ol, increased with the catalyst particle size. The observed selectivity dependence on the particle size was explained by the concentration profiles of the reactants in the catalyst particles. As a result of an insufficiently fast mass-transfer, the alkene concentration inside the larger particles is higher, causing deeper hydrogenation to occur.

1.4 Scope and outline of this thesis

The aim of the work described in this thesis is to synthesize macro-structured carbon nanofibers materials on large Titania particles and cordierite monolith, with properties that can avoid or diminish internal mass transfer limitations. Their supported palladium catalysts were compared with some catalysts, including palladium catalysts supported on activated carbon (Pd/AC), meso-porous carbon (Pd/MC) and carbon nanofibers (Pd/CNF). Their catalytic properties were evaluated for selective hydrogenation of citral, cinnamaldehyde and 4-carboxybenzaldehyde to determine if as-prepared macro-structured carbon nanofibers catalysts offer advantages in enhancing the activity and the selectivity in these reactions.

Chapter 2 describes the direct growth of CNFs on large Titania particles (C/TiO_2), using nickel and nickel-copper alloy as the catalyst, respectively. The textural and structural

properties of C/TiO_2 are characterized. Results revealed that the addition of a little Cu promoter in CNFs growth helped to the improvement in textural and structural properties of C/TiO_2. As-prepared structured CNFs support possessed suitable surface areas and dominant meso-porous structures. Pd catalyst supported on C/TiO_2 (Pd/C/TiO_2) exhibited high selectivity to citronellal in selective hydrogenation of citral, which was attributed to the elimination of internal diffusion limitations due to its mesoporous structure. **Chapter 3** focuses on the influence of structural properties on catalytic performance in citral selective hydrogenation over C/TiO_2 supported Pd catalyst (Pd/C/TiO_2). Internal diffusion limitations of the reactants in Pd/C/TiO_2 were estimated with Weisz-Prater criterion and compared to those of commercial Pd/AC catalyst. The results indicate negligible internal diffusion limitation inside Pd/C/TiO_2 due to the dominant meso-porous structures, which made citronellal become the main product in the reaction. In contrast, Pd on AC gives much more deep hydrogenation to 3,7-dimethyloctanol, because the micropores in this catalyst induces significant internal mass transport limitation.

Chapter 4 demonstrates the synthesis of carbon nanofiber-titania-cordierite monolith composite, i.e. CNF/TiO_2/monolith, and its application as catalyst support in selective hydrogenation of cinnamaldehyde (CAL) to hydrocinnamic aldehyde (HCAL). Attachment strength of the CNFs and acid-resistant properties of the composite had been studied to evaluate its mechanical stability in practical conditions. The effects of supported Pd particles, oxygen-containing surface groups and internal diffusion limitation on catalytic performance over Pd/CNF/TiO_2/monolith were further studied. CNF/TiO_2/monolith exhibited excellent catalytic activity for selective hydrogenation of CAL to HCAL, as compared to traditional carbon-supported catalysts including Pd/AC and Pd/MC. The low acidic oxygen-containing surface groups, as well as macro- and mesoporous structure are responsible for the high selectivity to the intermediate HCAL.

Chapter 5 estimated the mass transfer behavior of substrates in Pd/CNF/monolith for 4-CBA hydrogenation using reaction kinetics models and results were compared to Pd/CNF and Pd/AC with different particle sizes. Results indicated that Pd/CNF and Pd/CNF/monolith possessed the higher selectivity to 4-HMBA at complete 4-CBA conversion in 4-CBA hydrogenation than macro-structured Pd/AC did, which was attributed to the predominant macro- and mesopore structure of Pd/CNF and Pd/CNF/monolith. However, when the particle size of Pd/AC decreased to 53-44 μm, internal diffusion limitation in it was removed due to

its short diffusion length, and calculated Weisz-Prater numbers, Thiele modulus and reaction rate ratio (k_1/k_2) in two steps of this consecutive reaction confirmed this result.

Finally, **Chapter 6** summarizes the results obtained in this work, including general conclusions and recommendations for the future.

References

[1] A. Molnar, A. Sarkany, M. Varga, J. Mol. Catal. A 173 (2001) 185-221.

[2] J. Aumo, J. Warna, T. Salmi, D. Y. Murzin, Chem. Eng. Sci. 61 (2006) 814-822.

[3] A. Bruehwiler, N. Semagina, M. Grasemann, A. Renken, L. Kiwi-Minsker, A. Saaler, H. Lehmann, W. Bonrath, F. Roessler, Ind. Eng. Chem. Res. 47 (2008) 6862-6869.

[4] T. Louis, Chemical Reactor Analysis and Applications for the Practicing Engineer (Hoboken: John Wiley & Sons, Inc., 2012), pp. 420.

[5] H. Scott Fogler, Elements of chemical reaction engineering (4th edition) (Upper Saddle River: Prentice Hall, 2005), pp. 761.

[6] E. P. van Elk, Gas-liquid reactions: Influence of liquid bulk and mass transfer on process performance, PhD Thesis, University of Twente, Enschede, The Netherlands (2001).

[7] B. K. Dutta, Principles of mass transfer and seperation processes (Delhi: PHI Learning Pvt. Ltd., 2007), pp. 127.

[8] E. Crezee, B. W. Hoffer, R. J. Berger, M. Makkee, F. Kapteijn, J. A. Moulijn, Appl. Catal. A: Gen 251 (2003) 1.

[9] H. Scott Fogler, Elements of chemical reaction engineering (4th edition) (Upper Saddle River: Prentice Hall, 2005), pp. 771.

[10] H. Scott Fogler, Elements of chemical reaction engineering (4th edition) (Upper Saddle River: Prentice Hall, 2005), pp. 773.

[11] H. Scott Fogler, Elements of chemical reaction engineering (4th edition) (Upper Saddle River: Prentice Hall, 2005), pp. 780.

[12] M. Albert Vannice, Kinetics of catalytic reactions (New York: Springer Science + Business Media, Inc. 2005), pp. 57.

[13] H. Scott Fogler, Elements of chemical reaction engineering (4th edition) (Upper Saddle River: Prentice Hall, 2005), pp. 831, 839.

[14] R.A. van Santen, P.W.N.M. van Leeuwen, J.A. Moulijn, B.A. Averill, Catalysis: an integrated approach (Second, revised and enlarged edition) (Oxford: Elsevier Science, 1999), pp. 402.

[15] H. Scott Fogler, Elements of chemical reaction engineering (4th edition) (Upper Saddle River: Prentice Hall, 2005), pp. 830.

[16] S. Mukherjee, M. A. Vannice, J. Catal. 243 (2006) 108-130.

[17] K. Pangarkar, T. J. Schildhauer, J. R. van Ommen, J. Nijenhuis, F. Kapteijn, J. A. Moulijn, Ind. Eng. Chem. Res. 47 (2008) 3720-3751.

[18] C. N. Satterfield, AIChE J. 21 (1975) 209-228.

[19] J. K. Chinthaginjala, Hairy foam: thin layers of carbon nanofibers as catalyst support for liquid phase reactions, PhD Thesis, University of Twente, Enschede, The Netherlands (2010).

[20] A. Holmen, H. J. Venvik, R. Myrstad, J. Zhu, D. Chen, Catal. Today 216 (2013) 150-157.

[21] M. T. Kreutzer, P. Du, J.J. Heiszwolf, F. Kapteijn, J. A. Moulijn, Chem. Eng. Sci. 56 (2001) 6015-6023.

[22] E. García-Bordejé, I. Kvande, D. Chen, M. Rønning, Adv. Mater. 18 (2006) 1589-1592.

[23] P. Tribolet, L. Kiwi-Minsker, Catal. Today 105 (2005) 337-343.

[24] J. K. Chinthaginjala, L. Lefferts, Carbon 47 (2009) 3175-3183.

[25] S. Pacheco Benito, L. Lefferts, Carbon 48 (2010) 2862-2872.

[26] P. Li, T. Li, J. H. Zhou, Z. J. Sui, Y. C. Dai, W. K. Yuan, D. Chen, Microporous Mesoporous Mater. 95 (2006) 1-7.

[27] J. H. Zhou, M. G. Zhang, L. Zhao, P. Li, X.G. Zhou, W. K. Yuan, Catal. Today 147S (2009) S225-S229.

[28] M. V. Twigg, J. T. Richardson, Ind. Eng. Chem. Res. 46 (2007) 4166-4177.

[29] B. Pereda-Ayo, J. A. Botas-Echevarríab, J. González-Casablancac, M.P. González-Marcosa, J. R. González-Velasco, Catal. Today 216 (2013) 50-56.

[30] N. Jarrah, J. G. van Ommen, L. Lefferts, Catal. Today 79-80 (2003) 29-33.

[31] J. A. Moulijn, M. Kreutzer, F. Kapteijn, Chem. Eng. 768 (2005) 32-34.

[32] R. T. K. Baker, M. A. Barber, P. S. Harris, F. S. Feates, R. J. J. Waite, J. Catal. 26 (1972) 51-62.

[33] K. P. de Jong and J. W. Geus, Catal. Rev. Sci. Eng. 42 (2000) 481-510.

[34] M. S. Hoogenraad. Growth and utilization of carbon fibers, PhD Thesis, Utrecht University (1995).

[35] J. M. Planeix, N. Coustel, B. Coq, V. Bretons, P. S. Kumbhar, R. Dutartre, P. Geneste, P. Bernier, P. M. Ajayan, J. Am. Chem. Soc. 116 (1994) 7935-7936.

[36] X. Zhang, Y. C. Guo, Z. C. Zhang, J. S. Gao, C. M. Xu, J. Catal. 292 (2012) 213-226.

[37] J. Zhu, M. H. Lu, M. S. Li, J. J. Zhu, Y. H. Shan, Mater. Chem. Phys. 132 (2012) 316-323.

[38] J. K. Chinthaginjala, K. Seshan, L. Lefferts, Ind. Eng. Chem. Res. 46 (2007) 3968-3978.

[39] C. Pham-Huu, N. Keller, G. Ehret, L.J. Charbonniere, R. Ziessel, M.J. Ledoux, J. Mol. Catal. A: Chem. 170 (2001) 155-163.

[40] X. Yu, B. Lin, B. Gong, J. Lin, R. Wang, K. Wei, Catal. Lett. 124 (2008) 168-173.

[41] S. Morales-Torres, A. F. Pérez-Cadenas, F. Kapteijn, F. Carrasco-Marín, F. J. Maldonado-Hódar, J. A. Moulijn, Appl. Catal. B: Environ. 89 (2009) 411-419.

[42] P. W. A. M. Wenmakers, J. van der Schaaf, F. M. Kuster, J. C. Schouten, J. Mater. Chem. 18 (2008) 2426-2436.

[43] J. K. Chinthaginjala, J. H. Bitter, L. Lefferts, Appl. Catal. A: Gen. 383 (2010) 24-32.

[44] Z. R. Ismagilov, N. V. Shikina, V. N. Kruchinin, N. A. Rudina, V. A. Ushakov, N. T. Vasenin, H. J. Veringa, Catal. Today 102-103 (2005) 85-93.

[45] M. Cantoro, V. B. Golovko, S. Hofmann, D. R. Williams, C. Ducati, J. Geng, B. O. Boskovic, B. Kleinsorge, D. A. Jefferson, A. C. Ferrari, B. F. G. Johnson, J. Robertson. Diam. Relat. Mater. 14 (2005) 733-738.

[46] J. Jia, X. Z. Duan, G. Qian, P. Li, X. G. Zhou, D. Chen, W. K. Yuan, Catal. Today 216 (2013) 254-260.

[47] D. B.Thakur, R. M. Tiggelaar, Y. Weber, J. G. E. Gardeniers, L. Lefferts, K. Seshan, Appl. Catal. B: Environ. 102 (2011) 243-250.

[48] G. Neri, L. Bonaccorsi, L. Mercadante, S. Galvagno, Ind. Eng. Chem. Res. 36 (1997) 3554-3562.

[49] S. Handjani, E. Marceau, J. Blanchard, J. Krafft, M. Che, M. Päivi, N. Kumar, J. Wärnå, D. Y. Murzin, J. Catal. 282 (2011) 228-236.

[50] J. Álvarez-Rodríguez, I. Rodríguez-Ramos, A. Guerrero-Ruiz, A. Arcoya, Appl. Catal. A: Gen. 401 (2011) 56-64.

[51] E. Bus, R. Prins, J. A. Bokhoven, Catal. Commun. 8 (2007) 1397-1402.

[52] C. M. Park, Encyclopedia of Chemical Technology, Vol 18. New York: Wiley, 1996. 991.

[53] Y. Chen, J. L. Fulton, W. Partenheimer. J. Am. Chem. Soc. 127 (2005) 14085-14093.

[54] D. E. James. US 4782181. 1988.

[55] F. Menegazzo, T. Fantinel, M. Signoretto, F. Pinna. Catal Commun, 8 (2007) 876-879.

[56] J. M. Winterbottom, R. Fishwick, H. Stitt, Can. J. Chem. Eng. 81 (2003) 588-596.

[57] U. K. Singh, M. A. Vannice, Appl. Catal. A 213 (2001) 1-24.

[58] T. A. Nijhuis, G. van Koten, F. Kapteijn, J. A. Moulijn, Catal. Today 79-80 (2003) 315-321.

[59] H. R. Yue, Y. J. Zhao, L. Zhao, J. Lv, S. P. Wang, J. L. Gong, X. B. Ma, AIChE J. 58 (2012) 2798-2809.

Chapter 2

Production of Macro-structured Carbon Nanofibers Catalyst Support Based on Titania Extrudate

Abstract

In this chapter, we reported the synthesis of a promising carbon-titania composite material, CNF/TiO_2. The composite was synthesized by methane decomposition over TiO_2 extrudates using Ni-Cu as a catalyst. CNF/TiO_2 synthesized was subsequently employed to prepare its supported palladium catalyst, Pd/CNF/TiO_2. The textural and structural properties of CNF/TiO_2 and Pd/CNF/TiO_2 were characterized by BET, SEM/EDS, TEM, ICP-AES, XRD and TG-DTG. Results revealed that the addition of a little Cu promoter in composite synthesis helped to the improvement in textural and structural properties of CNF/TiO_2. The optimal composite prepared had a BET surface area of 60 m^2/g and 97% of its pore space were mesopore. It contained 38% of carbon composed of 90% of carbon nanofibers and 10% of amorphous carbon. Pd/CNF/TiO_2 prepared held the similar textural and structural properties as CNF/TiO_2 did. Although the comparatively lower catalytic activity caused by the lower palladium dispersion, Pd/CNF/TiO_2 exhibited the high citronellal selectivity (90%) at 90% citral conversion, which was attributed to the elimination of internal diffusion limitations due to its mesoporous structure.

This part of work has been published as Research Article: J. Zhu, M. Lu, M. Li, J. Zhu, Y. Shan, *Mater. Chem. Phys.* 132 (2012) 316-323.

2.1 Introduction

Selective hydrogenation is one of the most important processes in fine chemical industries. The properties and qualities of hydrogenation products can be significantly affected by the activity and structure of the employed catalyst [1, 2]. Particularly, the support material is one of the significant factors in the catalyst. Alumina, silica and activated carbons are commonly served as the traditional supports to prepare the catalysts to use in multiphase reactions.

In the past few years, significant attention has been drawn to the carbon nanofiber (CNF) due to its exceptional mechanical and electronic properties [3]. CNF has been shown to be important in the field of catalysis [3-5]. Compared to traditional catalyst supports (alumina, silica and activated carbons), metals supported onto CNF can exhibit unusually high catalytic activity and selectivity patterns [6].

However, most studies have focused on developing nanoscopic CNFs, which are difficult to use in fixed-bed catalytic reactors. Several studies have been recently published in which macroscopic CNFs had been synthesized on a variety of hosts such as alumina[7,8], silica[9,10], monolith[11], nickel foam[12, 13] and graphite[14] for the purpose of preparing catalyst supports. They are now becoming the significant process intensification technologies in gas-solid and gas-liquid-solid reactions, due to their unique advantages that they offer the controlling hydrodynamics, transport phenomena, and reaction kinetics in comparison with traditional ones [15].

In this chapter, we reported a novel macroscopic CNFs material, which is synthesized by depositing CNFs layers over titania extrudates (Figure 2.1a), named carbon-titania composite (CNF/TiO_2) (Figure 2.1b). Compared with other formed hosts, TiO_2 sticks possesses several prominent advantages including the high chemical resistance to make it be utilized in harsh environments such as highly acidic or basic medium, as well as the high mechanical strength that reduces the risk of breaking during reaction. The synthesized CNF/TiO_2 and its supported palladium catalyst had been characterized using various methods. Meanwhile, the CNF/TiO_2 supported palladium catalyst had also been prepared. Its catalytic performance had been evaluated in selective hydrogenation of citral to citronellal and compared with that of the commercial catalyst, i.e., formed activated carbon supported palladium. The possible formation mechanism of hydrogenation products was also discussed.

2.2 Experimental

2.2.1 Preparation and characterization of CNF/TiO_2 composite

TiO_2 extrudates with the stick shape (Sinopec Yangzi, China, ϕ 2×5 mm; 18.2 m^2/g; Figure 2.1a) were used as the host in this study to prepare CNF/TiO_2 composite material. Specifically, TiO_2 was impregnated with aqueous solution of $Ni(NO_3)_2 \cdot 6H_2O$ or the mixture of $Ni(NO_3)_2 \cdot 6H_2O$ and $Cu(NO_3)_2 \cdot 3H_2O$ (A.R, Sinopharm, China), in which the nickel loadings were kept fixed at 6 wt.%. The mole ratio of Ni to Cu in the mixture solution was varied within the range from 4:1 to 8:1. The samples were dried overnight at 393 K prior to calcination at 773 K for 2 h. After they were reduced in the tube at 873 K in a stream of N_2 / H_2 (80:20) (99.999%, Wuxi Tianhong, China) for 3 h, monometallic Ni/TiO_2 and bimetallic Ni-Cu/TiO_2 were obtained. Methane (99.999%, Wuxi Tianhong, China) was then passed through the tube to decompose at 873 K for 5 h. After refluxing in concentrated HNO_3 for 60 min to remove exposed nickel and copper metal particles, the composite supports CNF/TiO_2 were finally synthesized (Figure 2.1b).

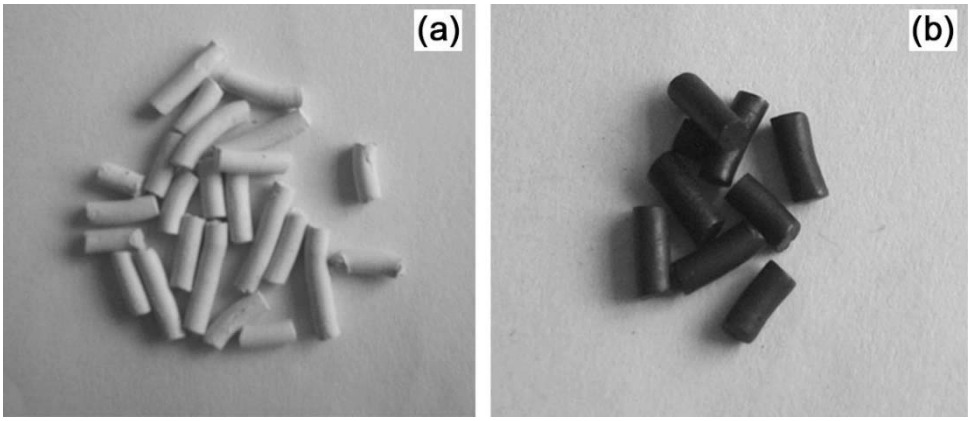

Figure 2.1: TiO_2 extrudates (a) and CNF/TiO_2 (b)

2.2.2 Preparation of CNF/TiO_2 supported Pd catalyst

0.5 wt.% of Pd catalyst was prepared by impregnation method. Firstly, the support CNF/TiO_2 was dispersed directly in an hydrochloric acid (HCl) solution (0.2 M) of palladium (II) chloride ($PdCl_2$) (Sinopharm, China) and stirred continuously for 6 h. The sample was then dried overnight at 393 K and stored in a desiccator. After reducing at 493 K in a stream of N_2/H_2 (80:20) for 2 h, the catalyst Pd/CNF/TiO_2 was finally prepared.

2.2.3 Characterization of the materials

CNF/TiO_2 composite and its supported Pd catalyst were characterized to test the textural

and structural properties. Methane decomposition was analyzed using Hiden QIC-20 online mass spectrometer. X-ray powder diffraction data were collected on Rigaku D/max 2500 diffractometer using CuKa (40 kV, 40 mA) radiation and a graphite monochromator. The BET specific surface areas were carried out with Micromeritics ASAP 2010 apparatus. The metals contents over supports and catalysts were determined by Vista-AX inductively coupled plasma atomic emission spectrometry (ICP-AES). Scanning electron images and elements distributions were recorded using a JEOL JSM-6360 LA scanning electron microscope & energy-dispersive X-ray spectroscopy (SEM/EDS). The morphologies and the properties of the metal particles on catalysts were obtained with JEM-2100 transmission electron microscopy (TEM). Thermogravimetric (TGA) and differential thermal (DTA) analysis were performed using a TA SDT Q600 instrument.

2.2.4 Activity test of Pd/CNF/TiO_2

The catalytic performance of Pd/CNF/TiO_2 has been evaluated in the reaction of selective hydrogenation of citral in liquid phase. The reaction was conducted in a 100 ml autoclave at 363 K and 3 MPa. The fleshed reduced catalysts (1 wt.%) were dispersed in the isopropanol (A.R, Sinopharm, China) solution of citral (10 wt.%, A.R, Sinopharm, China) and then they were treated under nitrogen and hydrogen flows successively to remove dissolved oxygen. The reaction pressure was maintained by injecting hydrogen. Small amounts of reaction samples were withdrawn from the reactor at different reaction times and analyzed using gas chromatography (VARIAN CP3800) equipped with a FID detector and a capillary column HP-5 using nitrogen as carrier gas. A formed activated carbon supported catalyst, named Pd/AC, (Pd loading 0.5 wt.%, BET specific surface area 810 m^2/g, micropore area 720 m^2/g, Sinopec Yangzi, China) and the blank CNF/TiO_2 without Pd loading were tested at the same conditions for comparison.

2.3 Results and discussion

2.3.1 The effect of promoter Cu on synthesis of CNF/TiO_2 composite materials

(1) Analysis of methane decomposition using online mass spectrometer

The methane decomposition over monometallic Ni/TiO_2 and bimetallic Ni-Cu/TiO_2 has been studied by monitoring residual CH_4 concentration after decomposition using an online mass spectrometer. The variations of CH_4 conversion as a function of reaction time are shown in Figure 2.2 for three samples.

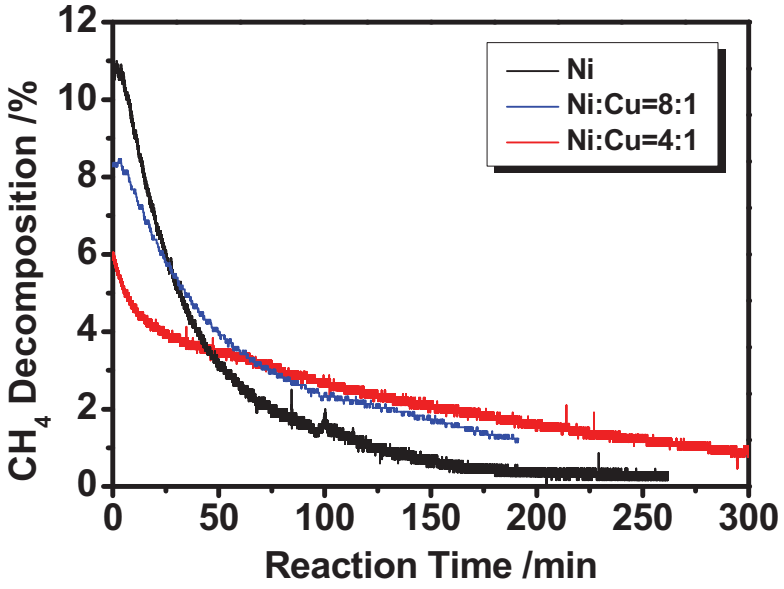

Figure 2.2: Methane decomposition versus reaction time over three Ni/TiO_2 and $Ni\text{-}Cu/TiO_2$ samples.

Specifically, Ni/TiO_2 showed the highest initial conversion (about 11%) for methane to carbon of all three samples. However, the conversion on Ni/TiO_2 decreased more steeply with time than that on $Ni\text{-}Cu/TiO_2$. After 250 min, the conversion on Ni/TiO_2 decreased to zero, indicating it complete deactivation, while the reaction with $Ni\text{-}Cu/TiO_2$ is still continuing although in a lower rate.

(2) BET analysis

The novel CNF/TiO_2 composite can be produced by depositing carbon onto TiO_2 host through methane decomposition. The textural properties of CNF/TiO_2 composites prepared using different precursors give different results, as shown in Table 2.1.

Table 2.1: Textural properties of the materials

Samples		Weight increased after methane decomposition (wt. %)	BET Surface Area(m^2/g)	Micropore Area(m^2/g)	Average Pore Diameter(nm)
TiO_2 host		/	18.3	3.1	14.2
CNF/TiO_2 composite	(I)	9	28.2	2.7	10.4
	(II)	38	60.3	1.8	6.2
	(III)	17	45.3	2.1	7.4
$Pd/CNF/TiO_2$		/	58.1	1.6	9.7

Note: CNF/TiO_2 composite were prepared through methane decomposition over $metal/TiO_2$ catalysts with different metal loadings: (I) 6 wt.% Ni loading over TiO_2; (II) Ni and Cu loading over TiO_2 (6 wt.% Ni, the

mole ratio of Ni to Cu: 8 to 1); (III) Ni and Cu loading over TiO_2 (6 wt.% Ni, the mole ratio of Ni to Cu: 4 to 1). CNF/TiO_2 composites prepared had all been treated in concentrated HNO_3 at 120°C for 60min. Pd/CNF/TiO_2 catalyst employed CNF/TiO_2 (II) as the support.

Generally, depositing carbon on TiO_2 hosts produce a significant increase in BET surface area. For example, compared with TiO_2 host, the weights of CNF/TiO_2 samples increased significantly with carbon deposition, especially in the case of CNF/TiO_2 (II), where it results in 38% increase, being the largest among the samples in this work and its BET surface area was 60 m^2/g, much larger than 18 m^2/g of TiO_2 host. Meanwhile, promoter Cu in the precursor imposed great influences on composite textural properties. The BET surface area of composite CNF/TiO_2 (II) and (III) were 60 m^2/g and 45 m^2/g respectively, much larger than 28 m^2/g of CNF/TiO_2 (I).

However, the variation occurred in textural properties between the sample CNF/TiO_2 (II) and CNF/TiO_2 (III) due to their different Cu contents in the precursors. Compared with CNF/TiO_2 (III), the sample CNF/TiO_2 (II) had the optimal textural properties: BET surface area was up to 60.3 m^2/g while the micropore area declined significantly to 1.8 m^2/g, accounting for only 3% of its total BET surface area, which may decrease internal diffusion limitations of the reactants in three phase catalytic reactions. In contrast, the micropore areas of TiO_2 host and CNF/TiO_2 (III) accounted for 16.9% and 4.6% of their total BET surface areas respectively.

These results could be explained that an excess Cu content in the precursor can inhibit the activity of Ni, thereafter slower the formation of carbon deposits and they were coincident with those of methane decomposition.

(3) XRD analysis

The XRD spectra of TiO_2, Ni/TiO_2, Ni-Cu/TiO_2 and CNF/TiO_2 before and after HNO_3 treatment were shown in Figure 2.2, which can provide valuable information about the crystalline phases of samples. Specifically, besides the common characteristic peaks of TiO_2 (anatase) (Figure 2.3a) at 2θ degree 25.3°, 36.9°, 37.7°, 38.5° and 48.0°, the XRD spectra of Ni/TiO_2 (Figure 2.3b) and Ni-Cu/TiO_2 (Figure 2.3c) also showed the peaks of Ni and Ni/Cu, respectively. Particularly, as a result of adding Cu promoter, the Ni (111) diffraction line in Ni-Cu/TiO_2 was shifted to the smaller angle, compared with that of Ni/TiO_2 (2θ from 44.46° to 44.22°). The same effect was found with the Ni (200) line. This shift is likely caused by dissolving the copper atoms into the Ni particles during the calcination as well as the

reduction process. Indeed, the copper atom radius (1.27 Å) was larger than a vacancy in the Ni lattice (0.52 Å), therefore, incorporation of the copper atom should increase the lattice constant, and, in turn, decrease the 2θ value. According to XRD analysis, the lattice constant of Ni after addition of copper was 3.5447 Å and the 2θ shift of Ni (111), -0.24°, corresponds to an increase of the lattice constant by 0.0159 Å. Note also, that no lines attributed to the Ni-Cu alloy structure were found in XRD measurements. In addition, the characteristic graphite (002) and graphite (101) peaks at 2θ (26.38°, 44.38°) was clearly evident (Figure 2.3d and 2.3e), indicating the dominance of graphite carbon deposit over host material after methane decomposition. It is noted that the peak of graphite (101) is close to that of nickel (111) at 2θ≈44.4°. Therefore, the peaks of graphite (101) and nickel (111) were likely overlapped each other before HNO_3 treatment (Figure 2.3d). While, with the removal of most exposed Ni and Cu, which was approved by the elements analysis (Table 2.2 & Figure 2.6b), the peaks of Cu and Ni (200) were not found in the spectrum (Figure 2.3e). So, we considered that the peak at 2θ=44.38° here represented graphite (101).

(4) SEM analysis

A large amount of CNFs covered the surfaces of TiO_2 after methane decomposition. The surface morphology of these samples has been examined using SEM and the images are shown in Figure 2.4a-2.4d.

Compared with the TiO_2 host (Figure 2.4a), the surface of CNF/TiO_2 (I) showed stubby structures with large diameters in a range of 100-120nm (Figure 2.4b). In contrast, CNFs covered on Ni-Cu/TiO_2 surface displayed the slight structures, as shown in Figure 2.4c and Figure 2.4d. The surface consisted of numerous fibers with a diameter in a range of 50-80nm. According to the mechanism of CNF growth [3], the diameter of CNF correlates with the size of the catalytic metal crystal. So, the variation in morphologies of CNFs between CNF/TiO_2 (I) and CNF/TiO_2 (II) (III) originated from the different sizes of Ni crystal. To Ni-Cu/TiO_2, incorporation of the copper into the nickel particles produced the small size of Ni crystals, which finally caused the formation of the slight structures of CNFs on Ni-Cu/TiO_2 surface. Combined BET and surface morphology analysis of CNF/TiO_2, a trace of Cu in the precursor can significantly improve the textural properties of CNF/TiO_2.

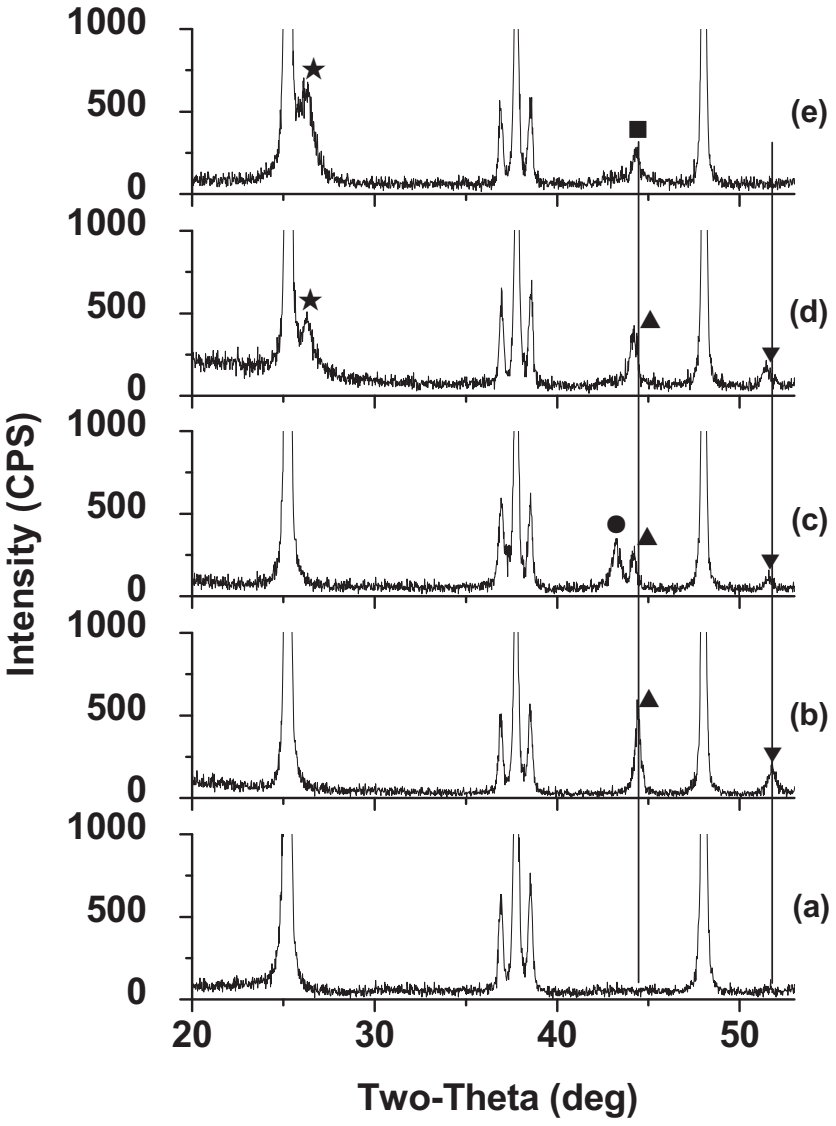

Figure 2.3: XRD patterns of pure TiO_2 support (a), Ni/TiO_2 with 6 wt.% Ni loading (b), $Ni\text{-}Cu/TiO_2$ with the mole ratio of Ni to Cu 8 to 1 (c), CNF/TiO_2 composite prepared by methane decomposition before HNO_3 treatment (d) and after HNO_3 treatment (e): ▲Ni (111); ▼ Ni (200); ● Cu (111); ★ Graphite (002); ■ Graphite (101).

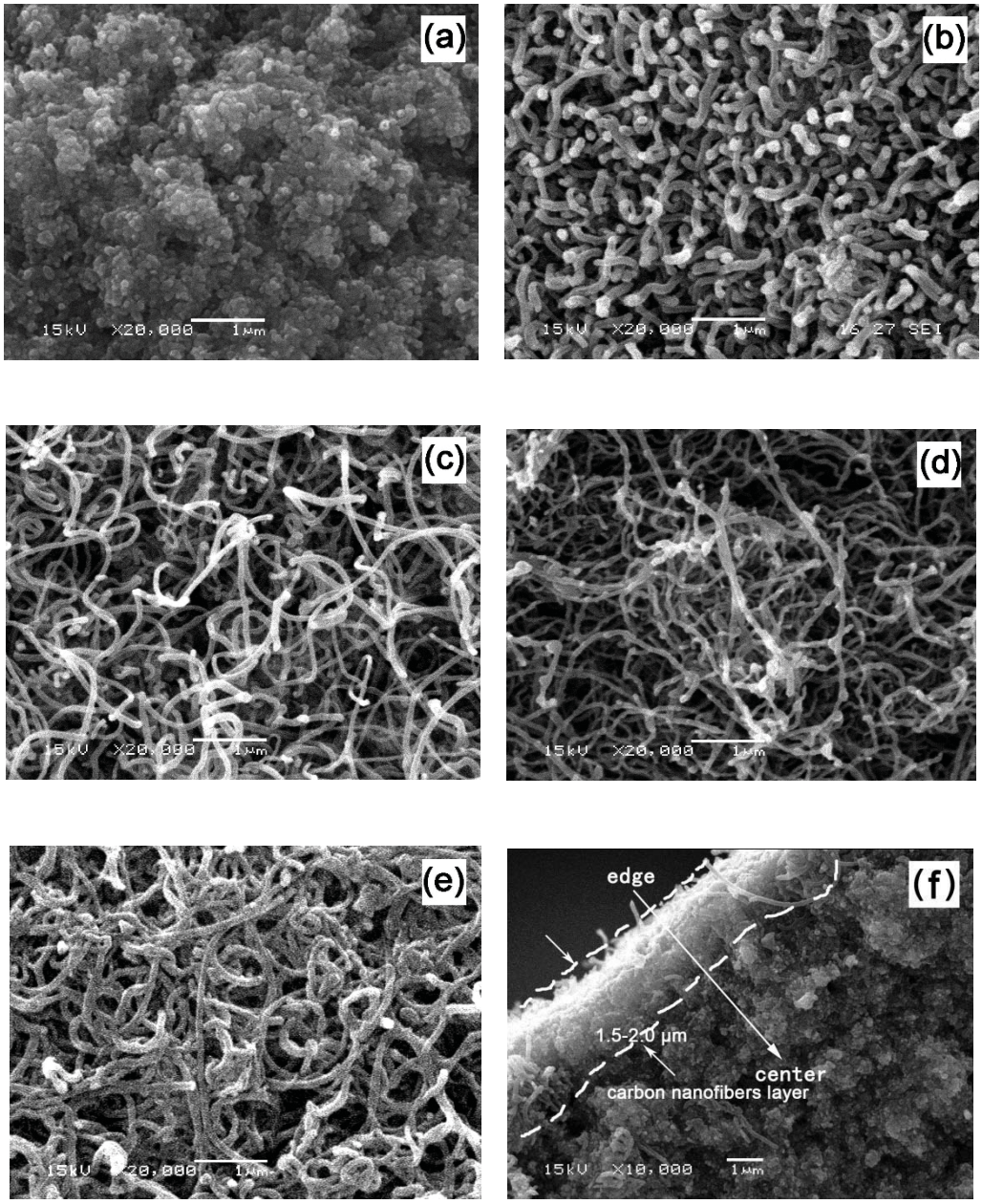

Figure 2.4: SEM images of the materials: (a) TiO_2 support; (b) the surface of CNF/TiO_2 (I); (c) the surface of CNF/TiO_2 (II); (d) the surface of CNF/TiO_2 (III); (e) the surface of CNF/TiO_2 (II) treated in concentrated HNO_3 for 60 min; (f) the cross section of CNF/TiO_2 (II).

Note: The meanings of CNF/TiO_2 (I), (II) and (III) were described in Table 2.1.

In conclusion, these test results indicate that Cu promoter can affect the formation of carbon deposit in two aspects: (i) the dissolution of copper atoms into the nickel particles can weaken the interactions between Ni crystals and produce the small size of Ni crystals, which could facilitate the production of CNF with small diameters on the host surface; (ii) there exists strong affinity between copper crystals and graphite carbon. The appearance of copper

can effectively prevent deposition of produced carbon onto the surface of Ni crystal, and consequently, slow the deactivation of Ni particles, thereafter keeping the growth of CNFs on Ni particles for a long time to increase its BET surface area and decrease its micropore area as well [16].

Considered the application of CNF/TiO_2 composite as the catalyst support, the sample CNF/TiO_2 (II) was more suitable than the others as its good textural properties. Therefore, CNF/TiO_2 (II) was selected as the support to prepare structured Pd catalyst in application for the selective hydrogenation of citral, which will be discussed in chapter 3 of the thesis. Particularly, the optimal ratio of Ni to Cu in the precursor was 8:1.

2.3.2 Textural and structural properties of CNF/TiO_2 and Pd/CNF/TiO_2

(1) Textural properties of the materials

As discussed in the section 2.3.1 (2), the sample CNF/TiO_2 (II) had the optimal textural properties: 60.3 m^2/g of BET surface area, while 1.8 m^2/g of micropore area, therefore it can be inferred that 97% of its pore space consisted of meso- and macropores. After Pd loading, the catalyst Pd/CNF/TiO_2 held the similar textural properties as CNF/TiO_2 did (Table 2.1) which indicated that as-prepared CNF/TiO_2 possessed a high material stability.

(2) Surface morphologies and element distributions of the materials

As shown by SEM images in Figure 2.4c, the surface of CNF/TiO_2 (II) covered with a significant amount of CNFs with diameters of 50-80 nm. The thickness of the deposition layer can be identified from a SEM image of CNF/TiO_2 (II) cross section in Figure 2.4f, i.e., 1.5-2.0 μm. Particularly, some CNFs appeared even in the interior of the host. The element distributions in the interior of the composite and the catalysts have been analyzed by SEM-EDS in this work.

Specifically, the local element compositions of 10 locations distributed evenly along a straight line from sample center to the edge were examined (Figure 2.5). The results are shown in Figure 2.6.

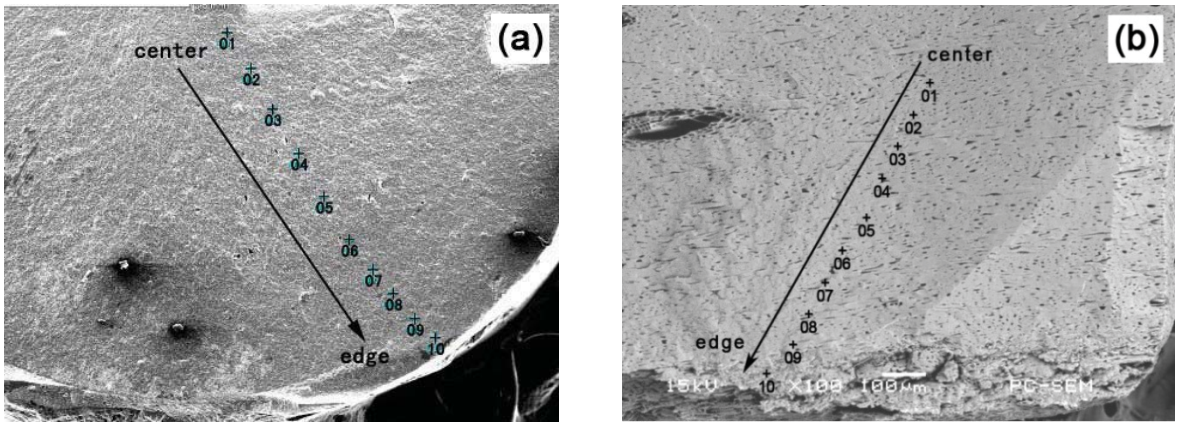

Figure 2.5: The locations selected in the sections of the materials: (a) CNF/TiO_2; (b) Pd/AC.

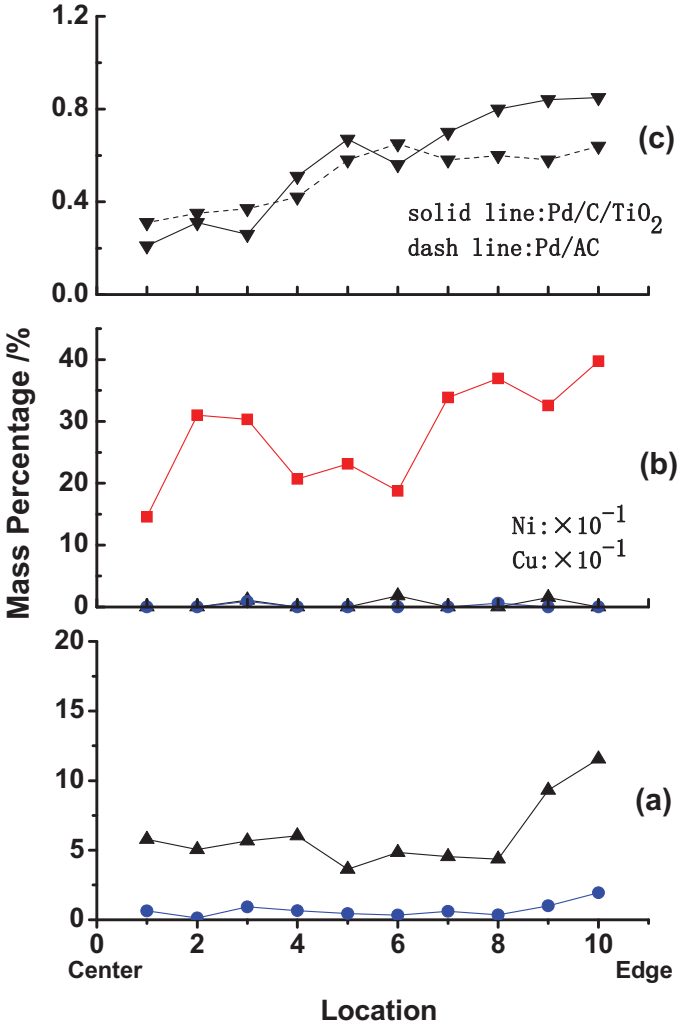

Figure 2.6: The element distributions inner materials: (a) Ni-Cu/TiO_2 (Ni:Cu 8:1); (b) CNF/TiO_2 (II) composite after concentrated HNO_3 treatment; (c) CNF/TiO_2 (II) supported Pd catalyst and Pd/AC catalyst (0.5% Pd loading). ■ Carbon; ▲ Nickel; ● Copper; ▼ Palladium.

Before carbon deposit, the mass percentages of element Ni and Cu in Ni-Cu/TiO_2 were

constant over most part of interior and increased significantly only near the sample edge (Figure 2.6a), indicating that the impregnation time of TiO_2 in $Ni(NO_3)_2$ and $Cu(NO_3)_2$ solution was sufficient to allow metallic salts adequately permeating into the material interior. After methane decomposition, large amount of carbon was found inside CNF/TiO_2, and the mass percentage of carbon coincided with the weight increase of TiO_2 host after carbon deposit (Figure 2.6b).

As the catalyst support, it is necessary for CNF/TiO_2 to remove the metal Ni and Cu particles, which introduced in the process of CNFs growth, to eliminate their effects on the catalytic reactions. Therefore, the samples were treated with concentrated HNO_3 to remove the exposed metal particles. The contents of Ni/Cu in the composite before and after HNO_3 treatment collected with ICP-AES were shown in Table 2.2. It indicated that 99.62% Ni and 99.58% Cu were removed after HNO_3 treatment and the metal residues in the composite became very little, in accordance with the results of Ni/Cu distributions in the interior of the composite (Figure 2.6b). Meanwhile, the structures of CNFs after HNO_3 treatment were partly collapsed but kept integrity relatively (Figure 2.4e).

Table 2.2: The contents of the metal Ni and Cu over CNF/TiO_2

Samples	Ni content (wt %)	Cu content (wt %)	Removal ratio of the metals after HNO_3 treatment (wt %)
CNF/TiO_2 composite (II) [1]	5.83	0.80	Ni: 99.62
CNF/TiO_2 composite (II) [2]	0.022	0.0034	Cu: 99.58

Note: The number 1 and 2 represented CNF/TiO_2 composite (II) before and after HNO_3 treatment, respectively.

(3) Carbon structures of the materials

The structure of carbon in the materials has been analyzed using XRD and TG-DTG. According to the mathematical model proposed by J.Mering & J.Maire [17], graphitization factor (G) is related to the crystal plane spacing distance of graphite (002) (d_{002}) via Equation 2.1:

$$G = (0.344 - d_{002})/(0.344 - 0.3354) \quad 2.1$$

Where 0.344 and 0.3354 nm denote the crystal plane spacing distance of non-graphite and ideal graphite, respectively.

The d_{002} of carbon deposits determined from XRD spectrum was 0.3364 nm with a

graphitization degree of 88%, proving that the dominant ingredient in carbon deposits was graphite.

Thermogravimetric analysis of CNF/TiO_2 and Pd/CNF/TiO_2 had been conducted to further determine the percentage of carbon deposited over the sample as well as its structural properties. The result was shown in Figure 2.7.

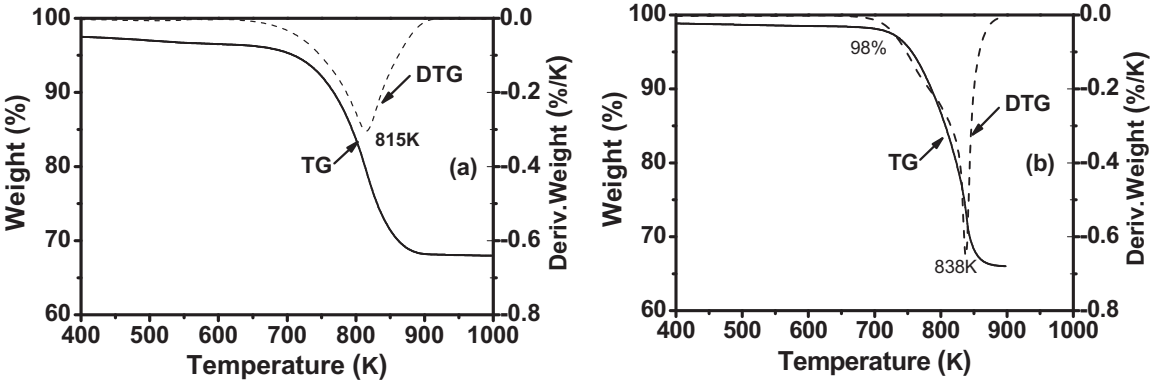

Figure 2.7: TG and DTG curves of CNF/TiO_2 (a) and Pd/CNF/TiO_2 (b) (Solid line corresponds TG curve; Dashed line corresponds to DTG curve).

Through the preparation process and elements analysis mentioned above, it was known that the composite CNF/TiO_2 is mainly composed of carbon and anatase. Specially, carbon can be oxygenated to carbon dioxide when heating in the air, which would cause to the weight loss of the composite. In Figure 2.7a, the total weight loss of the sample in temperature range from 573K to 973K was 35%, as calculated from TG curve, being equal to that of weight increase in CNF/TiO_2 (II) (Table 2.1), which indicated that the carbon deposit over TiO_2 host was about 35%. On the other hand, amorphous carbon and graphite carbon have their own characteristic oxidation temperatures. Generally, a higher oxidation temperature always indicates a purer and less defective material. The oxidation temperature of amorphous carbon is relatively low, i.e., in a range of 573 to 673 K, while is high in graphite carbon, ranging from 673 to 973 K [18]. Therefore, the structure of carbon deposits can be well estimated from the TG-DTG curve. Particularly, it can be inferred from the TG curve that over 90% weight loss occurred between 673K and 973K with the DTG peak at 815 K while only 10% weight loss occurred between 573K and 673K. Therefore, it is reasonable to conclude that about 90% carbon deposits produced via methane decomposition are graphite, which is pretty close to that estimated based on XRD analysis. It should be noted that CNFs have graphite structures [19]. However, the CNF structure in the interior of CNF/TiO_2 was not clearly observed by using SEM (Figure 2.2f) because there existed amorphous carbon, which might

cover CNF structure. Therefore, we supposed that the graphite in the interior of CNF/TiO_2 was actually CNF.

Figure 2.7b described the TD-DTG curve of CNF/TiO_2 (II) supported Pd catalyst. It was found that the structure of the catalyst kept identical to CNF/TiO_2 (II). In Figure 2.7b, over 95% weight loss occurred between 673K and 973K with the DTG peak at 838 K while only 5% weight loss occurred between 573K and 673K. It was inferred that during the preparation of the Pd catalyst, some of the amorphous carbon were removed which increased the content of CNFs to 95% in carbon deposit over the catalyst, compared with the composite CNF/TiO_2 (90%).

In summary, results showed that the carbon deposit in the composite was mainly composed of CNFs and the mesopore structure dominated the pore space of the material, which was highly beneficial to the elimination of internal diffusion limitation in catalytic reactions. Meanwhile, the composite had a solid and stable structure which also made it suitable as the catalyst support.

2.3.3 Evaluation of Pd/CNF/TiO_2 catalytic performance

(1) The properties of Pd particles in Pd/CNF/TiO_2

After the preparation of the catalyst, the actual Pd loading and Pd distribution over Pd/CNF/TiO_2 were determined with ICP-AES and EDS, respectively. The results were compared to those of Pd/AC. In Figure 2.6c, the mass percentage of the element palladium increased with the distance to the center of Pd/CNF/TiO_2, which would facilitate the reaction occurrence mainly on or near the exterior part of the catalyst. The same tendency was found in Pd/AC.

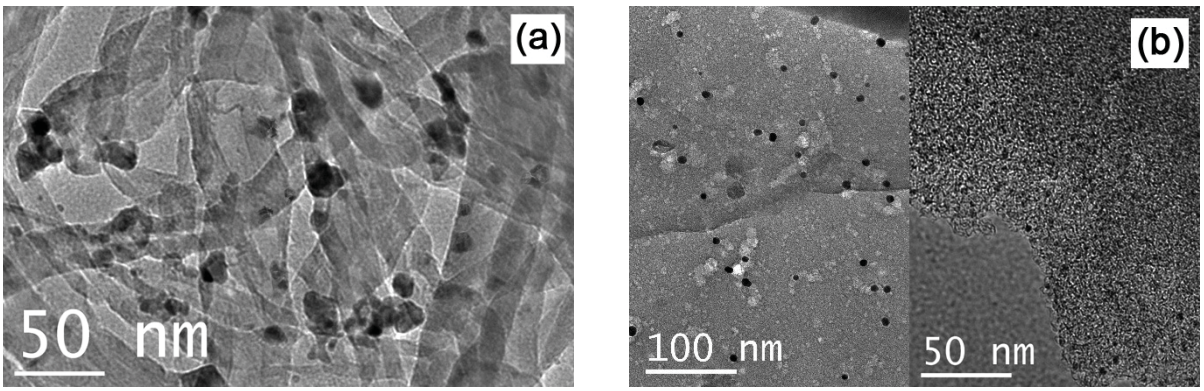

Figure 2.8: TEM images of Pd/CNF/TiO_2 (a) and Pd/AC (b).

Table 2.3: The actual Pd loading and average particle size over the catalysts

Samples	Actual Pd loading (wt %)	Average size of Pd particle (nm)
Pd/CNF/TiO_2 catalyst	0.51	~15
Pd/AC catalyst	0.48	3-8

Figure 2.8 displayed TEM images of the mashed Pd/CNF/TiO_2 and Pd/AC, showing some discrepancies in morphology and Pd particle properties between two catalysts. In Pd/CNF/TiO_2, Pd particles with the average size of 15nm (Table 2.3) were loaded on the fibers. While, obviously, some agglomerate of Pd particles were also occurred on the fibers. In contrast, Pd/AC was found to have the higher Pd dispersion and smaller Pd particle size than the former. Particularly, Pd particles with the average size of 8nm were observed to deposit on the outside surface of the activated carbon substrate (the left half of Figure 2.8b), while only 3-4nm interior the catalyst (the right half of Figure 2.8b). An explanation for the different palladium dispersions on the two catalysts might be their different BET surface area (Table 2.1). The larger surface area enhanced the Pd dispersion and narrowed the Pd particle size distribution in Pd/AC; conversely, the smaller surface area of Pd/CNF/TiO_2 resulted in the formation of poorly dispersed catalyst with large sized Pd particles, which would lead to the lower catalytic activity, compared with that of Pd/AC.

(2) Evaluation of Pd/CNF/TiO_2 catalytic performance

In this study, the selectivities to citronellal and 3,7-dimethyloctanol over Pd/CNF/TiO_2 in citral hydrogenation was evaluated and the results were compared with those of commercial Pd/AC catalyst. Citral was chosen as a model compound for hydrogenation reaction because it is a typical α,β unsaturated aldehydes. And citronellal, an intermediate product of the consecutive reactions of citral hydrogenation, is easy to hydrogenate deeply to citronellol and finally to 3,7-dimethyloctanol (Figure 2.9) due to significant internal diffusion inside micropores of catalysts [19].

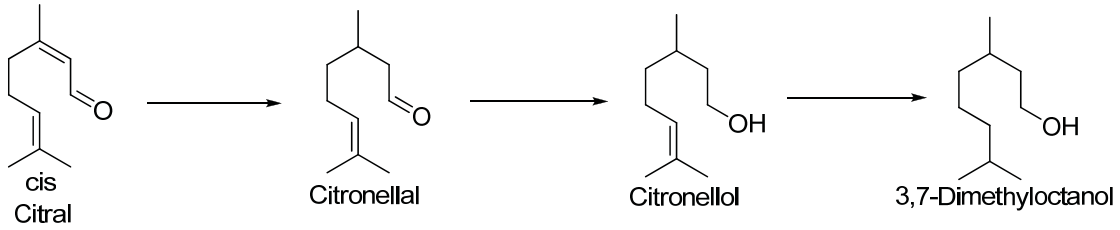

Figure 2.9: Consecutive reaction scheme of citral hydrogenation.

As shown in Figure 2.10, the citral conversion over Pd/CNF/TiO_2 was 90% after 32 h

while less than 2% at the same period over the blank sample, CNF/TiO_2, which confirmed that the effects of Ni and Cu residue in CNF/TiO_2 on the activity of citral hydrogenation was negligible. It could be explained that most of the exposed Ni and Cu were removed by HNO_3 treatment. Meanwhile, it took 4h for Pd/AC catalyst to reach 90% citral conversion, much faster than that of Pd/CNF/TiO_2. The low catalytic activity of Pd/CNF/TiO_2 might be due to relatively lower palladium dispersion of the catalyst, as explained in the first part of this section.

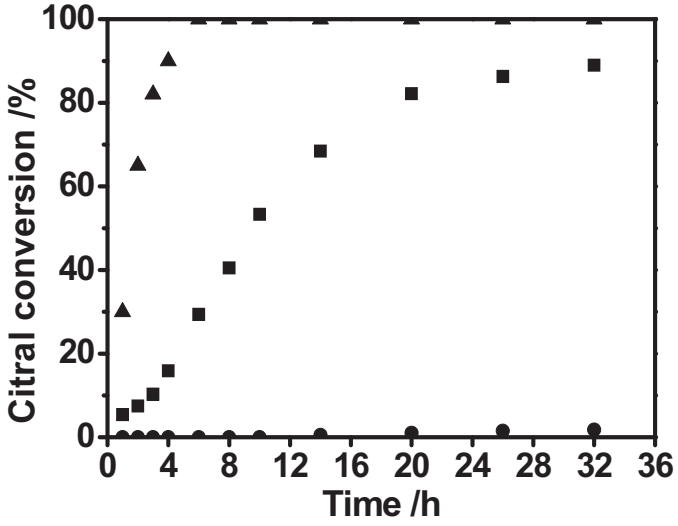

Figure 2.10: Citral conversion versus reaction time in citral hydrogenation at 363 K and 3 MPa over Pd/CNF/TiO_2 (■), Pd/AC (▲) and blank composite CNF/TiO_2 (●)

However, Pd/CNF/TiO_2 displayed higher selectivity to citronellal in citral hydrogenation than that of commercial Pd/AC (Figure 2.11). Particularly, at the citral conversion 90%, the citronellal selectivity of Pd/CNF/TiO_2 can be as high as 90%, being much higher than that of Pd/AC, 35%. However, the selectivity to 3,7-dimethyloctanol, the final product of citral hydrogenation, climbed up to nearly 60% over Pd/AC at the citral conversion 90%, while maintained less than 10% over Pd/CNF/TiO_2 at the same citral conversion. Considered the different support structures of the two catalysts, the distinction in selectivities between Pd/CNF/TiO_2 and Pd/AC is very likely due to their internal diffusion difference inside micropores. Particularly, Pd/CNF/TiO_2 had much fewer micropores (3%) than Pd/AC did (89%), thereafter, the internal diffusion inside micropores in Pd/CNF/TiO_2 was less important than that in Pd/AC. When citral was firstly hydrogenated to citronellal over Pd/CNF/TiO_2, the intermediate product citronellal was easily desorbed from Pd crystal to the solution. While over Pd/AC, citronellal can be confined inside the micropores long enough to be completely

converted to the final product 3,7-dimethyloctanol due to its slow internal diffusion rate. It explains why the selectivity to the intermediate citronellal over Pd/AC decreased faster than that over Pd/CNF/TiO_2 as the citral conversion increased. Therefore, Pd/CNF/TiO_2 may exhibit a higher selectivity to the intermediate product citronellal than Pd/AC did.

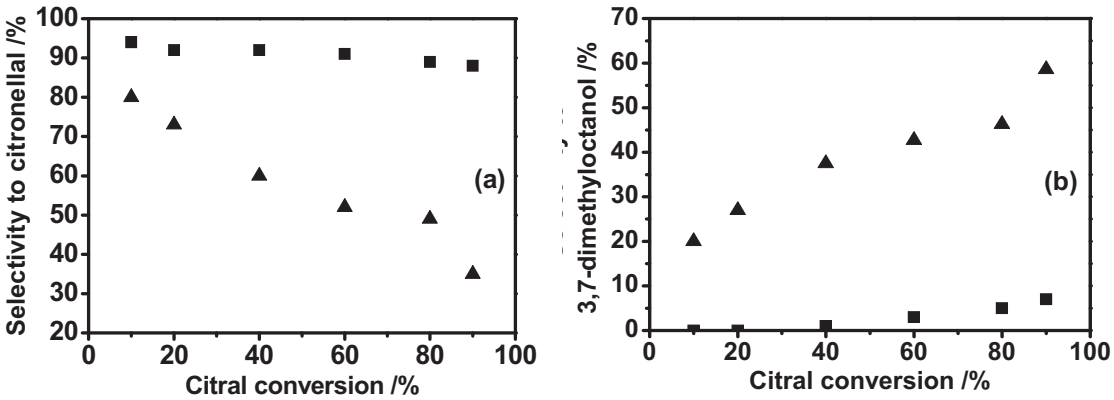

Figure 2.11: Selectivities to citronellal (a) and 3,7-dimethyloctanol (b) versus citral conversion in citral hydrogenation at 363 K and 3 MPa over commercial Pd/AC (▲) and Pd/CNF/TiO_2 (■).

2.4 Conclusions

A promising carbon-titania composite material CNF/TiO_2 that can be utilized as a structured catalyst support has been synthesized and characterized. It was prepared through methane decomposition over the TiO_2 extrudates. The suitable mole ratio of Ni to Cu in Ni-Cu/TiO_2 employed in carbon deposit was found to be 8:1. Results showed that the synthesized CNF/TiO_2 had the good textural and structural properties: the BET surface area was 60 m^2/g and the mesopore structure dominated the pore space of the material, which is beneficial for eliminating mass transfer limitations. Meanwhile, the dominant ingredient of carbon deposit over the composite was CNFs. Pd catalyst supported over CNF/TiO_2 exhibited a higher selectivity to the intermediate product citronellal (90%) than commercial Pd/AC (35%) at citral conversion of 90% in citral hydrogenation, which was attributed to the elimination of the internal diffusion limitation due to its mesoporous structures. The results indicate that as-prepared CNF/TiO_2 is an effective catalyst support with good textural stability and high chemical durability in potential applications for three phase catalytic reactors, i.e., citronellal production through citral hydrogenation in this thesis.

References

[1] I. M. J. Vilella, S. R. de Miguel, C. Salinas-Martínez de Lecea, Á. Linares-Solano, O. A.

Scelza, Appl. Catal. A: Gen. 281 (2005) 247-258.

[2] J. Álvarez-Rodríguez, M. Cerro-Alarcón, A. Guerrero-Ruiz, I. Rodríguez-Ramos, A. Arcoya, Appl. Catal. A: Gen. 348 (2008) 241-250.

[3] K. P. De Jong, J. W. Geus, Catal. Rev. Sci. Eng. 42 (2000) 481-510.

[4] W. Z. Li, C. H. Liang, J. S. Qiu, W. J. Zhou, H. M. Han, Z. B. Wei, G. Q. Sun, Q. Xin, Carbon 40 (2002) 791-794.

[5] N. M. Rodriguez, J. Mater. Res. 8 (1993) 29-33.

[6] R. Vieira, M. J. Ledoux, C. Pham-Huu, Appl. Catal. A: Gen. 274 (2004) 1-8.

[7] P. L. Liu, L. Lefferts, Chem. Res. Appl. 18 (2006) 1077-1083.

[8] W. L. Mi, Y. S. Lin, B. Q. Zhang, Y. D. Li, Mod. Chem. Ind. 25 (2005) 37-39.

[9] P. L. Liu, L. Lefferts, Chin. J. Chem. Eng. 14 (2006) 294-300.

[10] Y. Yamada, Y. Hosono, N. Murakoshi, N. Higashi, H. Ichi-oka, T. Miyake, N. Ikenaga, T. Suzuki, Diam. Relat. Mater. 15 (2006) 1080-1084.

[11] J. P. R. Vissers, F. P. M. Mercx, S. M. A. M. Bouwens, V. H. J. de Beer, R. Prins, J. Catal. 114 (1988) 291-302.

[12] H. S. Yang, Z. D. Xu, X. N. Lu, G. T. Wu, M. Wang, W. Z. Li, Chin. J. Chem. Phys. 13 (2000) 324-328.

[13] P. Tribolet, L. Kiwi-Minsker. Catal. Today 105 (2005) 337-343.

[14] P. Li, T. Li, J. H. Zhou, Z. J. Sui, Y. C. Dai, W. K. Yuan, D. Chen. Micropor. Mesopor. Mater. 95 (2006) 1-7.

[15] B. H. Chen, Z. G. Lei, F. Kapteijn, E. Tronconi, G. Groppi, Catal. Today 216 (2013) 1.

[16] Z. Zhang, T. Tang, G. D. Lu, Chem. Res. Appl. 19 (2007) 1.

[17] C. J. Li, B. X. Ma, X. X. Huo, New Carbon Mater. 14 (1999) 19.

[18] T. Tsoufis, P. Xidas, L. Jankovic, D. Gournis, A. Saranti, T. Bakas, M. A. Karakassides, Diam. Relat. Mater. 16 (2007) 155-160.

[19] U. K. Singh, M. A. Vannice, J. Catal. 199 (2001) 73-84.

Chapter 3

Influence of Structural Properties on Catalytic Performance in Citral Selective Hydrogenation over Macro-structured Carbon-Titania Supported Pd Catalyst

Abstract

Macro-structured CNF/TiO_2 prepared in chapter 2 was employed to support palladium catalyst (Pd/CNF/TiO_2). The effects of structural properties on catalytic performance in citral hydrogenation were estimated in calculation and compared with a commercial activated carbon supported palladium catalyst (Pd/AC). The results showed that although the reaction rate was comparatively low over Pd/CNF/TiO_2, which spent approximately 24 hours to reach 90% citral conversion, fourfold time of Pd/AC, the selectivity to citronellal in citral hydrogenation kept high (approximately 85%) at the same citral conversion, while decreasing to 40% over Pd/AC. The comparatively lower reaction rate over Pd/CNF/TiO_2 was attributed to the less surface Pd sites (3.94 μmol/g cat) than that on Pd/AC (12.2 μmol/g cat). Further calculation discovered the similar initial turnover frequency values over two catalysts (approximately 0.1 s^{-1}), which implied that citral hydrogenation is structure-insensitive over Pd catalysts and crystallite size effects have a little influence on the differences in the kinetics between two catalysts. The high selectivity to citronellal over Pd/CNF/TiO_2 was due to the negligible internal diffusion limitation inside the catalyst, which was proved by the calculating Weisz-Prater numbers (less than 0.3 of each reactant). In contrast, the pore structures, mainly composed of micro pores, caused the serious internal diffusion limitation over Pd/AC, which finally led to the increase on the selectivity to the deep hydrogenated product, 3,7-dimethyloctanol.

This part of work has been published as Research Article: J. Zhu, M. Lu, M. Li, J. Zhu, *Catal. Sci. Technol.* 3 (2013) 737-744.

3.1 Introduction

Selective hydrogenation is one of the key processes in fine chemical industries. The properties of hydrogenation products can be significantly affected by the activity and structure of the employed catalyst. In heterogeneous catalysis, how to eliminate the mass transfer limitations inside the catalyst particles, thereafter gathering the intermediate products with high selectivity increasingly attract the researchers' attentions. For example, citral, a typical α,β-unsaturated aldehydes, was usually selected as a model molecule in that there are three sites of hydrogenation: a conjugate double bond (C=C), a carbonyl group (C=O) and an isolated double bond (C=C). The selective hydrogenation of citral is a rather complex reaction network involving 6-8 important intermediates and a number of series-parallel reactions. Since palladium catalyst is very active in the hydrogenation of the C=C bond [1], citral in the reaction is easily hydrogenated to citronellal on it, followed by the deep hydrogenation to citronellol and finally to 3,7-dimethyloctan-1-ol (Figure 3.1) due to slow internal diffusion inside micropores of the catalysts [2]. Several systematic studies on citral selective hydrogenation have been reported. These studies covered some important aspects such as active metals [3-6] and catalyst supports [7-9]. Specifically, Yilmaz et al. [7] reported the highest selectivity (90%) to citronellal, at complete conversion of citral over Pd/natural zeolite with the particle sizes between 100 and 400 mesh, which was explained by the active metal properties and the absence of significant internal diffusion limitations.

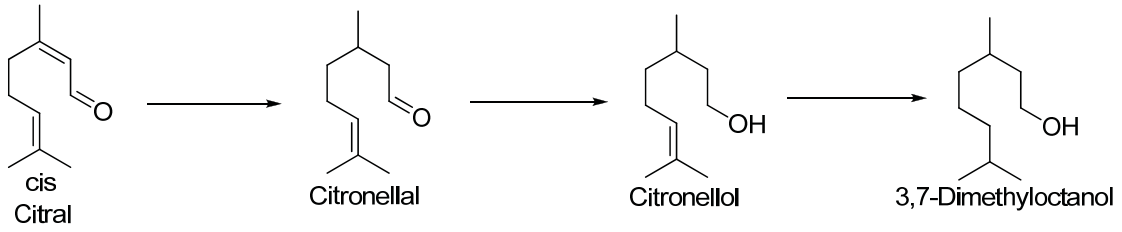

Figure 3.1: Consecutive reaction scheme of citral hydrogenation.

Although the effects of internal diffusion limitations can be reduced in microscopic powdered catalyst particles, the powdered catalysts have to be separated from the products at the end of reaction via a costly filtration step, which can lead to the loss of catalysts and cause seriously environmental problems [10]. These disadvantages restrict the industrial applications of the powdered catalysts.

Currently, some studies on evaluating mass transfer effects in catalytic reactions,

especially internal diffusion over structured catalysts, have increasingly become the focus of researchers' attention. As the process is scaled up, the conditions are shifted from kinetic control to diffusion control. Therefore, increasing the catalyst particle size would affect the activity and selectivity. Zhu et al. [11] studied the internal diffusion process in irregular A301 catalyst particles in ammonia synthesis and calculated the internal diffusion effectiveness factors based on multi-component diffusion reaction model. The calculation result was verified to coincide with the experiment test. J. Aumo et al. [12] studied kinetics and mass transfer effects for the complex three-phase hydrogenation in large Ni/alumina catalyst pellets. The model described well the behavior of the system, and it can be used for studies on reaction intensification. Zhang et al. [13] and Chen et al. [14] investigated the effects of the internal diffusions on the hydrogenation of 4-carboxybenzaldehyde (4-CBA) over Pd/activated carbon catalyst and F-T synthesis over Co/ZrO_2 catalyst, respectively. The results indicated that the size of the catalyst had the significant effects on the performances of two catalytic reactions, and some methods could be utilized to reduce the effects of internal diffusion, such as expanding the pore diameters of the supports, increasing active compositions deposited on the outside surface of the catalysts and reducing the sizes of catalyst particles to the suitable ones as well.

To evaluate the presence or absence of pore diffusion limitations inside the catalysts, Weisz-Prater criterion [15] is usually introduced in calculation. M.A. Vannice et al. [16] studied the effect of the solvent on the liquid-phase hydrogenation of citral over a Pt/SiO_2 catalyst. And numerous tests using the Weisz-Prater criterion verified that all data for each solvent were obtained in the regime of kinetic control. M.J.H. Simmons et al. [17] also studied enantioselective hydrogenation of dimethyl itaconate with immobilised rhodium-duphos complex in a recirculating fixed-bed reactor. By calculating the value of the Thiele Modulus, the employing catalyst was proved not to be subject to internal diffusion limitation.

In this chapter, one macro-structured carbon nanofiber support, CNF/TiO_2, which was synthesized in chapter 2, was employed to prepare palladium catalyst ($Pd/CNF/TiO_2$) and its catalytic performance was evaluated in selective hydrogenation of citral. The effect of the structural properties of $Pd/CNF/TiO_2$ on catalytic hydrogenation was evaluated by theoretical calculation and further proved in the experiments. The result was compared with that of a commercial catalyst, i.e., structured activated carbon supported palladium (Pd/AC) to investigate the potential of $Pd/CNF/TiO_2$ for commercial applications.

3.2 Experimental

3.2.1 Synthesis and characterizations of Pd/CNF/TiO_2

The composite CNF/TiO_2 prepared in chapter 2 was employed to support Pd catalyst, i.e. Pd/CNF/TiO_2. Specifically, CNF/TiO_2 was immersed with an hydrochloric acid (HCl) solution (0.2 M) of palladium (II) chloride ($PdCl_2$) (0.5 wt% Pd loading) (Sinopharm, China) and stirred continuously for 6 h. The resulting sample was dried overnight at 393 K and stored in a desiccator. After reducing at 493 K in a stream of N_2/H_2 (80:20) for 2 h, the catalyst Pd/CNF/TiO_2 was finally prepared.

The as-prepared Pd/CNF/TiO_2 was characterized to test the textural and structural properties. BET surface area and the average pore diameter of the catalyst were calculated from the nitrogen adsorption isotherm obtained at 77K using an ASAP 2010 sorptometer (Micromeritics). The palladium contents over the catalysts were determined by Vista-AX inductively coupled plasma atomic emission spectrometry (ICP-AES). Scanning electron images and elements distributions were recorded using a JEOL JSM-6360 LA scanning electron microscope & energy-dispersive X-ray spectroscopy (SEM/EDX). The morphologies and the properties of the palladium particles on catalysts were obtained with JEM-2100 transmission electron microscopy (TEM). A commercial formed activated carbon supported palladium catalyst (Pd loading 0.5 wt.%, irregular particles, $\phi \approx 4$ mm, 810 m^2/g, Sinopec Yangzi, China), named Pd/AC, was tested at the same conditions for comparison.

3.2.2 Estimation of catalytic properties on Pd/CNF/TiO_2

The catalytic performance on Pd/CNF/TiO_2 was evaluated in selective hydrogenation of citral, and the result was compared to that of the commercial Pd/AC. The experiments for revealing the intrinsic hydrogenation kinetics were carried out in a 100 ml pressurized autoclave. By dispersing approximately 1.0 g of the catalysts (2 wt.%) into a total mass of 50 g of isopropanol (A.R, Sinopharm, China) solution of citral (5 wt.%, A.R, Sinopharm, China), the autoclave was sufficiently flushed with nitrogen flow and the following hydrogen to remove dissolved oxygen. The reaction was commenced by switching on the stirring to 1000 rpm, which was verified to be sufficient to exclude external diffusion. The reaction were conducted at 353 K and 3 MPa total pressure, which was maintained by continuously injecting hydrogen into the reactor. Small amounts of reaction samples were withdrawn from the reactor at different reaction times and analyzed by gas chromatography (VARIAN CP3800) equipped with a FID detector and capillary column HP-5 using nitrogen as carrier gas. Initial

reaction conditions for citral hydrogenation were listed in Table 3.1.

Table 3.1: Initial reaction conditions for citral hydrogenation

Reaction condition	value
Reaction temperature, T (K)	353
Pressure, P (MPa)	3.0
Agitation, A (rpm)	1000
Mass of isopropanol, m_{IPA} (g)	47.5
Mass of citral, m_{citral} (g)	2.5
H_2 solubility, C_{H2} (mol/cm^3)	1.47×10^{-4} [a]
Mass of the catalyst, m_{cat} (g)	1.0

Note: (a) Based on the literature of Francesconi et. al. [18].

3.3 Results and discussion

3.3.1 Structural properties of Pd/CNF/TiO_2

As described in the section of "*Experimental*", the preparation of Pd/CNF/TiO_2 in this study employed CNF/TiO_2 composite as the catalyst support, which was synthesized by depositing carbon over the formed TiO_2. The structural properties of Pd/CNF/TiO_2 were characterized and the results were compared with those of commercial formed Pd/AC, as shown in Figure 3.2-3.5.

Based on Figure 3.2a, Pd/CNF/TiO_2 particle has the profile of cylinder shape with the average length of approximately 3.0 mm and diameter of 1.0 mm. The surface of the catalyst covered a significant amount of CNFs with diameters of 50-80 nm (Figure 3.2b). They intertwined each other to form pore structures. The thickness of the deposition layer can be identified from a SEM image of the catalyst section in Figure 3.2c, i.e., 1.5-2.0 μm. In comparison, the commercial Pd/AC particle has the profile of irregular shape with the average size of 3.0 mm (Figure 3.3a), whose surface is smoother than that of Pd/CNF/TiO_2 particle (Figure 3.3b). It is noted that, on surface of Pd/AC, some small substrates conglutinate (Figure 3.3b), which might be some fragments produced in the process of Pd/AC preparation.

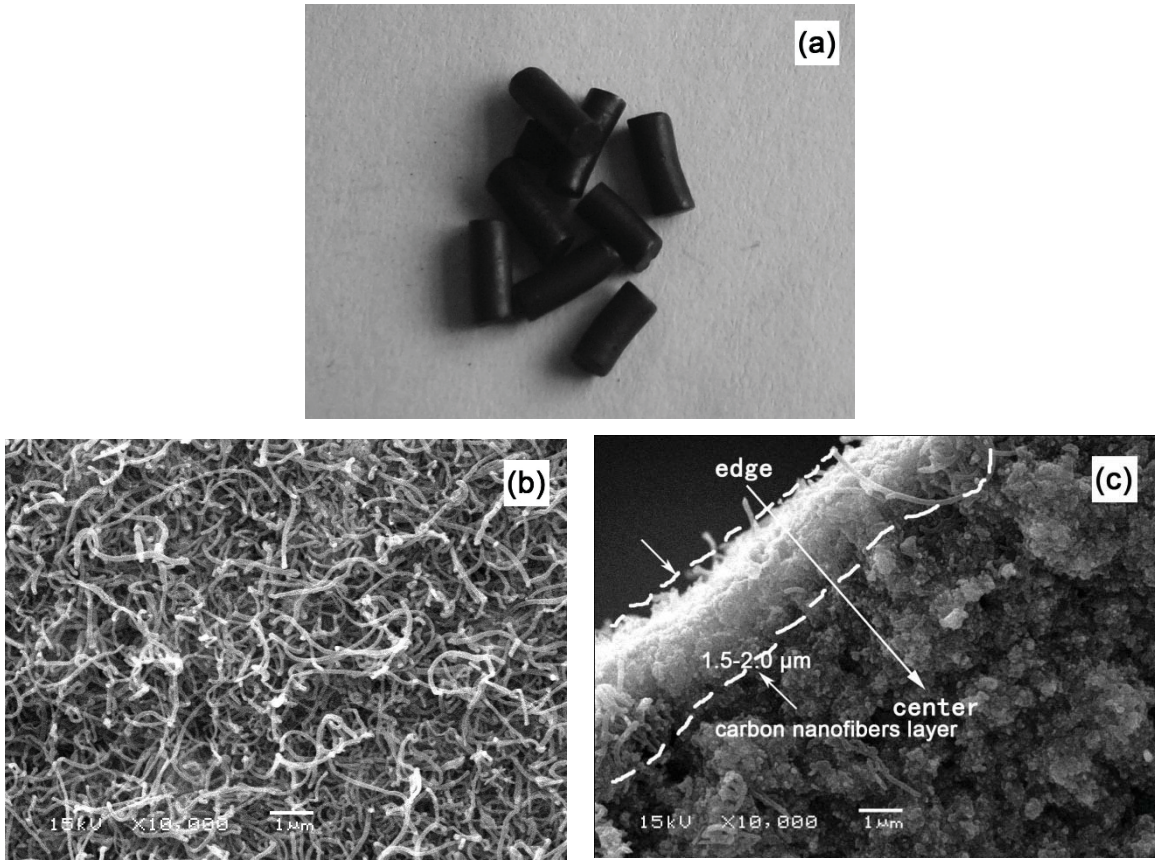

Figure 3.2: The profile and morphology of Pd/CNF/TiO_2 catalyst: (a) the profile of Pd/CNF/TiO_2; (b) SEM image of the surface on Pd/CNF/TiO_2; (c) SEM image of the cross section of Pd/CNF/TiO_2.

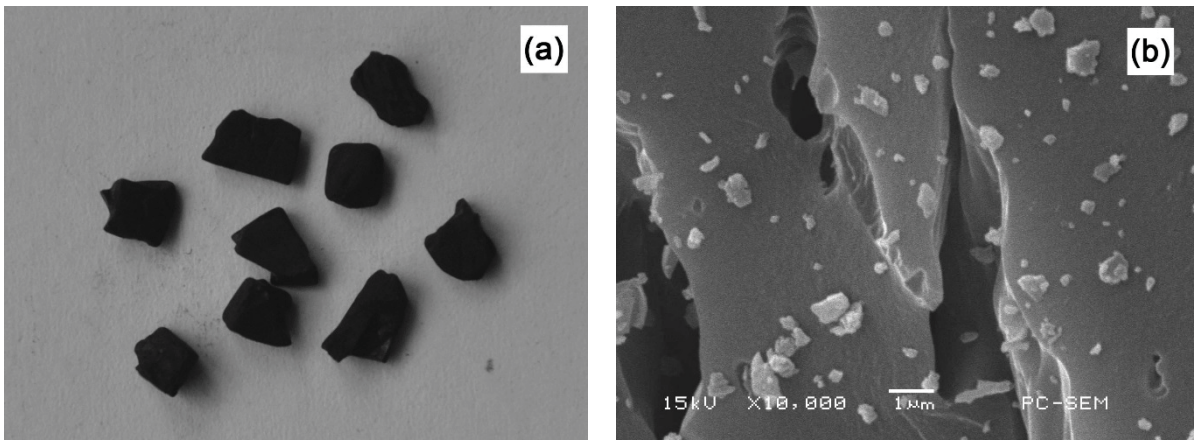

Figure 3.3: The profile and morphology of the commercial Pd/AC catalyst: (a) the profile of Pd/AC; (b) the SEM image of the surface on Pd/AC.

In order to analyze the palladium distribution in the catalyst, 10 positions with the same spacing distance were assigned from the center to the edge of the catalyst section. Elemental distribution on each position was measured by EDX, as indicated in section 2.3.2(2). The

mass percentage of palladium was tested in each position and results revealed some information of two catalysts (Figure 3.4). The mass percentage of the element palladium in Pd/CNF/TiO_2 increased with the distance to the center of the catalyst. More active sites of palladium in the exterior part of the catalyst than interior would facilitate the catalytic reaction occurrence mainly on or near the exterior part of the catalyst. The same tendency of Pd distribution was found in Pd/AC.

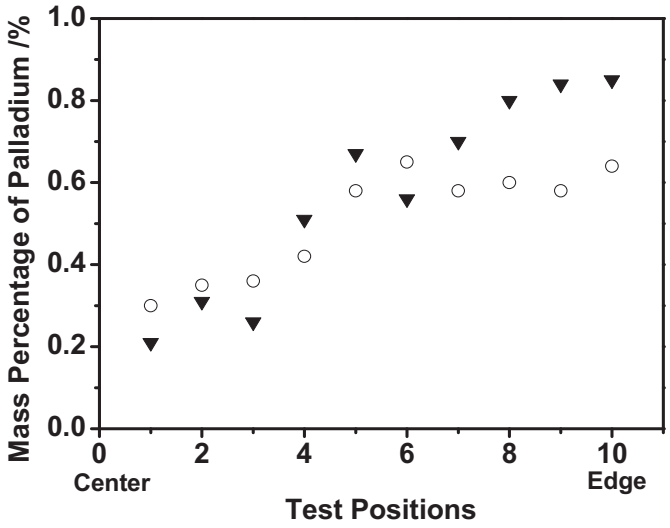

Figure 3.4: The palladium distributions in the cross sections of Pd/CNF/TiO_2 (▼) and Pd/AC (○).

The sizes and dispersions of palladium particles on catalysts could also be obtained in TEM images (Figure 3.5). Palladium particles in Pd/AC possess the small size (average size 4.7 nm), compared with that of Pd/CNF/TiO_2 (average size 14.5 nm). Based on the hemispherical model of metal particles on surface of the catalyst, palladium dispersions on Pd/AC and Pd/CNF/TiO_2 were calculated to be 25.88% and 8.39%, respectively. The high palladium dispersion on Pd/AC was attributed to its large BET surface area (810 m^2/g), while only 58 m^2/g of Pd/CNF/TiO_2 (Table 3.2).

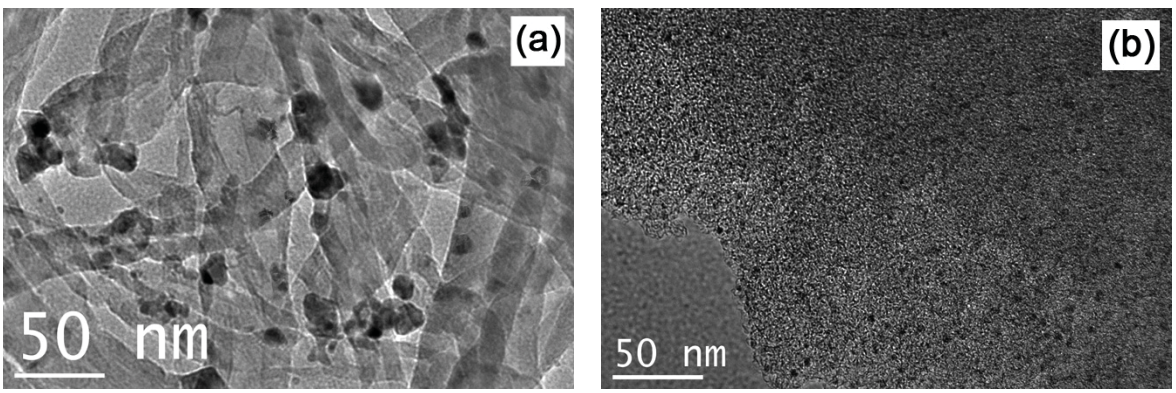

Figure 3.5: TEM images of Pd/CNF/TiO_2 (a) and Pd/AC (b)

Table 3.2: Properties of Pd/CNF/TiO_2 and commercial Pd/AC

	Catalyst	0.5% Pd/CNF/TiO_2	0.5 % Pd/AC
Bulk properties	Bulk density of the catalyst, ρ (g/cm^3)	1.28	0.48
	Average radius of catalyst particle, R_p (cm)	0.05 [a]	0.15 [a]
Textural properties	BET surface area, S_{total} (m^2/g)	58	810
	Micro-pore area, S_{micro} (m^2/g)	2	720
	Average pore radius, r_p (nm)	5.86	1.60
Palladium properties	Actual Pd loading (%)	0.51	0.48
	Average Pd particle size (nm)	10.8	4.7
	Pd dispersion (%)	8.39 [b]	25.88 [b]

Note: (a) The max length of the particle's cross section as the average size;

(b) Based on the hemispherical model of metal particles on surface of the catalyst.

3.3.2 Catalytic properties on Pd/CNF/TiO_2

The catalytic properties in citral hydrogenation over Pd/CNF/TiO_2 was evaluated and compared to that of commercial Pd/AC catalyst. Citral conversions and product distributions in citral hydrogenation over two catalysts were shown in Figure 3.6 and 3.7.

Under the same reaction conditions, including the mass of the catalyst, Pd loading and the initial citral concentration, the reaction rate of citral hydrogenation on Pd/AC was much faster than that on Pd/CNF/TiO_2. For example, the citral conversion over Pd/AC was 90% after 6 h, while it took nearly 24 h for Pd/CNF/TiO_2, fourfold time of the former catalyst, to reach the same conversion (Figure 3.6). However, Pd/CNF/TiO_2 possessed the higher selectivity to the intermediate, citronellal, in the reaction, than that over Pd/AC. Particularly, at the citral conversion of about 90%, the selectivity to citronellal over Pd/CNF/TiO_2 can be as high as 85% (Figure 3.7a), being much higher than that over Pd/AC, 40% (Figure 3.7b); while the selectivity to 3,7-dimethyloctanol, the final product in citral hydrogenation, climbed up to approximately 55% at the same citral conversion over Pd/AC catalyst (Figure 3.7b).

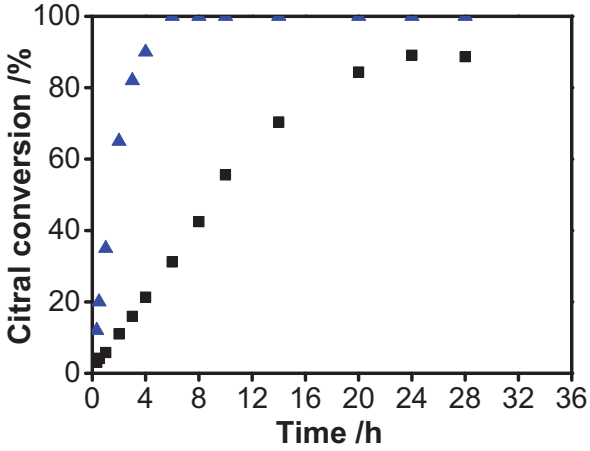

Figure 3.6: Citral conversion versus reaction time in citral hydrogenation over Pd/CNF/TiO_2 (■) and commercial Pd/AC (▲).

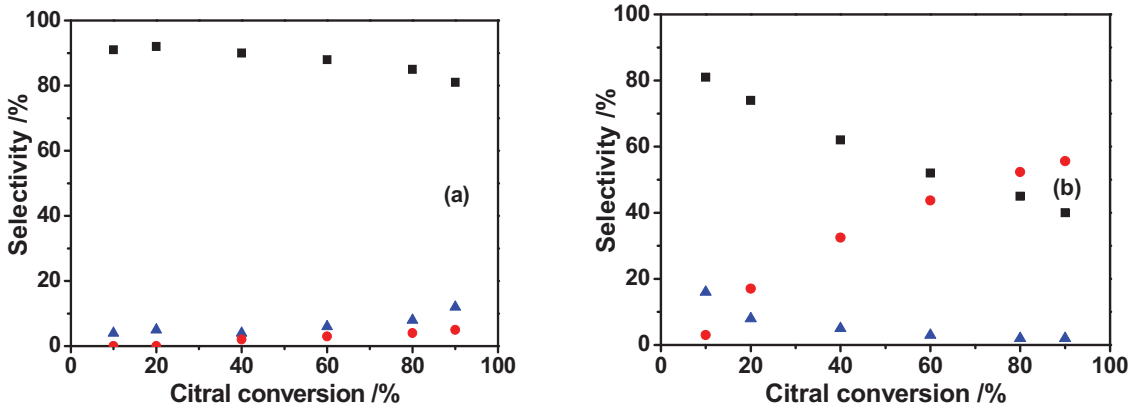

Figure 3.7: The product distribution versus citral conversion in citral hydrogenation over Pd/CNF/TiO_2 (a) and commercial Pd/AC (b): ■ Citronellal; ▲Citronellol; ● 3,7-dimethyloctanol;

The glaring discrepancy on catalytic properties between Pd/AC and Pd/CNF/TiO_2 could probably be attributed to some factors, including the number of surface Pd sites and mass transfer limitations [17, 19, 20]. Based on Pd loadings and dispersions (Table 3.2), the molar number of surface Pd sites was calculated to be 12.2 μmol/g cat on Pd/AC and 3.94 μmol/g cat on Pd/CNF/TiO_2. High dispersion of Pd on Pd/AC (25.88%) due to its large BET surface area (810 m^2/g), led to more surface Pd sites on Pd/AC. This was the main reason to obtain the comparatively higher reaction rate over Pd/AC than that over Pd/CNF/TiO_2.

Initial reaction rate in turnover frequency (TOF) was calculated using Equation 3.1 at citral conversion of approximately 10% because this initial reaction stage would make sure that the hydrogenation rate could not be affected by the changes of citral concentration.

$$TOF = \left(\frac{m_{citral} \times con.\%}{M_{citral} \times t} \right) \times \left(N_{Pd} \right)^{-1} \quad 3.1$$

Where mcitral and Mcitral are the mass of citral and its molecular weight (Table 1), respectively; con.% and t are the initial citral conversion and the reaction time (Figure 3.6), respectively; And NPd is the molar number of surface Pd sites.

Figure 3.6 showed that it took 20 min and 90 min to reach 10% citral conversions in Pd/AC and Pd/CNF/TiO_2 catalytic system, respectively. Therefore, the initial TOF was calculated to be 0.11 s^{-1} for Pd/AC and 0.082 s^{-1} for Pd/CNF/TiO_2. The similar initial TOFs in 0.5 wt% Pd/AC and 0.5 wt% Pd/CNF/TiO_2 catalytic systems implied that citral hydrogenation over Pd catalysts is probably structure-insensitive and crystallite size effects are not expected to have a significant influence on the differences in the kinetics between two catalysts. The result was in accordance with the study of M.A. Vannice et al. [19]. Therefore, the reaction rate and product distribution for citral hydrogenation in this study were presumed to be unaffected by crystallite size effects over Pd/AC and Pd/CNF/TiO_2 catalysts.

Finally, we would focus on discussing the effect of internal diffusion limitation for citral selective hydrogenation over two catalysts.

3.3.3 Modeling the internal diffusion limitation in the catalyst (Weisz-Prater Criterion)

In a first order reaction, the effect of internal diffusion behavior of the reactants could be estimated using Weisz-Prater criterion (W-P criterion, N_{WP}), expressed in Equation 3.2. Weisz-Prater number (N_{WP}) is particularly useful because it provides a dimensionless number containing only observable parameters that can be readily measured or calculated, which was discussed in chapter 1.

$$N_{W-P} = \frac{\Re \cdot R_P^2}{C_S \cdot D_{eff}} \quad 3.2$$

Where $\Re$ is the initial reaction rate; R_P is the catalyst particle radius, Cs is the substrate concentration on catalyst surface; D_{eff} is the effective diffusivity of the substrate in the pores of the catalyst.

W-P criterion asserted that if $N_{W-P}<0.3$, rates for all reactions with an order of 2 or less should have negligible mass transfer limitations, while a value for $N_{W-P}>6$ indicates the definite diffusion control. If the W-P criterion gives a non-definitive value in the borderline region (between 0.3 and 6), additional calculations can be performed using reactant concentrations and rates taken at different reaction times [16]. In order to use the W-P

criterion successfully, it is important to accurately determine the effective diffusivity of the reactant (D_{eff}) and the initial reaction rate ($\Re$) in a given catalyst system.

Prior to calculation, we made two valid assumptions on citral hydrogenation to simplify the computation process:

I. The intermediate products have the same physical properties as citral. The composition of the solution in the pores will change as the citral reacts, but the intermediate products in this reaction are similar to citral in molecular size and configuration, so it is assumed that they have the similar physical properties.

II. The physical properties of the liquid phase are essentially unchanged during the reaction. The initial concentration of citral in the reaction is calculated to be 2.0 mole percent, i.e., the dilute solution, and the products will exist in even smaller concentrations. Therefore, the physical properties of the liquid phase are assumed to be unchanged during the reaction, which would maintain the effective diffusivity to be constant.

Seeing that two assumptions mentioned above are reasonable in the practical reactions, the W-P criterion calculated using the initial reaction conditions is a satisfactory model to estimate the effect of internal diffusion behavior on citral hydrogenation.

Determining Weisz–Prater criterion to evaluate internal diffusion behavior, is generally complicated for complex reactant (or solvent) molecules, because their experimentally measured bulk diffusivities (D_b) have rarely been reported. In a liquid-phase system, these parameters are needed to estimate effective diffusivities (D_{eff}), within the pore structure of the catalyst. The calculation of D_b need to determine the physical properties of the reactants as well as the solvent, including critical volume (V_c), pressure (P), density (ρ), viscosity (η) and vaporization enthalpy (L^{vap}). Once D_b is known, D_{eff} can be estimated. When combining D_{eff} with k, and R_P, Thiele modulus and Weisz-Prater number allowed to be finally calculated based on Equation 3.4 and 3.5.

Table 3.2 listed some properties of Pd/CNF/TiO_2 and commercial Pd/AC, which were measured by catalyst characterization including density test, nitrogen adsorption and TEM. Table 3.3 gave some physiochemical parameters of the reactants and solvent in the reaction system, which might be used in calculation of bulk diffusivities. They were determined with the methods derived from some handbooks [21-23].

Table 3.3: Physical properties of the reactants and solvent in the reaction system

Reactants and solvent	r（nm）	M (g·mol^{-1})	ρ (g/cm^3)	V_b [(a)] (m^3·kmol^{-1})	χ	L^{vap} (J·kmol^{-1}×10^7)	η (Pa·s×10^{-4})
H_2	0.12	2		0.0286			
Citral	0.39	152	0.780	0.171	1 [(b)]	4.55	5.01 [(c)]
Isopropanol	0.25	60	0.784	0.081	1 [(b)]	3.99	5.20

Note: (a) Tyn-Calus Method, V_b=0.285·$V_c^{1.048}$ (V_c: critical volume)

(b) The solvent association parameter is taken as 1, since the citral and isopropanol are both non-polar.

(c) Empirical expression of the viscosity of citral: lgη=509.12· (T^{-1}-3.42×10^{-3})-3.0 (T: reaction temperature, K)

3.3.4 Estimation of the effective diffusivity (D_{eff}) of reactants in Pd/CNF/TiO_2

In citral hydrogenation, there were two diffusing reactants, i.e., citral and hydrogen. They have different diffusivities in the reaction system due to their different physical and chemical properties. So, it is necessary to calculate the effective diffusivities of each in the liquid-filled pores. Based on assumption I mentioned in the section 3.3.3, the intermediates in the pores have the same diffusivities as citral. So, the estimation of intrapaticle diffusion in citral hydrogenation needs to consider the diffusion behaviors of merely two reactants.

(1) Diffusivity of H_2 in citral / isopropanol binary liquid phase system ($D_{H_2,mixt}$)

Citral hydrogenation in this work involved binary liquid phase, i.e., the reactant citral and the solvent isopropanol, which made the reaction a multi-component diffusion system. The diffusivity of H_2 in citral / isopropanol ($D_{H_2,mixt}$) can be estimated using Equation 3.3 [24]:

$$D_{H_2,mixt}=\frac{\left(D_{H_2,citral}\cdot\eta_{citral}^{0.5}\right)^{x_{citral}}\left(D_{H_2,IPA}\cdot\eta_{IPA}^{0.5}\right)^{x_{IPA}}}{\eta_{mixt}^{0.5}} \qquad 3.3$$

where $D_{H_2,citral}$ or $D_{H_2,IPA}$ represents the diffusivity of hydrogen in citral or isopropanol, respectively; η_{citral} and η_{IPA} represent the viscosities of two liquids, respectively.

The viscosity of the mixture (η_{mixt}) required in equation 3.3 might be computed from the relationship in Equation 3.4 [20]:

$$\eta_{mixt}=\eta_{citral}^{x_{citral}}\cdot\eta_{IPA}^{x_{IPA}} \qquad 3.4$$

where x_{citral} or x_{IPA} is the mole fraction of citral or isopropanol in their mixture.

According to equation 3.4, $D_{H_2,mixt}$ is determined by the diffusivity of H_2 in each liquid of citral and isopropanol, as well as the viscosity of each liquid.

Based on the method of Wilke and Chang [25], diffusivity of a dilute gas solute in a liquid solvent ($D_{1,2}$) could be expressed in Equation 3.5:

$$D_{1,2} = 1.1728 \times 10^{-16} \frac{T\sqrt{\chi \cdot M_2}}{\eta_2 \cdot V_1^{0.6}} \qquad 3.5$$

where T is the reaction temperature; χ is the solvent association parameter; M_2 is the molecular weight of solvent; η_2 is the viscosity of the solvent under the reaction temperature; and V_1 is the molar volume of the gas solute at normal boiling point.

In this section, H_2 was considered as the diffusing reactant, and the diffusivity of H_2 in citral or isopropanol can be estimated using Equation 3.5. The physical properties of citral and isopropanol (IPA) are listed in Table 3.2. So, the diffusivities of H_2 in citral and isopropanol were calculated to be 8.6×10^{-5} cm^2/s and 2×10^{-5} cm^2/s, respectively.

After the calculation of $D_{H_2,citral}$ and $D_{H_2,IPA}$, the values were introduced in Equation 3.3. Thus, we solved the diffusivity of H_2 in citral / isopropanol binary liquid phase system, i.e., $D_{H_2,mixt}$=6.34×10^{-5} cm^2/s.

(2) Diffusivity of citral in citral / isopropanol binary liquid phase system ($D_{citral,mixt}$)

In this section, citral is considered to be the diffusing component. As the low mole fraction of citral in isopropanol (x_{citral}= 2 mol %), Equation 3.6, which is applicable to a dilute solute (< 10 mol %) in a non-water solvent [26], could be used to estimate the diffusivity of citral in binary liquid phase system ($D_{citral,mixt}$).

$$D_{citral,mixt} \approx D_{citral,IPA} = 4.4\times10^{-15} \frac{T}{\eta_{IPA}} \left(\frac{V_{IPA}}{V_{citral}}\right)^{1/6} \left(\frac{L_{IPA}^{vap}}{L_{citral}^{vap}}\right)^{1/2} \qquad 3.6$$

where T is the reaction temperature; η_{IPA} is the viscosity of the solvent isopropanol under the reaction temperature; V is the molar volume of at normal boiling point; L^{vap} is the enthalpy of vaporization at normal boiling point.

With the values of the parameters in Table 1, the value of $D_{citral,\ mixt}$ was computed to be 2.46×10^{-5} cm^2/s.

(3) Effective diffusivity of the reactants in the pores of the catalyst (D_{eff})

In three-phase catalytic system, the reactant molecules diffuse in liquid-filled pores of the catalyst. The conventional model of effective diffusivity (D_{eff}) obtained from the bulk diffusivity (D_b), catalyst porosity (ε) and tortuosity (τ) was modified by incorporating empirical constants [27], as shown in Equation 3.7:

$$D_{eff} = D_b \cdot \frac{\varepsilon}{\tau} \cdot \left(A \cdot e^{-B\lambda} \cdot t\right) \quad 3.7$$

Here, λ is the ratio of the diffusing molecule radius to the average pore radius of the catalyst (i.e., $r_{molecule}/r_{pore}$); A and B are empirical constants based on the catalyst and the type of diffusing molecule. Ternan et al. [28], developed an expression for effective diffusivity involving only one empirical constant (P), as shown in Equation 3.8, which simplified the calculation greatly.

$$D_{eff} = D_b \cdot \frac{(1-\lambda)^2}{1+P \cdot \lambda} \quad 3.8$$

Here, P is a fitting parameter determined individually for catalysts. Based on the report of Satterfield [29], the value of P was calculated to be 16.3, which was employed in this study to estimate D_{eff} in Pd/CNF/TiO_2 and Pd/AC catalyst.

$D_{H_2,mixt}$ and $D_{Citral,mixt}$, calculated in the section 3.4.1 and 3.4.2, were then introduced in equation (8) to estimate the effective diffusivities in the pores of two catalysts.

To calculate the effective diffusivities, structural properties of Pd/CNF/TiO_2 and commercial formed Pd/AC required were listed in Table 2.

Through calculation, the effective diffusivity of the hydrogen and citral in the pores of Pd/CNF/TiO_2 were:

$D_{eff/H2}$=4.59×10^{-5} cm^2/s; $D_{eff/citral}$ =1.03×10^{-5} cm^2/s;

While in commercial Pd/AC:

$D'_{eff/H2}$=2.44×10^{-5} cm^2/s; $D'_{eff/citral}$ =2.89×10^{-6} cm^2/s.

3.3.5 Estimation of Weisz-Prater criterion on mass transfer limitation over Pd/CNF/TiO_2

(1) Calculation of initial global reaction rate ($\Re$)

Initial global reaction rate ($\Re$) on the catalyst could be estimated at the reaction stage of approximately 10% citral conversion and expressed in Equation 3.9:

$$\Re = \left(\frac{m_{citral} \times con\%}{M_{citral} \times t}\right) \times \left(\frac{m_{cat}}{\rho_{cat}}\right)^{-1} \quad 3.9$$

where m_{citral}, M_{citral}, $con.\%$ and t are defined as the same as that in the expression of TOF; m_{cat}

and ρ_{cat} are the mass of the catalyst and its bulk density, respectively (Table 3.2).

Since the parameters in the expression were all known, the maximum initial global reaction rate was calculated to be 1.18 μmol/s·cm^3 cat for Pd/AC and 0.316 μmol/s·cm^3 cat for Pd/CNF/TiO_2.

(2) Estimation of Weisz-Prater criterion

Effective diffusivity (D_{eff}), catalyst particle radius (R_P) and Initial global reaction rate ($\Re$), which are essential to calculate Weisz-Prater number, had all been known in the section 3.3.3 and 3.3.5. The calculation results of W-P criterion for each reactant were summarized in Table 3.4.

Table 3.4: Internal diffusion limitations for citral hydrogenation over Pd/AC and Pd/CNF/TiO_2

Sample	Reactant	Weisz-Prater number (N_{WP})
Pd/AC	Citral	35.91
	H_2	7.4
Pd/CNF/TiO_2	Citral	0.29
	H_2	0.11

The calculating results inferred that in Pd/CNF/TiO_2, $N_{W\text{-}P}$ for each reactant was less than 0.3, which satisfied the condition assuring the elimination of significant internal diffusion limitations in citral hydrogenation in isopropanol; However, in Pd/AC, $N_{W\text{-}P}$ for each reactant was more than 6, which implied the serious internal diffusion limitations of the reactants in Pd/AC. It is noted that in each catalytic system, the $N_{W\text{-}P}$ number for citral was higher than that for hydrogen, indicating a higher probability that the internal diffusion of citral, rather than hydrogen, would suppress the rate of reaction. It could be explained by the drastic differences in molecular size of hydrogen and citral. Generally, the smaller the molecular size of the reactant, the more easily it diffuses inside the catalyst particles. Thus, the lower $N_{W\text{-}P}$ number of hydrogen, which suggests the less internal diffusion limitation, is attributed to its smaller size than that of citral for a same type of catalyst.

The estimation to internal diffusion limitation in this study explained well the rationality of product distributions on citral hydrogenation over Pd/CNF/TiO_2 and commercial Pd/AC (Figure 3.7). The discrepancy on product distributions is likely to be determined by the different structural properties of two catalysts. As shown in Table 3.2, the pores of Pd/CNF/TiO_2 with the average diameter 11.72 nm are mainly composed of meso- and macro-pores. Its micro-pore area occupies only 3.45% of the total surface area. In comparison,

there distribute numerous micro-pores in the interior part of Pd/AC with the average diameter 3.2 nm and micro-pore area occupies approximately 88% of the total.

3.3.6 Mechanism of citral hydrogenation on Pd/AC and Pd/CNF/TiO_2

The mechanism of the reaction on Pd/AC and Pd/CNF/TiO_2 was shown in Figure 3.8. It speculated that when the reactants H_2 and citral diffused along the apertures in Pd/CNF/TiO_2, they suffered the less diffusion resistance due to the numerous meso- and macro-pores of the catalyst. Once citronellal, the intermediate product, was synthesized in the pores, it desorbed from Pd crystal to the solution and easily diffused toward outside of the pores, which made it little probability to hydrogenate deeply to citronellol, even 3,7-dimethyloctanol (Figure 3.8a-3.8b). However, when the reaction took place inside Pd/AC catalyst, citronellal might have stayed there for a long time to further hydrogenated to citronellol and 3,7-dimethyloctanol due to the serious diffusion limitation (Figure 3.8c).

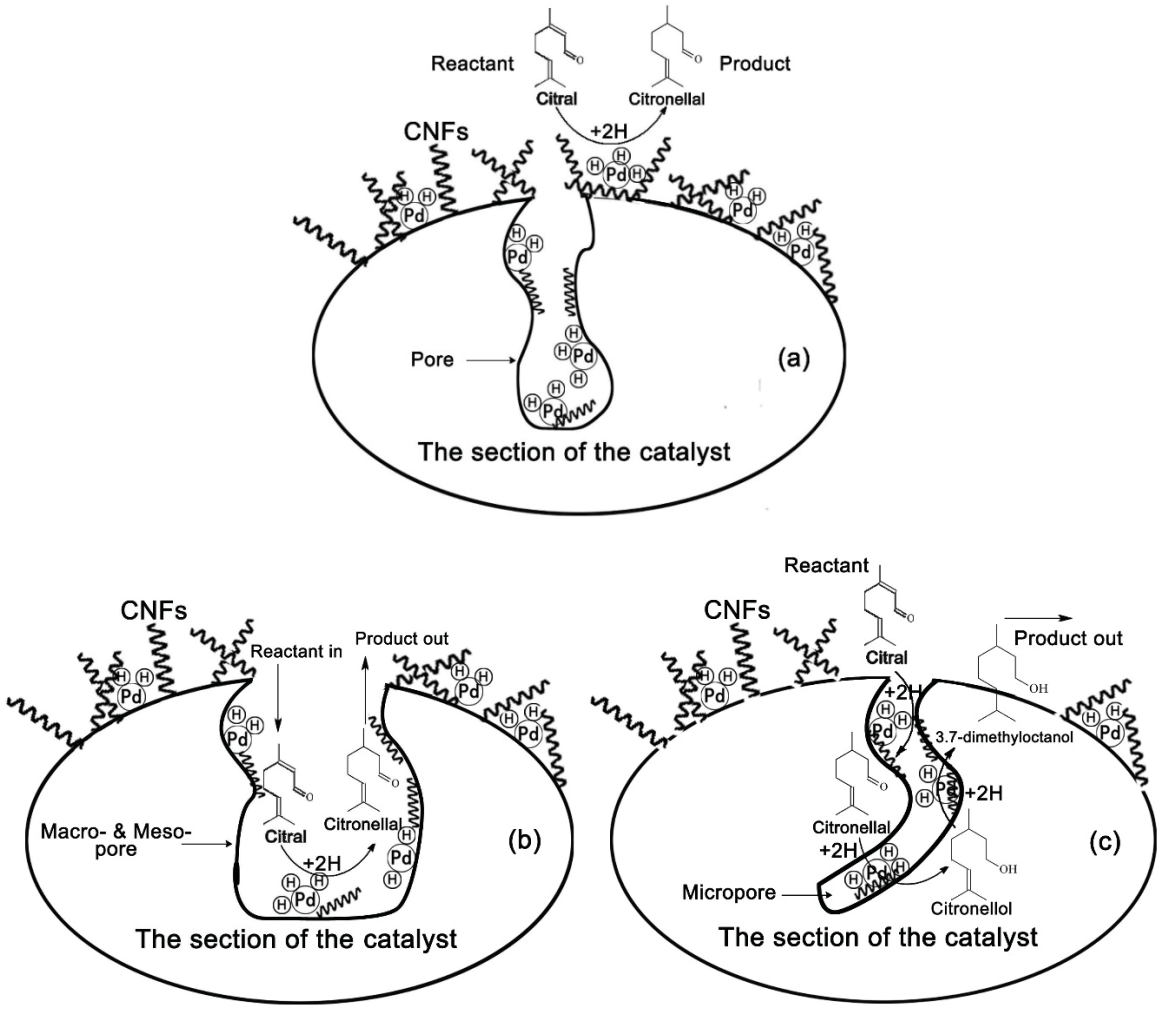

Figure 3.8: The process of citral hydrogenation over the catalyst: (a) on external surface of the catalyst; (b) in the macro- and mesopores; (c) in the micropores

3.4 Conclusions

The catalytic properties over macro-structured Pd/CNF/TiO_2 and Pd/AC for citral hydrogenation were estimated in calculation. The comparatively lower reaction rate over Pd/CNF/TiO_2 than that over Pd/AC was attributed to its low Pd dispersion. Weisz-Prater criterion were employed to estimate the internal diffusion limitations of reactants in the catalyst. The calculating results inferred the absence of internal diffusion limitations in Pd/CNF/TiO_2. It proved the rationality of high citronellal selectivity in citral hydrogenation over it. Meso- and macro-pores, the dominant structures of apertures in Pd/CNF/TiO_2, resulted in the elimination of internal diffusion limitation in the catalyst. These results showed that CNF/TiO_2, an effective catalyst support, has a potential application in three phase catalytic reactions, especially those controlled by internal diffusion.

Nomenclature

Cs	concentration on catalyst surface, mol/cm^3
D_b	bulk diffusivity, m^2/s
D_{eff}	effective diffusivity in the pores of the catalyst, m^2/s
k	reaction rate constant, h^{-1}
L^{vap}	enthalpy of vaporization at normal boiling point, J/kmol
M	molecular weight, g/mol
m	the mass of the reactant, solvent, or the catalyst, g
N	the number of hydrogenation active sites, mol/g cat
n^0	the initial mole amount of reactants, mol
P	the fitting parameter in the expression of effective diffusivity
ρ	density of the material, g/cm^3
R_P	the catalyst particle radius, cm
r	molecular radius or the average pore radius of the catalyst, nm
t	reaction time, s
λ	the ratio of molecular radius to average pore radius of the catalyst, $r_{molecule}/r_{pore}$
V	molar volume at normal boiling point, m^3/kmol
x	mole fraction of component in the solution, mol %
χ	solvent association parameter
ϕ	Thiele modulus

η viscosity of the liquid or the solution, Pa·s

θ porosity of the catalyst

References

[1] F. Delbecq, P. Sautet, J. Catal. 152 (1995) 217-236.

[2] J. Álvarez-Rodríguez, A. Guerrero-Ruiz, Catal. Today 107-108 (2005) 302-309.

[3] J. Álvarez-Rodríguez, I. Rodríguez-Ramos, A. Guerrero-Ruiz, A. Arcoya, Appl. Catal. A: Gen. 401 (2011) 56-64.

[4] A. Vicente, T. Ekou, G. Lafaye, C. Especel, P. Marécot, C. T. Williams, J. Catal. 275 (2010) 202-210.

[5] A. Vicente, G. Lafaye, C. Especel, P. Marécot, C. T. Williams, J. catal. 283 (2011) 133-142.

[6] C. Caballero, J. Valencia, M. Barrera, A. Gil, Powder Tech. 203 (2010) 412-414.

[7] S. Yilmaz, S. Ucar, L. Artok, H. Gulec, Appl. Catal. A: Gen. 287 (2005) 261-266.

[8] J. Álvarez-Rodríguez, I. Rodríguez-Ramos, A. Guerrero-Ruiz, E. Gallegos-Suarez, A. Arcoya, Chem. Eng. J. 204-206 (2012) 169-178.

[9] T. Ekou, C. Especel, S. Royer, Catal. Today 173 (2011) 44-52.

[10] L. Kiwi-Minsker, I. Yuranov, V. Höller, A. Renken, Chem. Eng. Sci. 54 (1999) 4785-4790.

[11] T. Li, M. S. Xu, B. C. Zhu, D. Y. Fang, J. Chem. Ind. Eng. 53 (2002) 1260-1264.

[12] J. Aumo, J. Wärnå, T. Salmi, D. Yu, Murzin, Chem. Eng. Sci. 61 (2006) 814-822.

[13] S. G. Zhang, J. H. Zhou, X. C. Xu, Z. J. Sui, X. G. Zhou, W. K. Yuan. Chem. React. Eng. Tech. 24 (2008) 509-515.

[14] C. B. Chen, J. G. Chen, K. G. Fang, Y. H. Sun, J. Fuel Chem. Tech. 38 (2010) 588-593.

[15] P. B. Weisz, Z. Phys. Chem. 11 (1957) 1-15.

[16] S. Mukherjee, M. A. Vannice, J. Catal. 243 (2006) 108-130.

[17] M. A. Al Herz, A. N. Tsoligkas, M. J. H. Simmons, J. Wood, Appl. Catal. A: Gen. 396 (2011) 148-158.

[18] J. Vicente, H. d′Angelo, A. Z. Francesconi, J. Chem. Eng. Data 46 (2001) 671-674.

[19] U. K. Singh, M. N. Sysak, M. A. Vannice, J. Catal. 191 (2000) 181-191.

[20] U. K. Singh, M. A. Vannice, J. Catal. 199 (2001) 73-84.

[21] B. E. Poling, J. M. Prausnitz, J. P. O'Connell, The properties of gases and liquids, fifth

ed., Chem. Ind. Press, Beijing, 2005.

[22] N. L. Chen, Solvents Handbook, third ed., Chem. Ind. Press, Beijing, 2002.

[23] G. Q. Liu, L. X. Ma, J. Liu, Handbook of physical properties in chemistry & chemical engineering (Organic volume), Chem. Ind. Press, Beijing, 2002.

[24] J. Leffler, H.T. Cullinan, Ind. Eng. Chem. Fund. 9 (1970) 84-88.

[25] C. R. Wilke, P. Chang, AIChE J. 1 (1955) 264-270.

[26] C.J. King, L. Hsueh, K. Mao, J. Chem. Eng. Data 10 (1965) 348-350.

[27] A. Chantong, F.E. Massoth, AIChE J. 29 (1983) 725-731.

[28] M. Ternan, Can. J. Chem. Eng. 65 (1987) 244-249.

[29] C. N. Satterfield, C. K. Colton, W. H. Pitcher, AIChE J. 19 (1973) 628-635.

Chapter 4

Carbon Nanofibers Grown on Anatase Washcoated Cordierite Monolith and its Supported Palladium Catalyst for Cinnamaldehyde Hydrogenation

Abstract

This chapter reported the synthesis of a promising carbon nanofiber-titania-cordierite monolith composite, i.e. CNF/TiO_2/monolith, and its application as the catalyst support in selectivity hydrogenation of cinnamaldehyde (CAL) to hydrocinnamic aldehyde (HCAL). The composite was synthesized through TiO_2 coating on the surface of the monolith and the following CNF growth on it. Synthesized CNF/TiO_2/monolith was subsequently employed to prepare its supported palladium catalysts, Pd/CNF/TiO_2/monolith. Attachment strength and acid-resistant properties of the composite had been studied to evaluate its structural stability in some severe conditions. And the effects of supported Pd particles, oxygen-containing surface groups and internal diffusion limitation on catalytic performance over Pd/CNF/TiO_2/monolith were further studied. Results revealed that total BET surface area of the composite was 31 m^2/g and the macro- and mesopore structure dominated the pore space of the material (about 93%). Meanwhile, 94% of the carbon deposit on the surface of the composite was CNF. TiO_2 and CNF coating was deemed to increase its textural and acid-resistant properties. Although relatively slow reaction rate over as-prepared Pd/CNF/TiO_2/monolith-R due to its small BET surface area and low Pd dispersion (about 15%), the selectivity to HCAL maintained high (about 90%) over it at 95% CAL conversion, the same as that over powdered Pd/CNF (about 93%), being much higher than that over Pd/AC (about 45%), Pd/MC and Pd/CNF/TiO_2/monolith-O (each about 82%). This was attributed to the removal of acidic oxygen-containing surface groups and the elimination of internal diffusion limitation on Pd/CNF/TiO_2/monolith-R.

This part of work has been published as Research Article: J. Zhu, Y. Jia, M. Li, M. Lu, J. Zhu, *Ind. Eng. Chem. Res.* 52 (2013) 1224-1233.

4.1 Introduction

Selective hydrogenation is one of the key processes in pharmaceutical and cosmetic industries. With the ever increasing demand for special chemicals, selective hydrogenations of α,β-unsaturated aldehydes become one of the current challenges to be tackled both from the fundamental and from the industrial standpoints [1]. Cinnamaldehyde (CAL), a typical α,β-unsaturated aldehyde, possesses two sites of hydrogenation: a carbonyl group (C=O) and a conjugate double bond (C=C), which leads to a complex reaction network of CAL selective hydrogenation involving two parallel reactions (Figure 4.1). Specifically, cinnamaldehyde can be initially hydrogenated to cinnamyl alcohol (COL) and hydrocinnamic aldeyde (HCAL), depending on whether the C=C double bond is hydrogenated or the C=O bond. Both intermediates are further hydrogenated to hydrocinnamic alcohol (HCOL), even 1-propylbenzene (1-PB) as the final product [2-4]. The performance of the hydrogenation reactions, especially the product selectivity, is significantly influenced by several factors including metal particle size [5-7], nature of the support [8-10], presence of promoters [11, 12] and reaction solvent [13, 14].

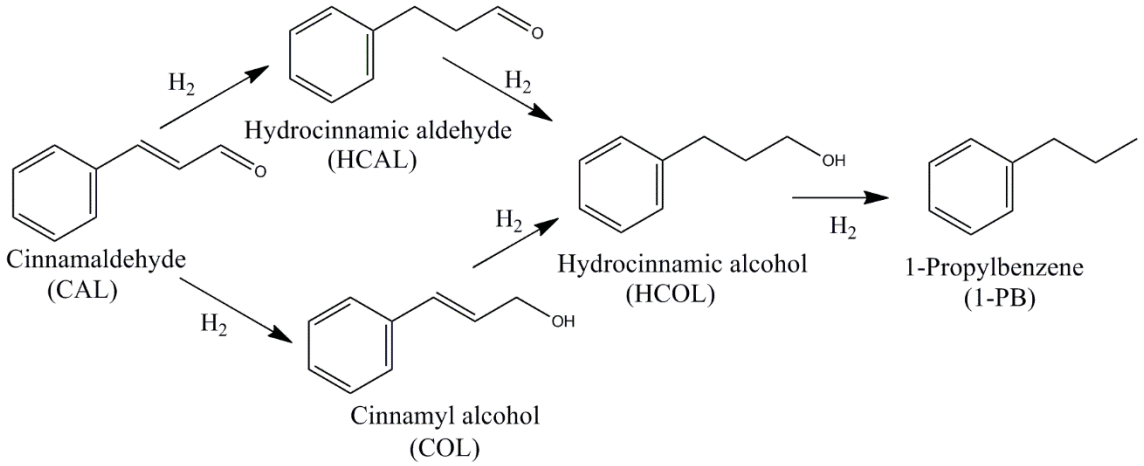

Figure 4.1: Consecutive reaction routes of cinnamaldehyde hydrogenation.

For this reason, many attempts have been made to promote the selectivity to different intermediates by taking advantage of some novel catalysts or catalytic systems. For example, Galletti et al. [15] synthesized Pd/γ-Al_2O_3 nanocatalysts using a simple and environmentally friendly microwave-assisted process. These new supported palladium nanocatalysts have shown interesting catalytic performances in terms of both activity and selectivity when

employed in CAL hydrogenation to HCAL in decalin, reaching from high to complete substrate conversions and selectivity up to 97% in HCAL at complete substrate conversion.

Recently, a new group of carbonaceous materials, carbon nanotube (CNT) and nanofiber (CNF), abbreviation as CNF(T), showed potential applications in various fields of materials research including catalysis, owing to their exceptional physical and chemical properties [16-18]. The use of CNF(T) as catalyst support is inspired by the unique properties of these materials including their unique structure-dependent optical, resistance to strong acids and bases, and high mechanical flexibility and strength, as well as improved carbon–metal interactions that have been found to enhance catalytic performance [19, 20]. In addition, they can form aggregates with high surface areas and pore volumes without micro porosity, which will prefer to improve product selectivity in selective hydrogenation. Zhang et al. [20] reported a striking enhancement of catalytic performance of gold nanoparticles (NPs) supported on CNTs for CAL hydrogenation in toluene and the results showed that the selectivity to HCAL was up to 91% at 95% CAL conversions.

Although owning some advantages mentioned above, CNF(T) in powder form suffer from some drawbacks for slurry phase operation. Obviously, the agglomeration of the nanofibers and the difficulty of filtration can adversely impact catalytic processes. In addition, CNF(T) powders are difficult to use directly in fixed-bed reactors due to a high pressure drop. Therefore, many studies on macro-structured CNF(T) and their prepared catalysts have been launched [21], for the purpose of resolving the disadvantages of the powdered catalysts employed in catalytic reactors, especially in fixed-bed ones. Some formed supports, including graphite felt [22], metallic filters and foams [23-25], can be employed to immobilize CNF(T) to develop the macro-structured CNF(T) supports. Ceramic monolith is another promising candidate as well.

Cordierite monolith, a formed industrial ceramics with the shape of honeycomb (Figure 4.2a), is widely used in new reactor applications such as chemical processing, refining industries, and catalytic combustion [26-28]. It has some distinct advantages including better mechanical strength, lower heat transfer capacity and lower thermal expansion coefficients [29]. Macro-porous structure, another feature of the monolith, will be in favor of selective hydrogenation by eliminating internal diffusion limitation in the reaction. However, both the low specific surface area of cordierite monolith (<1 m^2/g) and weak metal-support interactions limit its application as the catalyst support. Therefore, a layer of coating with high specific surface area is usually synthesized in the process of the catalyst preparation to cover

the surface of monolith to increase its effective surface area, thereafter improving the metal dispersion on it. In early works of Chen et al. [30], Lefferts et al. [31] and Monzón et al. [32], CNF(T) washcoated cordierite monoliths were synthesized with different methods. Notably, β-zeolite or γ-alumina layer is often used to cover the bare monolith prior to the growth of CNF(T) in order to supply sufficient number of cationic exchange sites to anchor the metallic particles responsible for the CNF (T) formation. Furthermore, Wang et al. [33] and Pérez-Cadenas et al. [34] synthesized ruthenium and palladium catalysts supported on CNF(T) washcoated monolith for the synthesis of ammonia and low-temperature combustion of BTX, respectively. The as-prepared catalysts displayed the excellent catalytic performance on target reactions.

In this chapter, we developed a novel CNF washcoated cordierite monolith. A layer of TiO_2 film, synthesized by a sol-gel route, was deposited over the bare monolith prior to the growth of CNF. The as-prepared macro-structured composite was named CNF/TiO_2/monolith. TiO_2, not β-zeolite or γ-alumina, was chosen to cover the monolith in composite preparation because it possesses several prominent advantages including the high chemical resistance to make the TiO_2-coated monolith utilize in highly acidic or basic medium, as well as its preferable electronic properties to help to improve the product selectivity in reactions [35, 36]. The catalytic behavior of Pd catalyst supported on CNF/TiO_2/monolith (Pd/CNF/TiO_2/monolith) was studied in selective hydrogenation of CAL to HCAL. The results were compared with those supported on formed activated carbon (Pd/AC), meso-porous carbon (Pd/MC) and the powdered carbon nanofiber (Pd/CNF). The possible formation mechanism of hydrogenation products was also discussed.

4.2 Experimental

4.2.1 Synthesis of CNF/TiO_2/monolith composite

The cylindrical cordierite monolithic substrates (length 2 cm, diameter 1 cm) had square channels, a cell density of 62 cells/cm^2 (400 cpsi) and a wall thickness of 0.18 mm (Nanjing Gaochun special ceramic company), as shown in Figure 4.2a. It was firstly coated with TiO_2 layer using a dip coating method [37]. In this case, cordierite monolith was impregnated with 2.0 wt. % tetrabutyl titanate / ethanol (A.R, Sinopharm, China) colloid. After withdrawal from the colloid 10 min later, excess liquid in the monolithic channels was removed with

pressurized air and then dried overnight in air at 393 K. Once they were calcined at 773 K for 3 h with a heating rate of 2.0 K/min in order to avoid cracks, TiO_2/monolith was obtained.

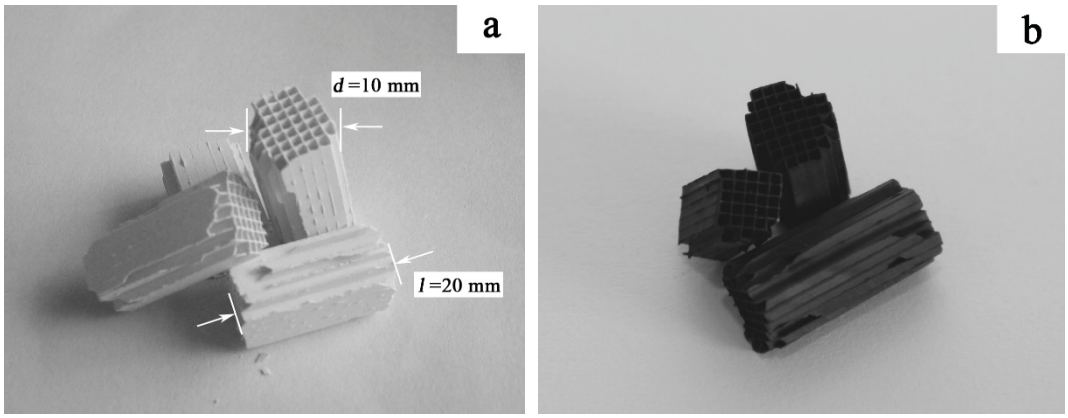

Figure 4.2: The profile of the materials: (a) cordierite monolith; (b) CNF/TiO_2/monolith composite.

For CNF coating, Ni was deposited by equilibrium impregnation of TiO_2/monolith supports with an aqueous solution of $Ni(NO_3)_2 \cdot 6H_2O$ (A.R, Sinopharm, China), in which the nickel loading was kept fixed at 4.0 wt.%. The samples were dried overnight at 393 K prior to calcination at 773 K for 2 h. After they were reduced in the tube at 873 K in a stream of N_2 / H_2 (80:20) (99.999%, Wuxi Tianhong, China) for 2 h, methane (99.999%, Wuxi Tianhong, China) was then passed through the tube to decompose at 873 K for 4 h. After refluxing in 20 wt.% HNO_3 at 393 K for 60 min to remove exposed nickel metal particles and create anchoring sites for metal deposition, the composite support CNF/TiO_2/monolith were finally synthesized.

4.2.2 Characterizations of CNF/TiO_2/monolith composite

CNF/TiO_2/monolith composite was characterized to test the textural and structural properties. X-ray powder diffraction data were collected on Rigaku D/max 2500 diffractometer using CuKa (40 kV, 40 mA) radiation and a graphite monochromator. Nitrogen adsorption-desorption measurements were carried out with Micromeritics ASAP 2010 apparatus. Surface morphology and element distributions on the materials were recorded using a JEOL JSM-6360 LA scanning electron microscope - energy dispersive spectrometer (SEM-EDS). The morphologies and the properties of the metal particles on catalysts were obtained with JEM-2100 transmission electron microscopy (TEM). Thermogravimetric (TGA) and differential thermal (DTA) analysis were performed using a TA SDT Q600 instrument.

The attachment strength of the nanofibers anchoring to the monolith was evaluated by monitoring the weight loss after treatment in an ultrasonic bath for 60 min. The acid-resistant

property of the composite was tested by refluxing bare monolith and CNF/TiO_2/monolith in 20 wt.% HNO_3 for 180 min and then calculating the weight loss of samples.

4.2.3 Preparation of CNF/TiO_2/monolith, MC and CNF supported Pd catalysts

0.5 wt.% of Pd catalyst was prepared by impregnation method. Specifically, the support CNF/TiO_2/monolith, which had been synthesized in the section 2.1, were impregnated into an aqueous solution of $PdCl_2$ (Pd≥59%, Sinopharm, China) and stirred continuously for 6 h. The samples were then dried overnight at 393 K and stored in a desiccator. Finally, the catalysts were reduced in a quartz tube at 493 K for 2 h. The catalysts prepared were named Pd/CNF/TiO_2/monolith-O. It could be further treated in N_2 at 773 K for 120 min to remove part of the surface oxides. The as-prepared sample was named Pd/CNF/TiO_2/monolith-R. 0.5 wt.% Pd/MC and Pd/CNF were synthesized through the same procedure as Pd/CNF/TiO_2/monolith-R did. In detail, MC (200 mesh, Changzhou Mesocarbon Co., China) and CNF (diameter in a range of 20-40 nm, Chengdu Organic chemical, China) supports were previously treated by refluxing in 20 wt.% HNO_3 at 393 K for 60 min prior to the preparation of Pd/MC and Pd/CNF and the as-prepared catalysts were then treated in N_2 at 773 K for 120 min.

4.2.4 Catalytic performance of Pd/CNF/TiO_2/monolith

The catalytic performance on Pd/CNF/TiO_2/monolith was evaluated in selective hydrogenation of CAL to HCAL, and the result was compared to that of Pd/MC, Pd/CNF and a commercial Pd catalyst supported on formed activated carbon, i.e. Pd/AC (0.5 wt% Pd loading, irregular particles, ϕ≈3 mm, 810 m^2/g, Sinopec Yangzi, China). The experiments for revealing the intrinsic hydrogenation kinetics were carried out in a 500 ml pressurized autoclave. Formed catalysts were placed in the baskets, which were fixed in the axle of the stirrer and the channel of monolith was parallel to the rotation direction of the stirrer (Figure 4.3). By dispersing approximately 5.0 g of the catalysts into 250 g toluene (A.R, Sinopharm, China) solution of CAL (A.R, Sinopharm, China) at the concentration of 5.0 wt.%, the autoclave was sufficiently flushed with nitrogen flow and the following hydrogen to remove dissolved oxygen. The reaction was commenced by switching on the stirring to 800 rpm, which was verified to be sufficient to exclude external diffusion. The experiments were conducted at 353 K and 2 MPa total pressure, which was maintained by continuously injecting hydrogen into the reactor. Small amounts of reaction samples were withdrawn from the reactor at different reaction times and analyzed by gas chromatography (VARIAN CP3800) equipped with a FID detector and capillary column HP-5 using nitrogen as carrier gas.

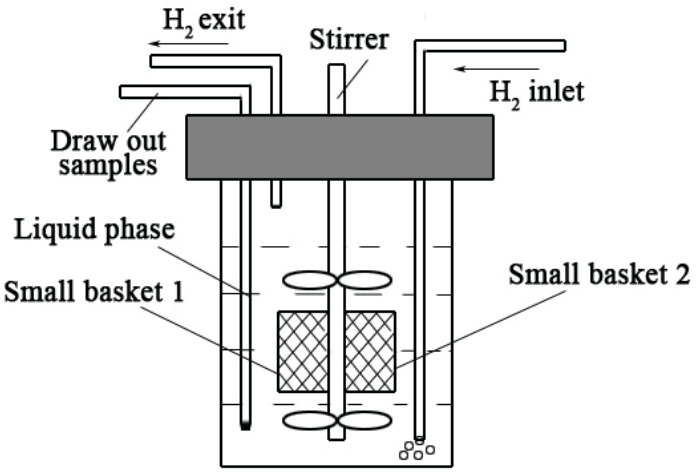

Figure 4.3: Scheme of the reaction setup.

4.3 Results and discussion

4.3.1 Textural and structural properties of CNF/TiO_2/monolith composite

(1) Surface morphological and elemental distribution analysis

As described in the section 4.2.1, CNF/TiO_2/monolith composite was synthesized by two stages: the coating of TiO_2 film over the monolith by dip coating method and then the growth of carbon nanofibers on TiO_2/monolith through methane decomposition. The obtained CNF/TiO_2/monolith (Figure 4.2b) maintained the same profile as the bare monolith (Figure 4.2a) and the carbon deposited evenly on its surface, which implied that the modification to the monolith in this work did not damage the main structure of it. This would favor the following preparation of macro-structured catalyst.

Further analysis on SEM images of monolith-based materials discovered that, TiO_2 coating, the bridge between monolith and carbon nanofibers, covered the whole surface of the base material (Figure 4.4a-4.4b). This smooth and dense film was expected to play the important roles on the textural and acid-resistant properties of the final composite. And after methane decomposition over TiO_2/monolith, surface of the composite covered a significant amount of CNFs with diameters of 30-60 nm (Figure 4.4c-4.4d). They intertwined each other to form pore structures. Compared with bare monolith (sample 1#, Table 4.2), carbon content on the surface of the composite accounted for more than 83 wt.% (sample 2#, Table 4.2), which implied the overwhelming carbon covering the monolith and be in accordance with the result of SEM images of the composite. CNFs, which covered the surface of the monolith, not

only supplied most of the BET surface area of the composite, but also determined the surface textural property of it.

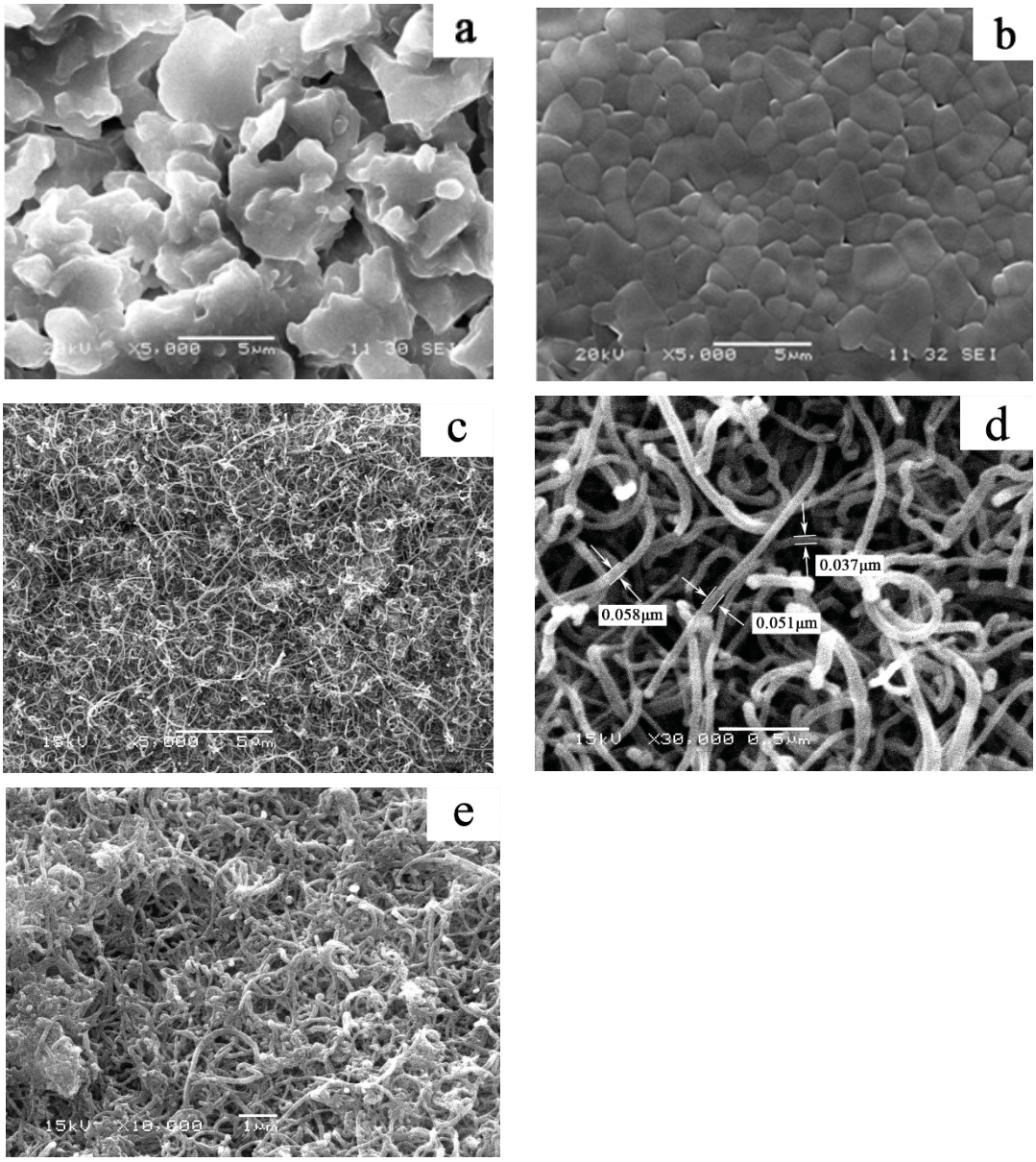

Figure 4.4: SEM images of the surfaces of materials: (a) bare cordierite monolith; (b) TiO_2/monolith composite; (c) CNF/TiO_2/monolith with low magnification (×5000); (d) CNF/TiO_2/monolith with high magnification (×30000); (e) CNF/TiO_2/monolith after acid corrosion test.

(2) Nitrogen adsorption-desorption analysis

Textural properties of monolith-based materials including total surface area, micropore area and average pore size could be analyzed by nitrogen adsorption-desorption measurements. Generally, the coating of TiO_2 and the following growth of carbon nanofibers on cordierite monolith could cause a significant increase in BET surface area (Table 4.1).

Specifically, CNF/TiO_2/monolith had the BET surface area as high as 31 m^2/g in this work, which was much larger than 0.60 m^2/g of bare monolith. According to the weight increase before and after methane decomposition over TiO_2/monolith (about 19 wt.%), the BET surface area per gram CNF was calculated to be approximate 160 m^2, in accordance with that of commercial powdered CNF.

Table 4.1 Physicochemical properties of the materials and their supported palladium catalysts

Sample	Carbon deposit in the monolith (wt. %) [a]	Total BET Surface Area (m^2/g)	Micropore Area (m^2/g)	Average Pore size (nm)	Actual Pd loading (wt%) [b]	Average Pd size (nm)	Pd dispersion (%) [c]
Bare monolith	-	0.6	-	10.1	-	-	-
TiO_2/monolith	-	3	-	8.7	-	-	-
CNF/TiO_2/monolith	18.7	31	2	12.8	-	-	-
Pd/CNF/TiO_2/monolith-O [d]	-	28	2	11.3	0.48	7.8	16
Pd/CNF/TiO_2/monolith-R [e]	-	29	2	10.7	0.45	8.2	15
Commercial Pd/AC	-	810	720	2.1	0.50	2.8	43
Pd/MC [f]	-	670	126	4.9	0.48	3.5	35
Pd/CNF [f]	-	180	10	6.1	0.52	5.6	22

Note: (a) calculated by the weight increase after methane decomposition;

(b) Determined with ICP-AES;

(c) Based on the hemispherical model of metal particles on surface of the catalyst.

(d) Composite refluxing in 20 wt% HNO_3 at 393 K for 60 min prior to the preparation of supported Pd catalyst;

(e) Prepared by heat-treating Pd/CNF/TiO_2/monolith-O in N_2 at 773 K for 120 min;

(f) MC and CNF refluxing in 20 wt% HNO_3 at 393 K for 60 min prior to the preparation of their supported Pd catalysts and as-prepared catalysts then heat-treating in N_2 at 773 K for 120 min.

Furthermore, the micropore area and average pore size of CNF/TiO_2/monolith was about 2 m^2/g and 12.8 nm, respectively (Table 4.1). Therefore, it can be inferred that 93% of its pore space consisted of meso- and macropores, which will benefit the decrease of internal diffusion limitation during multiphase catalytic reactions. And after Pd loading, Pd/CNF/TiO_2/monolith

catalyst holding the similar textural properties as CNF/TiO_2/monolith did (Table 4.1) indicated the high material stability of prepared composite.

(3) Thermogravimetric analysis

Since the oxidation temperature of carbon is in a range of 573K to 973K, thermogravimetric analysis could been conducted to determine the percentage of carbon deposited on the surface of monolith, as well as its structural properties. The result was shown in Figure 4.5.

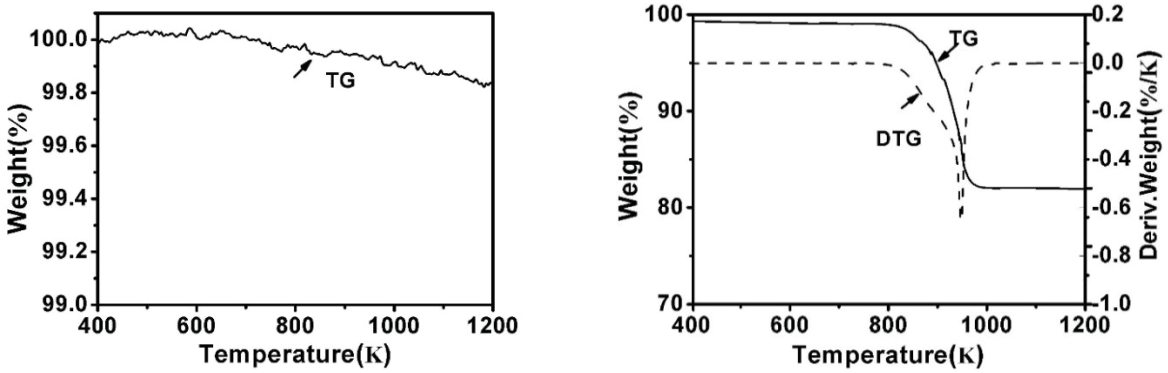

Figure 4.5: TG and DTG curves of materials including TiO_2/monolith (a) and CNF/TiO_2/monolith (b).

The total weight loss of CNF/TiO_2/monolith in temperature range from 573K to 973K was about 17 wt.% (Figure 4.5b), as calculated from TG curve, being near to that of weight increase in the monolith (about 19 wt.%, Table 1). Noted that TiO_2/monolith before carbon deposition had no obvious weight loss (< 0.2 wt.%) at the same temperature range as CNF/TiO_2/monolith did (Figure 4.5a), which implied that the weight loss in CNF/TiO_2/monolith mainly derived from the carbon deposited on its surface. Herein, carbon content on the monolith accounted for about 17 wt.% of the total weight of the composite after methane decomposition.

In addition, amorphous carbon and graphite carbon have their own characteristic oxidation temperatures. A higher oxidation temperature always indicates a purer and less defective material. The oxidation temperature of amorphous carbon is relatively low, i.e., in a range of 573 to 673 K, while that of graphite carbon is ranging from 673 to 973 K [38]. Therefore, the structure of carbon deposits can be well estimated from the DTG curve. Particularly, it can be inferred from the TG curve in Figure 3b that over 97 wt.% weight loss occurred between 673 K and 973 K with the DTG peak at 938 K while only a little weight

loss occurred between 573 K and 673 K. Therefore, it is reasonable to conclude that about 97 wt.% carbon produced by methane decomposition are graphite. It should be noted that CNF has the graphite structure [39]. Combining the SEM images of the composite surface (Figure 4.4c-4.4d) with thermogravimetric analysis, we supposed that the graphite covering the surface of the composite was mainly CNF.

(4) XRD analysis

The structure of CNF/TiO_2/monolith was further analyzed using XRD. Compared with the cordierite (Figure 4.6a), the XRD spectrum of CNF/TiO_2/monolith (Figure 4.6e) showed the evident characteristic peak of graphite (002) at 2θ (26.38°), in accordance with that of commercial powdered CNF (Figure 4.6d), indicating the dominant CNF deposit on the surface of monolith after methane decomposition. However, the spread peaks of XRD spectrum at 2θ (20°-30°) in both MC and AC (Figure 4.6b-4.6c) implied their microcrystalline structures or the blend of crystalline and amorphous structures. The difference in crystal formation among these carbon supports will affect the textural and electronic properties of their supported catalyst, which are important factors in evaluating catalytic performance.

According to the mathematical model in reference [40], graphitization factor (G) is related to the crystal plane spacing distance of graphite (002) (d_{002}) via the Equation 4.1:

$$G= (0.344-d_{002})/(0.344-0.3354) \quad 4.1$$

in which 0.344 and 0.3354 nm is the crystal plane spacing distance of non-graphite and ideal graphite, respectively.

The d_{002} of carbon deposits determined from XRD spectrum was 0.3359 nm with a graphitization degree of 94%, which coincided with that of thermogravimetric analysis.

Meanwhile, the characteristic peaks of anatase at 2θ (25.30°, 36.96°, 37.76°, 48.02°) also indicated that tetrabutyl titanate sol covering the surface of cordierite monolith was decomposed to anatase in calcination, which would help to improve the product selectivity in catalysis due to its excellent electronic properties.

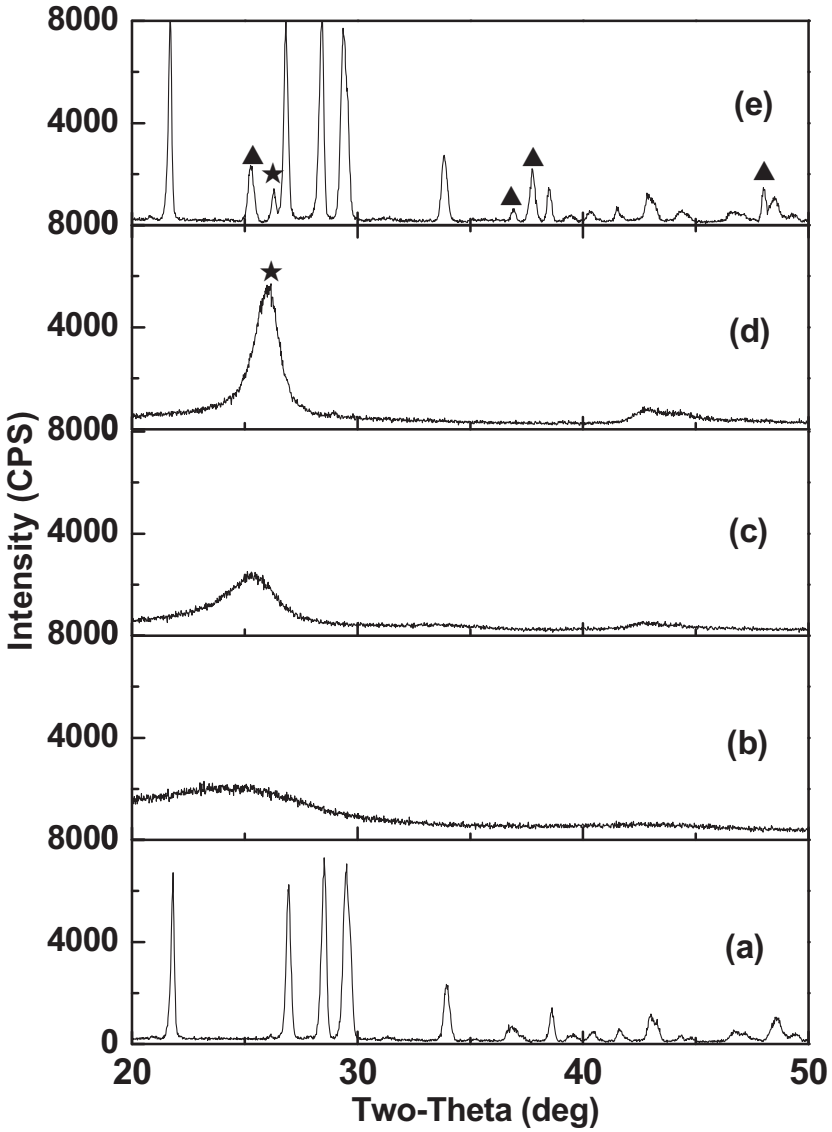

Figure 4.6: XRD pattern of materials including cordierite (a), formed activated carbon (b), mesoporous carbon (c), carbon nanofiber (d) and CNF/TiO_2/monolith (e): ▲ Anatase; ★ Graphite (002).

4.3.2 Attachment strength and acid-resistant properties of CNF/TiO_2/monolith composite

Since a catalyst often needs to stand some severe reaction conditions including strong shearing force and highly acidic or basic medium, it is essential for a catalyst support to maintain its structural stability in those surroundings. In this work, attachment strength of CNF anchoring to the monolith and acid-resistant property of the composite had been studied to evaluate its structural stability.

Based on Table 4.2, the weight loss of the composite (sample 3#) after 60 min treatment in the ultrasonic bath was only 1.4 wt.% of the total, and the carbon composition in the monolith decreased from 83.42 wt.% (sample 2#) to 81.35 wt.%, which implied the removal of a little bit unsolidified CNFs or amorphous carbon particles on the composite. This confirmed the strong anchoring of the CNFs to the monolith.

Table 4.2 Average surface element distributions on cordierite monolith materials before and after the tests of CNF attachment strength and acid corrosion

Samples	Weight loss after treatment (wt. %)	Surface element distribution (wt. %) [a]					
		C	Ti	O	Al	Si	Mg
Original samples							
1# Bare monolith	-	-	0.54	45.13	16.93	27.06	6.86
2# CNF/TiO_2/monolith	-	83.42	7.25	6.92	0.86	1.13	0.21
Samples after CNF attachment strength test [b]							
3# CNF/TiO_2/monolith	1.4	81.35	8.23	7.86	0.94	1.29	0.31
Samples after acid erosion test [c]							
4# Bare monolith	9.2	-	-	46.64	4.97	46.18	2.13
5# CNF/TiO_2/monolith	1.9	79.72	7.64	10.24	0.73	1.39	0.20

Note: (a) measured by scanning electron microscope - energy dispersive spectrometer (SEM-EDS).

(b) samples treated in an ultrasonic bath for 60 min to test the attachment strength of CNFs anchoring to the monolith;

(c) samples treated in boiling HNO_3 solution (20 wt%) for 180 min to test the resistance to acid erosion;

The chemical composition of the cordierite ($2MgO{\cdot}2Al_2O_3{\cdot}5SiO_2$) determines its weak resistance to the acid, which restrict its application in the reaction involving acidic substances. For example, the weight loss of the bare monolith (sample 4#) after refluxing in boiling HNO_3 solution (20 wt%) for 180 min was up to 9.2 wt.% of the total, and some MgO and Al_2O_3 compositions in the monolith had been removed due to acid corrosion. Surface elemental distribution further indicated that the content of Mg on the surface of bare monolith greatly

decreased from 6.86 wt.% to 2.13 wt.% and the content of Al from 16.93 wt.% to 4.97 wt.%, which caused the increase of Si content in final on the surface of monolith.

In contrast, after TiO_2 coating and CNF deposit, the as-prepared CNF/TiO_2/monolith composite exhibited the high acid-resistant property. Specifically, the composite (sample 5#) had the little weight loss (only 1.9 wt. %), far below that of the bare monolith (sample 4#). Meanwhile, the structures of CNFs after HNO_3 treatment were partly collapsed but kept integrity relatively (Figure 4.4e).The strong acid resistance of CNF/TiO_2/monolith was attributed to the dense TiO_2 and CNF coating on the surface of monolith, which protected it from the acid corrosion. Noted that the weight ratio of oxygen to carbon (O/C) on the surface of CNF/TiO_2/monolith after acid corrosion increased from 0.083 to 0.128 (Table 4.1), which inferred the formation of some oxygen-containing surface groups such as carbonyl groups (-C=O) and carboxyl ones (-COOH) due to HNO_3 oxidation.

In conclusion, the analysis to the composite indicated that the carbon deposit on the surface of the monolith was mainly composed of CNF and the macro- and mesopore structures dominated the pore space of the material, which was highly conducive to the elimination of internal diffusion limitation in catalytic reactions. Meanwhile, the solid and stable structure of the composite also made it suitable as the catalyst support in some severe reaction conditions.

4.3.3 Catalytic performance of Pd catalyst supported on CNF/TiO_2/monolith

(1) Effect of supported Pd particles

As one of the most important factors in catalysis, the properties of metal particles, including crystallite size and surface metal sites, will take great effects on catalytic activity. In this work, the sizes and dispersions of palladium particles on catalysts could be obtained in TEM images (Figure 4.7) and summarized in Table 1. Specifically, palladium particles in Pd/AC possessed the smallest size (average 2.8 nm) of four employed catalysts, and the largest in Pd/CNF/TiO_2/monolith (average 8.1 nm). Based on the hemispherical model of metal particles on surface of the catalyst, palladium dispersions on Pd/AC, Pd/MC, Pd/CNF and Pd/CNF/TiO_2/monolith-O(R) were calculated to be 43%, 35%, 22% and 16% (15%), respectively.

Moreover, based on Pd loadings and dispersions (Table 4.1), the molar number of surface Pd sites (N_{Pd}) was further calculated to be 20.4 μmol/g·cat (Pd/AC), 16.3 μmol/g·cat (Pd/MC), 10.2 μmol/g·cat (Pd/CNF) and about 7.3 (7.1) μmol/g·cat (Pd/CNF/TiO_2/monolith-O(R)), respectively. High palladium dispersion on Pd/AC due to its

large BET surface area (810 m^2/g), as shown in Table 4.1, led to more surface Pd sites on Pd/AC. This was the main reason to obtain the comparatively higher reaction rate over Pd/AC than that over other employed catalysts. For example, CAL conversion over Pd/AC was 95% after 180 min, while it took nearly 600 min for Pd/CNF/TiO_2/monolith, more than threefold time of the former catalyst, to reach the same conversion (Figure 4.8).

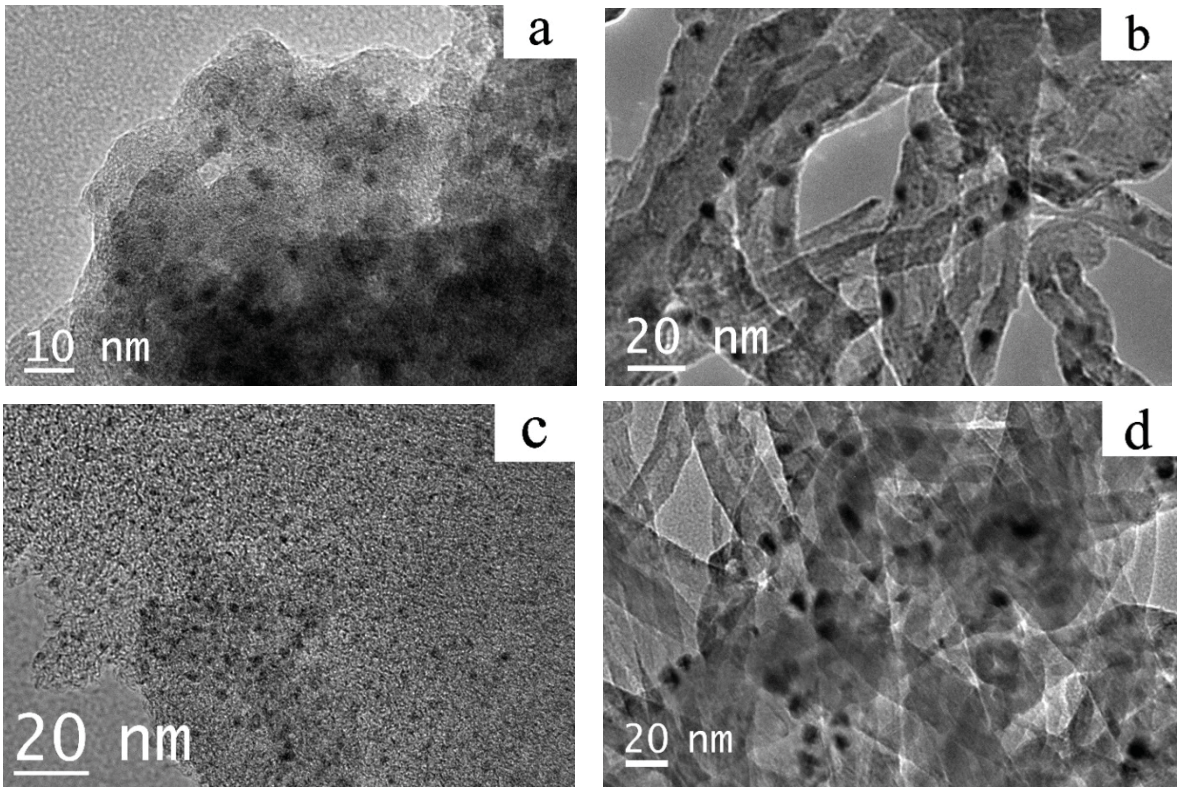

Figure 4.7: TEM images of Pd catalysts: (a) Pd/MC; (b) Pd/CNF; (c) Pd/AC; (d) Pd/CNF/TiO_2/monolith-R

The concept of initial turnover frequency (TOF) for the catalyst was employed here to estimate the crystallite size effect on the kinetics in catalysis. It might be calculated using Equation 4.2 at CAL conversion of approximately 10% in order to get the intrinsic kinetic data.

$$TOF = \left(\frac{m_{CAL} \times con.\%}{M_{CAL} \times t} \right) \times \left(N_{Pd} \right)^{-1} \qquad 4.2$$

Where $m_{CAL}$and M_{CAL} are the mass of CAL and its molecular weight, respectively; *con.%* and *t* are the initial citral conversion and the reaction time (Figure 6) , respectively; And N_{Pd} is the molar number of surface Pd sites.

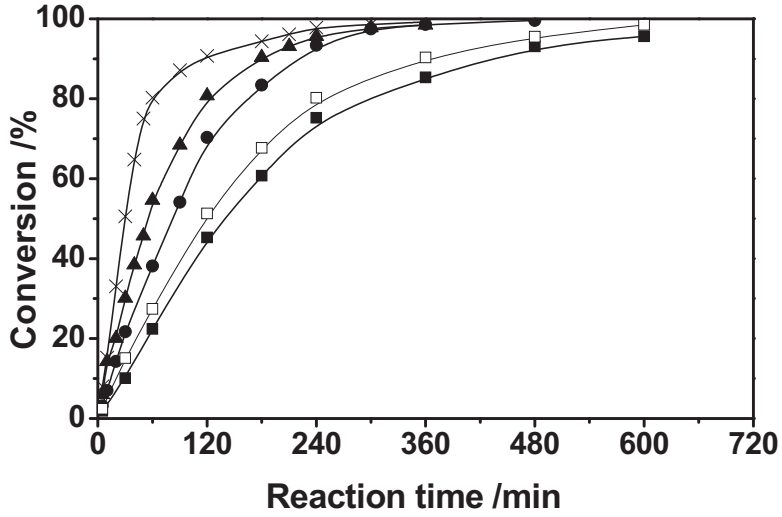

Figure 4.8: Cinnamaldehyde conversion versus reaction time in cinnamaldehyde hydrogenation over 0.5 wt% Pd/AC (×), 0.5 wt% Pd/CNF (●), 0.5 wt% Pd/MC (▲), 0.5 wt% Pd/CNF/TiO_2/monolith-R (■) and 0.5 wt% Pd/CNF/TiO_2/monolith-O (□).

Therefore, the initial TOFs were calculated from the curves of Figure 6 to be 0.25 s^{-1} for Pd/AC, 0.23 s^{-1} for Pd/MC, 0.20 s^{-1} for Pd/CNF, 0.16 s^{-1} for Pd/CNF/TiO_2/monolith-O and 0.21 s^{-1} for Pd/CNF/TiO_2/monolith-R, respectively. Considered the similar surface O/C weight ratios of Pd/MC, Pd/CNF and Pd/CNF/TiO_2/monolith-R, the similar initial TOFs in three catalytic systems implied that Pd particle size is not expected to have a significant influence on the differences in the kinetics among the catalysts.

However, Pd particle size did affect the product distribution in the reaction. According to Figure 4.9, selectivity to COL in Pd/CNF/TiO_2/monolith-R maintained nearly 8.0 % at CAL conversion of 20 %; while that in Pd/MC and Pd/CNF only approximately 4.0 % and 5.5 % at the same conversion. Since little deep hydrogenation of COL to HCOL in three catalysts at 20% conversion, the difference of COL distribution in Pd/MC, Pd/CNF and Pd/CNF/TiO_2/monolith-R was ascribed to Pd particle size effect. The result was in accordance with the study of Gallezot et al. [41] and Chizari et al. [42] Particle size effect asserts that an increase of metal particle size, especially larger than 2-3 nm, favors the selectivity to COL and this trend can be attributed to a steric effect whereby the planar CAL molecule can not adsorb parallel to a flat metal surface because of the steric repulsion of the aromatic ring. By tilting away from the metal surface, the CAL molecule facilitates end-on adsorption and the C=C bond is protected and hence the selectivity to COL is improved.

(2) Effect of oxygen-containing surface groups

Energy Dispersive Spectrometer (EDS) measurements were done to establish the amount of oxygen on the surface of the catalysts. Table 4.3 gave the O/C weight ratios of five employed catalysts. Results showed that, O/C weight ratio on the surface of the commercial Pd/AC obtained the highest value (0.11) in the catalysts, which implied the existence of amount of oxygen-containing groups on its surface.

Table 4.3 Average surface element distribution of oxygen and carbon on the catalysts

Sample	Surface element distribution (wt. %)		O/C weight ratio (wt./wt.)
	C	O	
Pd/CNF/TiO_2/monolith-O	80.69	8.23	0.10
Pd/CNF/TiO_2/monolith-R	82.86	4.86	0.06
Pd/AC	88.06	9.90	0.11
Pd/MC	96.14	2.23	0.02
Pd/CNF	94.79	2.56	0.03

However, the heat-treating in Nitrogen at 773 K could eliminate most of acidic oxygen-containing groups from the surface. The fact that O/C weight ratio of Pd/CNF/TiO_2/monolith after heat-treating decreased much from 0.10 to 0.06 (Table 3) proved the efficiency of this treatment. It is well established that when oxygen-containing groups on a carbon support are heated under inert atmosphere, almost acidic oxygen-containing groups including carboxyl and carbonyl groups completely decomposed at 973 K [43, 44]. Meanwhile, upon heating under inert atmosphere, some sintering occurred because the average particle size of Pd/CNF/TiO_2/monolith became slightly larger after heating at 773 K (Table 1). Nevertheless, the sintering was very limited, which implied the high thermostability of the catalyst. It should be noted that part of oxygen present on Pd/CNF/TiO_2/monolith surface derived from TiO_2, rather than acidic groups produced from HNO_3 oxidization. This part of oxygen was hard to remove by heat-treating in nitrogen, which led to comparatively higher O/C value than that on the surface of Pd/MC (0.02) and Pd/CNF (0.03).

Oxygen-containing surface groups had some influence on CAL selective hydrogenation including its reaction rate and product distribution. To begin with, as mentioned in section 3.3(1), initial TOF was calculated to be 0.21 s^{-1} for Pd/CNF/TiO_2/monolith-R, larger than that

for Pd/CNF/TiO_2/monolith-O (0.16 s^{-1}), which indicated the increase in activity after the removal of oxygen-containing surface groups.

In addition, Figure 4.9 showed that selectivity to HCAL in Pd/CNF/TiO_2/monolith-R maintained beyond 90 % at CAL conversion of 90 % and that to COL lower than 8%; In contrast, Pd/CNF/TiO_2/monolith-O obtained comparatively high COL selectivity (more than 13%) at the same conversion. In view of the same textural properties and particle sizes of two catalysts, the change in COL selectivity was related to the amount of oxygen-containing surface groups. Pd/MC and Pd/CNF, the other two catalysts with low O/C weight ratio, had the same trend in COL selectivity as Pd/CNF/TiO_2/monolith-R did.

The experiment results relating to the influence of oxygen-containing surface groups on product distribution were consistent with those reported by Toebes M. L., et al [9]. It is possibly explained by the changing modes of adsorption on carbon support. After the heat-treating in nitrogen, the carbon surface changed gradually from polar to non-polar due to the removal of the oxygen-containing surface groups. This change in polarity can alter the preferential adsorption mode of CAL and, thus, a shift in selectivity. Specifically, Non-polar surface is in favor of the adsorption of aromatic ring, which facilitate the hydrogenation of C=C bond and hence the selectivity to COL decrease, vice versa. Equally, the high surface oxygen content on commercial Pd/AC was very likely to lead to comparatively high COL selectivity (more than 7%) at the beginning of the reaction when excluding its effect of particle size (< 3 nm).

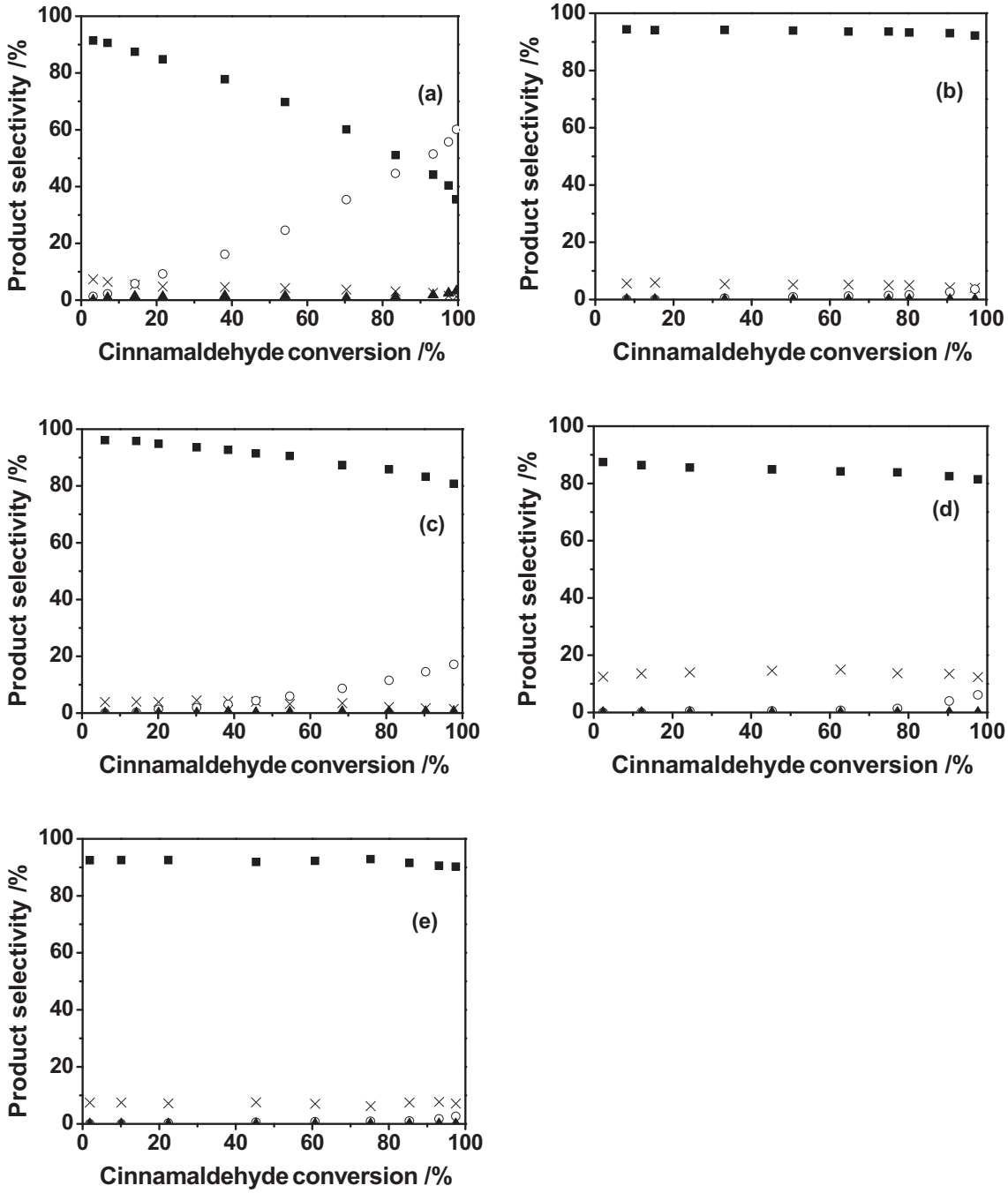

Figure 4.9: Product distribution versus conversion in cinnamaldehyde hydrogenation over 0.5 wt% Pd catalysts including Pd/AC (a), Pd/CNF (b), Pd/MC (c), Pd/CNF/TiO_2/monolith-O (d) and Pd/CNF/TiO_2/monolith-R (e): ■ HCAL, × COL, ○ HCOL and ▲ 1-PB.

(3) Effect of mass transfer limitation

Based on product distributions in CAL hydrogenation over five catalysts, Pd/CNF and Pd/CNF/TiO_2/monolith-R showed the higher selectivity to HCAL than that over other three catalysts (Figure 4.9). Particularly, at CAL conversion of 95%, HCAL selectivity over

Pd/CNF and Pd/CNF/TiO_2/monolith-R were as high as 93% and 90%, respectively, being much higher than that over Pd/AC (approximately 45%); However, the selectivity to HCOL, the product of deep hydrogenation, climbed up to more than 50% over Pd/AC at CAL conversion of 95%, while maintained about 3% over Pd/CNF and Pd/CNF/TiO_2/monolith-R at the same CAL conversion. Noted that, although Pd/CNF/TiO_2/monolith-O had the comparatively lower selectivity to HCAL (approximately 82%) than Pd/CNF and Pd/CNF/TiO_2/monolith-R did due to the effect of oxygen-containing surface groups, selectivity to HCOL over it equally maintained the low level (approximately 5%).

Considered the different textural properties of the catalysts, the distinction in selectivity is very likely due to their mass transfer limitations inside micropores. Particularly, the micropore area on Pd/C/TiO_2/monolith-O(R) and Pd/CNF accounted for only 6.9% and 5.5%, respectively, significantly less than that on Pd/AC (88.9%) (Table 4.1). Herein, we supposed that, when CAL was hydrogenated to HCAL or COL in Pd/C/TiO_2/monolith-O(R) and Pd/CNF, the pores with large size would favored the departure of intermediates to the main solution; While in Pd/AC, HCAL and COL were confined inside the micropores long enough to be further converted to HCOL, even 1-PB due to its serious internal diffusion limitation. It explains why selectivity to the intermediates HCAL and COL over Pd/AC decreased faster than that over Pd/C/TiO_2/monolith-O(R) and Pd/CNF with the reaction continuing.

As discussed in this section, the as-prepared Pd/CNF/TiO_2/monolith-R catalyst exhibited excellent catalytic activity for selective hydrogenation of CAL to HCAL, the similar as powdered Pd/CNF. Although the relatively less surface Pd sites over Pd/CNF/TiO_2/monolith-R than that over Pd/AC, Pd/MC and Pd/CNF due to its small BET surface area led to the decrease of the reaction rate, low acidic oxygen-containing surface groups, as well as macro- and mesoporous structure caused the high selectivity to HCAL over Pd/CNF/TiO_2/monolith-R.

4.4 Conclusions

Macro-structured CNF/TiO_2/monolith composite was synthesized by TiO_2 coating on the surface of the cordierite monolith and the following CNF growth on it. TiO_2 film and CNF coating significantly improved the textural and acid-resistant properties of the composite. The Pd catalyst supported on CNF/TiO_2/monolith, compared with some traditional carbon-supported catalysts including Pd/AC and Pd/MC, exhibited excellent catalytic activity

for selective hydrogenation of CAL to HCAL, the similar as the powdered Pd/CNF. Despite the disadvantage of relatively slow reaction rate on Pd/CNF/TiO_2/monolith-R due to its small BET surface area, low acidic oxygen-containing surface groups, as well as macro- and mesoporous structure made it get the high selectivity to the intermediate HCAL. As a macro-structured CNF support, CNF/TiO_2/monolith is potential in fixed-bed reactions for selective hydrogenations, especially those reactions which are controlled by internal diffusion limitation.

References

[1] G. Neri, L. Bonaccorsi, L. Mercadante, S. Galvagno, Ind. Eng. Chem. Res. 36 (1997) 3554-3562.

[2] A. B. Merlo, B. F. Machado, V. Vetere, J. L. Faria, M. L. Casella, Appl. Catal. A: Gen. 383 (2010) 43-49.

[3] S. Handjani, E. Marceau, J. Blanchard, J. Krafft, M. Che, M. Päivi, N. Kumar, J. Wärnå, D. Y. Murzin, J. Catal. 282 (2011) 228-236.

[4] R. Zheng, M. D. Porosoff, J. L. Weiner, S. Lu, Y. Zhu, J. G. Chen, Appl. Catal. A: Gen. 419-420 (2012) 126-132.

[5] L. Mercadante, G. Neri, C. Milone, A. Donato, S. Galvagno, J. Mol. Catal. A: Chem. 105 (1996) 93-101.

[6] M. Jang, J. K. Park, E. W. Shin, Micropor. Mesopor. Mater. 75 (2004) 159-168.

[7] E. Bus, R. Prins, J. A. van Bokhoven, Catal. Commun. 8 (2007) 1397-1402.

[8] R. Malathi, R. P. Viswanath, Appl. Catal. A: Gen. 208 (2001) 323-327.

[9] M. L. Toebes, T. A. Nijhuis, J. Hájek, J. H. Bitter, A. J. van Dillen, D. Yu. Murzin, K. P. de Jong, Chem. Eng. Sci. 60 (2005) 5682-5695.

[10] A. J. Plomp, H. Vuori, A. O. I. Krause, K. P. de Jong, J. H. Bitter, Appl. Catal. A: Gen. 351 (2008) 9-15.

[11] J.L. Margitfalvi, I. Borbáth, M. Hegedűs, A. Tompos, Appl. Catal. A: Gen. 229 (2002) 35-49.

[12] G. F. Santori, M. L. Casella, O. A. Ferretti, J. Mol. Catal. A: Chem. 186 (2002) 223-239.

[13] U. K. Singh, M.A. Vannice, Appl. Catal. A: Gen. 213 (2001) 1-24.

[14] H. Yamada, S. Goto, J. Chem. Eng. Jpn. 36 (2003) 586-589.

[15] A. M. R. Galletti, C. Antonetti, A. M. Venezia, G. Giambastiani, Appl. Catal. A: Gen. 386 (2010) 124-131.

[16] W. Liang, S. Yokojima, M. F. Ng, G. Chen, G. He, J. Am. Chem. Soc. 123 (2001) 9830-9836.

[17] S. Iijima, Nature, 354 (1991) 56-58.

[18] J. K. Chinthaginjala, L. Lefferts, Appl. Catal. B: Environ. 101 (2010) 144-149.

[19] J. M. Planeix, N. Coustel, B. Coq, V. Bretons, P. S. Kumbhar, R. Dutartre, P. Geneste, P. Bernier, P. M. Ajayan, J. Am. Chem. Soc. 116 (1994) 7935-7936.

[20] X. Zhang, Y. C. Guo, Z. C. Zhang, J. S. Gao, C. M. Xu, J. Catal. 292 (2012) 213-226.

[21] J. K. Chinthaginjala, K. Seshan, L. Lefferts, Ind. Eng. Chem. Res. 46 (2007) 3968-3978.

[22] P. Li, T. Li, J. H. Zhou, Z. J. Sui, Y. C. Dai, W. K. Yuan, D. Chen. Micropor. Mesopor. Mater. 95 (2006) 1-7.

[23] N. A. Jarrah, F. Li, J. G. van Ommen, L. Lefferts, J. Mater. Chem. 15 (2005) 1946-1953.

[24] P. Tribolet, L. Kiwi-Minsker. Catal. Today, 105 (2005) 337-343.

[25] J. K. Chinthaginjala, J. H. Bitter, L. Lefferts, Appl. Catal. A: Gen. 383 (2010) 24-32.

[26] Q. Liu, Z. Liu, W. Wu, Catal. Today 147 (2009) S285-S289.

[27] C. Hung, J. Hazard. Mater. 180 (2010) 561-565.

[28] L. E. Gómez, I. S. Tiscornia, A. V. Boix, E. E. Miró, Appl. Catal. A: Gen. 401 (2011) 124-133.

[29] P. Avila, M. Montes, E. E. Miró, Chem. Eng. J. 109 (2005) 11-36.

[30] E. García-Bordejé, I. Kvande, D. Chen, M. Rønning, Adv. Mater. 18 (2006) 1589-1592.

[31] N. Jarrah, J. G. van Ommen, L. Lefferts, Catal. Today 79-80 (2003) 29-33.

[32] M.A. Ulla, A. Valera, T. Ubieto, N. Latorre, E. Romeo, V.G. Milt, A. Monzón, Catal. Today, 133-135 (2008) 7-12.

[33] X. Yu, B. Lin, B. Gong, J. Lin, R. Wang, K. Wei, Catal. Lett. 124 (2008) 168-173.

[34] S. Morales-Torres, A.F. Pérez-Cadenas, F. Kapteijn, F. Carrasco-Marín, F. J. Maldonado-Hódar, J. A. Moulijn, Appl. Catal. B: Environ. 89 (2009) 411-419.

[35] P. Weerachawanasak, P. Praserthdam, M. Arai, J. Panpranot, J. Mol. Catal. A: Chem. 279 (2008) 133-139.

[36] M. Englisch, A. Jentys, J. A. Lercher, J. catal. 166 (1997) 25-35.

[37] Q. H. Tian, G. L. Zhao, G. R. Han, J. Inorg. Mater. 19 (2004) 147-152.

[38] T. Tsoufis, P. Xidas, L. Jankovic, D. Gournis, A. Saranti, T. Bakas, M. A. Karakassides, Diam. Relat. Mater. 16 (2007) 155-160.

[39] J. M. Wu, J. J. Yao, H. P. Yang, Y. N. Fan, B. L. Xu, Acta. Chim. Sinica. 68 (2010) 1349-1356.

[40] C. J. Li, B. X. Ma, X. X. Huo, New Carbon Mater. 14 (1999) 22-28.

[41] P. Gallezot, D. Richard, Catal. Rev. Sci. Eng. 40 (1998) 81-126.

[42] K. Chizari, I. Janowska, M. Houllé, I. Florea, O. Ersen, T. Romero, P. Bernhardt, M. J. Ledoux, C. Pham-Huu, Appl. Catal. A: Gen. 380 (2010) 72-80.

[43] F. Rodriguez-Reinoso, Carbon 36 (1998) 159-175.

[44] T. G. Ros, A. J. van Dillen, J. W. Geus, D. C. Koningsberger, Chem. Eur. J. 8 (2002) 1151-1162.

Chapter 5

Influence of Internal Diffusion on Selective Hydrogenation of 4-Carboxybenzaldehyde over Palladium Catalysts Supported on Carbon Nanofiber Coated Monolith

Abstract

In this study, a macro-structured Pd catalyst supported on carbon nanofiber coated on cordierite monolith (Pd/CNF/TiO_2/monolith) was employed for hydrogenation of 4-CBA. The effect of mass transfer on the catalyst performance was studied experimentally and the results are described using a simple kinetic model. The results were compared to Pd catalysts supported on activated carbon (Pd/AC) and on carbon nanofibers aggregates (Pd/CNF). Catalytic performance of the Pd/CNF/TiO_2/monolith is similar to Pd/CNF and the Pd/AC with particles as small as 50 micron (Pd/AC50), whereas Pd/AC with larger support particles revealed a lower activity per Pd active surface site, due to internal mass transfer limitation. Also the selectivity to the intermediate hydrogenation product (4-HMBA), versus deep hydrogenation to p-TA, is clearly affected by internal mass transfer. Pd/AC with large particles (3000 μm) achieves a maximum yield to the intermediate product of only 35%, whereas all the other catalysts achieve typically 70%. Remarkably, the conversion level at which the maximum yield of the intermediate product is achieved is highest for the Pd/CNF/TiO_2/monolith. This advantage is assigned to superior internal mass transfer properties, thanks to high porosity, low tortuosity and short diffusion length of the CNF layer. Clearly, the CNF/TiO_2/monolith applied as a fixed bed outperforms slurry phase catalysts, abandoning the need of a filtration section.

This part of work has been published as Research Article: J. Zhu, F. Wu, M. Li, J. Zhu, J. G. van Ommen, L. Lefferts, *Appl. Catal. A: Gen.* 498 (2015) 222-229.

5.1 Introduction

Activated carbon (AC) is commonly used as a catalyst support in chemical industry due to its advantages including high surface area and resistance to acid [1-3]. However, like two sides of a coin, its high micro-porosity, the main contributor to its high surface area, can also be the origin of significant internal mass transfer limitation in the catalyst. This effect might be reduced by decreasing the particle size, at the expense of increasing the costs for catalyst filtration as well as catalyst loss [4]. For the purpose of preventing these disadvantages, many attempts have been made to develop mesoporous structured supports, allowing operation in a fixed-bed reactor without significant internal diffusion limitation.

Macro-structured carbon nanofibers, which could be prepared by depositing carbon nanofibers (CNFs) on the surface of a preformed base material, is a candidate to substitute activated carbon. CNFs possess exceptional properties including its open structure, high external surface area and high pore volume in absence of any micro porosity [5-7]. For example, macro-structured CNFs supports were developed on metal foam [8-11] and carbon felt [6, 12] in recent years. Pd catalysts on these supports were reported to exhibit a high catalytic activity in selective hydrogenation of nitrite and oxidative dehydrogenation of ethylbenzene.

Cordierite monoliths are widely used in new reactor applications in chemical and petro-chemical processing, as well as catalytic combustion and cleaning of exhaust gases [13-15]. It offers several advantages such as a high geometric external surface, short diffusion lengths, structural durability, a low pressure drop and a low thermal expansion coefficient and mechanical stability [16, 17]. These features also make monolithic structures suitable for three-phase catalytic reactions because it combines the advantages of slurry reactors and trickle-bed ones, while eliminating their disadvantages [18, 19].

However, its small surface area (<1 m^2/g) limits its direct applications in catalysis. Therefore, a coating with high specific surface area is usually deposited, covering the surface of monolith, in order to increase its effective surface area, facilitating high metal dispersions. Such thin washcoated layers are usually made by depositing an oxide layer (alumina, silica, etc) with texture and porosity similar to traditional catalyst support particles. Different parameters can be adjusted, such as thickness of the layer, governing the diffusion length and porosity of the layer. But the porous washcoated layers generally suffer from relatively low

pore volume and high tortuosity, hampering internal mass transfer. It urges the use of alternative thin layers such as entangled carbon nanofibers (CNFs) or nanotubes (CNTs) as support to satisfy the demands (high pore volume, high surface area and low tortuosity) for effective internal mass transfer [18, 20]. In our previous work [17], we prepared a CNF coated cordierite monolith support (CNF/TiO_2/monolith) with a "sandwich" structure, where the CNFs layer was grown on the titania (TiO_2) film coated monolith. Results showed that after the CNF coating, its textural and acid-resistant properties improved greatly, compared with the bare monolith, while the CNF's are strongly anchored to the monolith. Moreover, CNF/TiO_2/monolith supported Pd catalyst (Pd/CNF/TiO_2/monolith) exhibited a high selectivity to the intermediate product in cinnamaldehyde hydrogenation, which was attributed to elimination of internal diffusion limitation in the catalyst. This confirmed the potential of CNF/TiO_2/monolith support in three-phase catalysis.

Purified terephthalic acid (PTA) is an important industrial raw material used for the manufacture of polyethylene terephthalate (PET), polybutylene terephthalate (PBT) and polytrimethylene terephthalate (PTT), which are mainly applied in the production of fibers, resins, films and fabrics [21,22]. In the process of two companies, i.e. Scientific Design and Amoco MC [23, 24], the terephthalic acid (TA) production is based on the liquid-phase oxidation of *p*-xylene (PX) using a homogeneous catalyst $Co(OAc)_2$, HBr, and a cocatalyst $Mn(OAc)_2$. The obtained crude terephthalic acid (CTA) usually contains approximately 2000-6000 μg/g of 4-carboxybenzaldehyde (4-CBA) as the main impurity, which would decrease the polymerization rate during the production of PET, PBT and PTT [25]. Therefore, the main upgrading step in refining CTA to PTA is the catalytic hydrogenation of 4-CBA to 4-(hydroxymethyl) benzoic acid (4-HMBA) and further to *p*-toluic acid (*p*-TA) in water (Figure 5.1) [26, 27]. 4-HMBA and *p*-TA are more soluble than 4-CBA and are thus much easier removed during PTA-crystallization, staying behind in the liquid. An activated carbon supported palladium catalyst (Pd/AC) is commonly used for PTA refinement [28], leading to the main product of *p*-TA due to the serious mass transfer limitation in Pd/AC. Nevertheless, only a few reports have focused on the product distribution, i.e. 4-HMBA and *p*-TA [29, 30].

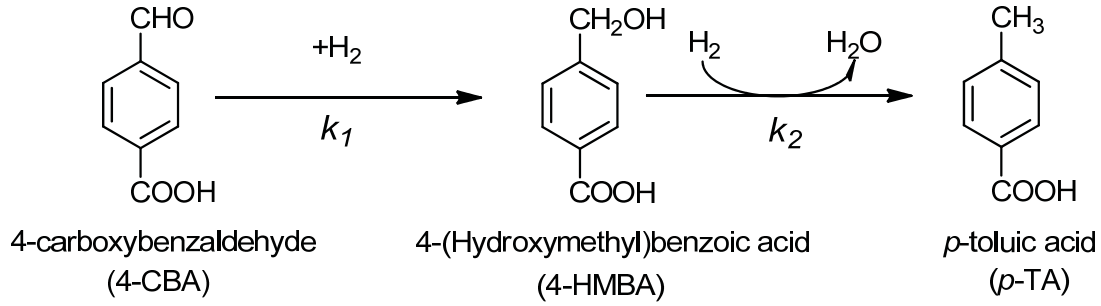

Figure 5.1: Pathway of 4-carboxybenzaldehyde hydrogenation

The formation of 4-HMBA is preferred over *p*-TA because 4-HMBA is better soluble in water, simplifying the separation. Furthermore, formation of 4-HMBA requires less hydrogen then p-TA. In addition, 4-HMBA is also an important monomer for the synthesis of the corresponding homopolymers, poly(p-methylenebenzoate) and its corresponding ester, methyl p-hydroxymethylbenzoate (mep-HMB) [31].

In this study, a macro-structured Pd/CNF/TiO_2/monolith catalyst was employed for the hydrogenation of 4-CBA. The effect of mass transfer on the catalyst performance was studied experimentally and the results are described using a simple kinetic model. For comparison, Pd catalysts supported on activated carbon (Pd/AC) and carbon nanofiber agglomerates (Pd/CNF) with the same Pd loading as that of Pd/CNF/TiO_2/monolith were investigated under the same working conditions.

5.2 Experimental

5.2.1 Preparation of CNF/TiO_2/monolith support

A cordierite monolith with the total BET surface area of less than 1 m^2/g, cell density of 62 cells/cm^2 (400 cpsi) and a wall thickness of 0.18 mm was purchased from Nanjing Gaochun ceramic company. The preparation procedure of CNF/monolith is described in detail in our previous publication [17]. In summary, bare monolith was first coated with a TiO_2 layer using a dip coating method. A Ni precursor was then introduced by impregnating TiO_2 coated monolith with a $Ni(NO_3)_2$ solution. The samples were dried overnight prior to calcination. After that, the samples were reduced in a gas mixture of N_2 and H_2, followed by CNF synthesis in methane resulting in 18.7 wt. % CNFs on the monolith. Finally, the exposed nickel metal particles were removed by leaching in HNO_3.

5.2.2 Pd deposition

A 0.5 wt% Pd catalyst was prepared by the adsorption method. Specifically, CNF

agglomerates (diameter of CNFs in a range of 20-40 nm, BET surface area 180 m^2/g, Chengdu Organic chemical, China) with the size of 177-149 μm were selected using 80 and 100 mesh sieves. The CNFs agglomerates were dispersed directly in a hydrochloric acid (HCl) solution (0.2 M) of palladium (II) chloride ($PdCl_2$, Sinopharm, China). CNF/TiO_2/monolith were placed in a home-made small basket with the size of ϕ 25×40 mm and the mean opening of the basket screen of 1.19 mm (16 mesh), which was fixed to the axle of a stirrer, and the stirrer was immersed in the $PdCl_2$ solution. The CNFs agglomerates and the CNF/TiO_2/monolith were stirred continuously for 4 hours. After that, the CNF/monolith was removed from the solution and the CNF agglomerates were filtered off, followed by drying overnight at 393 K. Finally the samples were reduced in a quartz tube at 493 K at a heating rate of 2 K/min in a stream of N_2/H_2 (80:20) for 2 h. The catalysts prepared were named Pd/CNF/TiO_2/monolith and Pd/CNF160, respectively.

5.2.3 Selection to a series of Pd/AC catalysts with different particle size

The commercial Pd/AC3000 pellets (Pd loading 0.5 wt%, homogeneous distribution, irregular particles, ϕ≈3 mm, 810 m^2/g, Sinopec Yangzi, China) were crushed to small particles with different sizes of 177-149 μm and 53-44 μm, using sieves of 80 and 100 mesh, 270 and 325 mesh (Shanghai Fengxing Sieve ManuACturing Co., Ltd.), respectively. The resulting samples were hence named Pd/AC160 and Pd/AC50. These Pd/AC catalysts were employed to study the effect of internal diffusion limitation in the particles.

5.2.4 Characterizations of Pd catalysts

The Pd/CNF/TiO_2/monolith, the Pd/CNF prepared in the section 5.2.2 and the Pd/AC3000 were characterized in detail. The BET specific surface areas were determined with a Micromeritics ASAP 2010 apparatus. Scanning electron images and elemental distributions were recorded using a JEOL JSM-6360 LA scanning electron microscope. The Pd particle sizes were obtained with a JEM-2100 transmission electron microscopy (TEM). Average Pd particle size of each catalyst was statistically measured by 2 TEM images with at least 50 particles. The Pd loading was determined by Vista-AX inductively coupled plasma atomic emission spectrometry (ICP-AES). The Pd dispersions were calculated using hemispherical model, in which, Pd hemispheres are assumed to be exposed as the metal particle surface [32].

5.2.5 Catalytic property of Pd catalysts on 4-CBA hydrogenation

The catalytic performance of Pd/CNF/TiO_2/monolith was evaluated in the 4-CBA hydrogenation, and the result was compared to that of the Pd/CNF160 and the Pd/AC serie

catalysts. The experiments were conducted in a 500 ml pressurized stirred basket semi-batch autoclave (Figure 5.2) at 363 K and 1.5 MPa hydrogen pressure. An electric-heating mantle outside the autoclave supplied the heat to the reactor, and hydrogen flow maintained the reaction pressure, together with a back-pressure regulator in the gas outlet. Macro-structured catalysts (Pd/CNF/TiO_2/monolith and Pd/AC3000) were placed in the baskets, as described in the section 2.2, while the powder catalyst Pd/CNF160, Pd/AC160 and Pd/AC50 were dispersed directly in the solution. Approximately 0.5 g of the catalysts was dispersed in a 200 ml aqueous solution of 4-CBA (0.2 wt.%, A.R, Sinopharm, China), and the autoclave was flushed with nitrogen before pressurizing with hydrogen, in order to remove dissolved oxygen. Starting the stirrer commenced the reaction. The detailed reaction conditions are summarized in Table 5.1. Samples (1 ml) were withdrawn from the reactor every 10-30 min, filtered immediately to separate the catalyst particles and analyzed by HPLC (Agilent LC 1260) equipped with a 250 mm long C-18 column and a UV detector (wavelength 254 nm). 4-CBA conversion (X), the selectivity towards the 4-HMBA (S_{HMBA}) and *p*-TA (S_{pTA}) were defined as Equation 5.1-5.3.

$$X = \frac{C^0_{CBA} - C_{CBA}}{C^0_{CBA}} \times 100\% \quad 5.1$$

$$S_{HMBA} = \frac{C_{HMBA}}{C^0_{CBA} - C_{CBA}} \times 100\% \quad 5.2$$

$$S_{pTA} = \frac{C_{pTA}}{C^0_{CBA} - C_{CBA}} \times 100\% \quad 5.3$$

where C_{CBA}, C_{HMBA} and C_{pTA} are the instant molar concentration of 4-CBA, 4-HMBA and *p*-TA during the reaction; C^0_{CBA} is the initial molar concentration of 4-CBA (13.3 μmol/ml, Table 5.1). The mass balance was close to or even better than 97%.

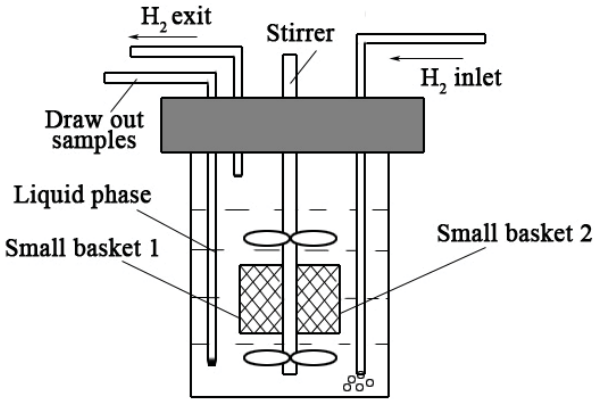

Figure 5.2: Scheme of the reaction setup.

Table 5.1 Reaction conditions for 4-CBA hydrogenation

Reaction condition	value
Reaction temperature, T (K)	363
Pressure, P (MPa)	2.0
Agitation, A (rpm)	200-1000
Mass of H_2O, m_{H2O} (g)	200
Mass of 4-CBA, m_{CBA} (g)	0.4
Mass of the catalyst, m_{cat} (g)	0.5
Initial concentration of 4-CBA, C^0_{CBA} (μmol/ml)	13.3

5.3 Results and discussion

5.3.1 Structure of Pd/CNF/TiO_2/monolith, Pd/CNF and Pd/AC

The structural properties of the catalysts including BET surface area, micropore area and average pore size were summarized in Table 5.2; it should be noted that the properties of Pd/AC160 and Pd/AC50 are very similar to Pd/AC3000, except for the diffusion length, obviously. Pd/AC had the highest BET surface area (810 m^2/g·cat) in these samples due to its predominant micropores (approximately 90% of total BET surface area). There was no significant change in surface area on grinding. In contrast, the Pd/CNF/TiO_2/monolith possessed low BET surface area (30 m^2/g·cat). However, considering the fact that the CNF/TiO_2/monolith contains 18.7 wt. % CNFs (Table 5.2), the BET surface area reached 160 m^2 per gram CNF (m^2/g·CNF), similar to CNFs agglomerates (180 m^2/g·cat). Based on the surface area, weight of the CNFs and assuming cylindrical shape and density equal to the density of graphite (1.8 g/cm^3), the diameter of the growing CNF on monolith and CNF agglomerates is estimated to be about 20 nm, in reasonable agreement with the observations in TEM pictures (25-30 nm, Figure 5.3b and 5.3c).

Table 5.2 Properties of palladium catalysts

	Pd/AC3000 [a]	Pd/CNF160	Pd/CNF/TiO_2/monolith
Carbon deposit on the monolith (wt. %)	-	-	18.7
Bulk density of catalyst, ρ (g/cm^3)	0.48	0.38	1.8
Average diffusion length, R_p (cm)	0.15	8×10-3	9×10-3
BET surface area, S_{total} ($m^2/g{\cdot}cat$)	810	180	30
Micropore area, S_{micro} ($m^2/g{\cdot}cat$)	720	10	2
Pore Volume, V_{pore} (cm^3/g)	0.43	0.27	0.085
Average pore size, d_p (nm)	2.1	6.1	11.3
Tortuosity, τ [b]	3.5	2.0	2.0
Porosity, $\theta = V_{pore}{\cdot}\rho$	0.21	0.10	0.15
Pd loading (wt.%) [c]	0.50	0.52	0.48
Pd loading per gram carbon (wt. %)	0.50	0.52	2.6
Pd particle size (nm) [d]	2.8 ± 0.6	5.6 ± 1.2	19.2 ± 3.1
Pd dispersion (%) [e]	43.4	21.7	6.3
Concentration of Pd-surface atoms (μmol/g C) [f]	20.4	10.2	16.1

Note: (a) Pd/AC160 and Pd/AC50 are similar to Pd/AC3000, except the average diffusion length (80 and 25 μm, respectively)

(b) According to the reference of R. Ocampo-Pérez et al. [33];

(c) Based on total weight;

(d) Mean value of 50 particles, ± the standard deviation (Figure S5.1);

(e) Calculated assuming hemispherical Pd particles on the surface of the support;

(f) Concentration of Pd surface atom (μmol) per gram of carbon.

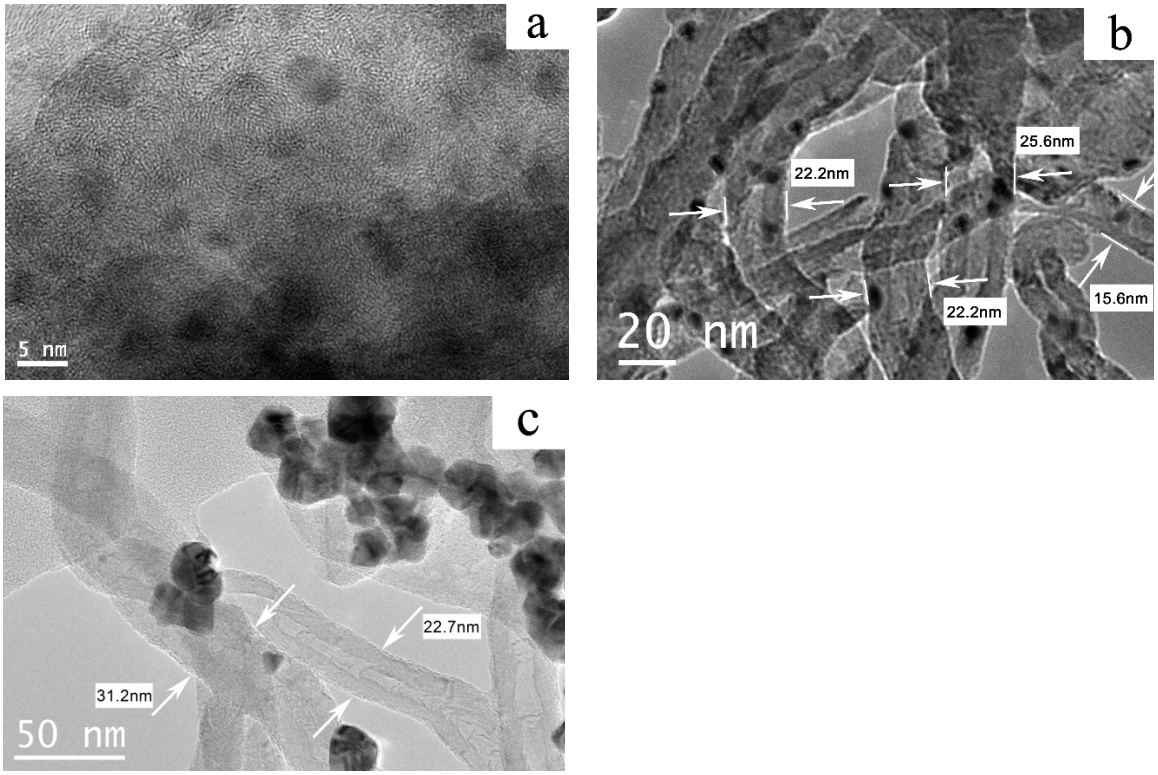

Figure 5.3: TEM images of Pd catalysts: (a) Pd/AC3000; (b) Pd/CNF160; (c) Pd/CNF/TiO_2/monolith.

In spite of the relatively low BET surface area, Pd/CNF/TiO_2/monolith possessed an excellent pore structure for selective hydrogenation. Its apparent micropore area was calculated, based on N_2 adsorption-desorption data, to be insignificant, and the average pore size 11.3 nm (Table 5.2), which inferred the mesoporous structure of the material. Note that the pore size distributions are calculated assuming capillary condensation; however, entangled CNFs actually do not really contain pores. Instead this structure resembles the inverse structure of a classical porous support [34]. Consequently, the pore size data results in apparent values.

Moreover, the size and dispersion of palladium particles were obtained from TEM images (Figure 5.3) and results were summarized in Table 5.2. The Pd dispersion increased from 6% on the Pd/CNF/TiO_2/monolith to 43% on Pd/AC3000 with increasing BET surface area of the support. Also, the Pd loading per gram of carbon is significantly higher on the Pd/CNF/TiO_2/monolith (2.6 *versus* 0.5 wt. %, Table 5.2), contributing to increasing particle size and decreasing dispersion. Remarkably, the concentration of Pd surface atoms on Pd/AC and Pd/CNF/TiO_2/monolith, i.e. the concentration of active sites, is rather similar as can be seen in Table 5.2 (see Equation 5.5). Furthermore, Pd is reasonably evenly distributed through the AC3000 support, as observed with SEM-EDX in Figure 5.4. As the catalyst support with

the longest diffusion distance (AC3000) resulted in homogeneous distribution of Pd, it seems reasonable to assume this is true for all catalysts in this study.

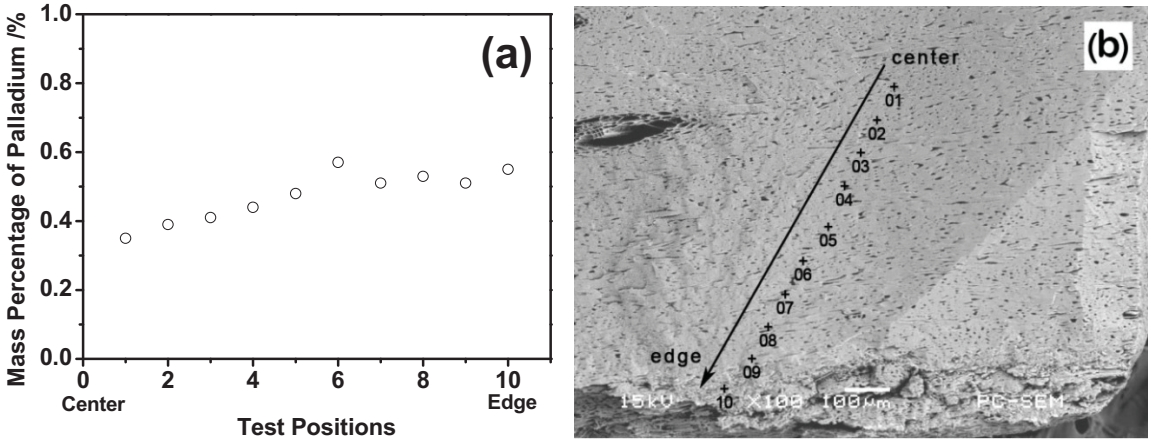

Figure 5.4: The concentration of Pd as function of the position at the cross section of AC3000 support (a); (b) indicates the position of the points chosen for Pd analysis at the cross section.

5.3.2 Catalytic performance

First, it was experimentally checked that a stirring speed of 800 rpm was sufficient to rule out any external transport limitation for both Pd/AC3000 and Pd/CNF/TiO_2/monolith, as described in supporting information (Figure S5.2). So, stirring speed of 800 rpm was employed in all experiments. The conversion of 4-CBA and product yield vs. reaction time on Pd/AC3000, Pd/CNF/TiO_2/monolith, Pd/AC50, Pd/AC160 and Pd/CNF160 are given in Figure 5.5. On Pd/AC3000 (Figure 5.5a), the conversion of 4-CBA completed in 22 h and the main product (96%) is the fully hydrogenated *p*-TA. The intermediate product 4-HMBA is dominant initially, but is disappearing almost completely when approaching full conversion (Figure 5.1), typical for a consecutive reaction scheme.

Compared with Pd/AC3000, Pd/CNF/TiO_2/monolith (Figure 5.5b) exhibits a lower observed activity for the two samples with identical Pd amounts; which is probably due to the lower Pd dispersion on Pd/CNF/TiO_2/monolith (Table 5.2 and Figure 5.3), considering the fact that the Pd loading and amount of catalyst used was constant. Moreover, the product distribution is very different, with 4-HMBA as the main product throughout. Pd/AC160, Pd/AC50 and Pd/CNF160 gave similar results (Figure 5.5c-5.5e).

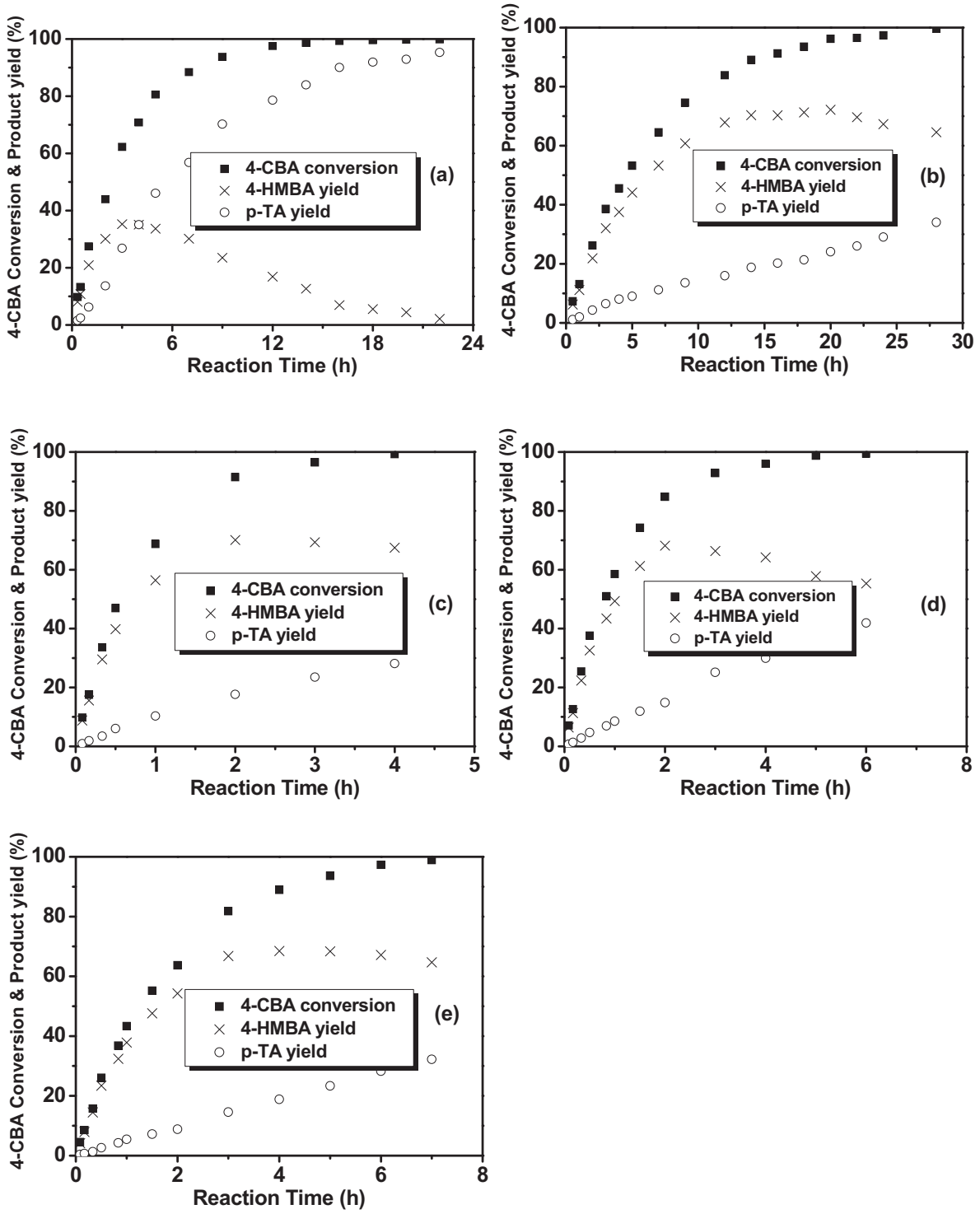

Figure 5.5: The 4-CBA conversion and product yield as a function of time over Pd/AC3000 (a), Pd/CNF/TiO_2/monolith (b), Pd/AC50 (c), Pd/AC160 (d) and Pd/CNF160 (e): ■ 4-CBA conversion; × 4-HMBA yield; ○ *p*-TA yield.

Since 4-CBA hydrogenation is generally considered as a first-order reaction in 4-CBA [1,

35, 36], whereas the hydrogen concentration was kept constant, apparent reaction rate constants (k_1) for 4-CBA hydrogenation (Figure 5.1) were calculated based on total conversion of 4-CBA over Pd catalysts by Equation 5.4 and fitted in Figure 5.6.

$$ln\frac{1}{1-X} = k_1 t \qquad 5.4$$

Where X represents the total conversion of 4-CBA at reaction time t.

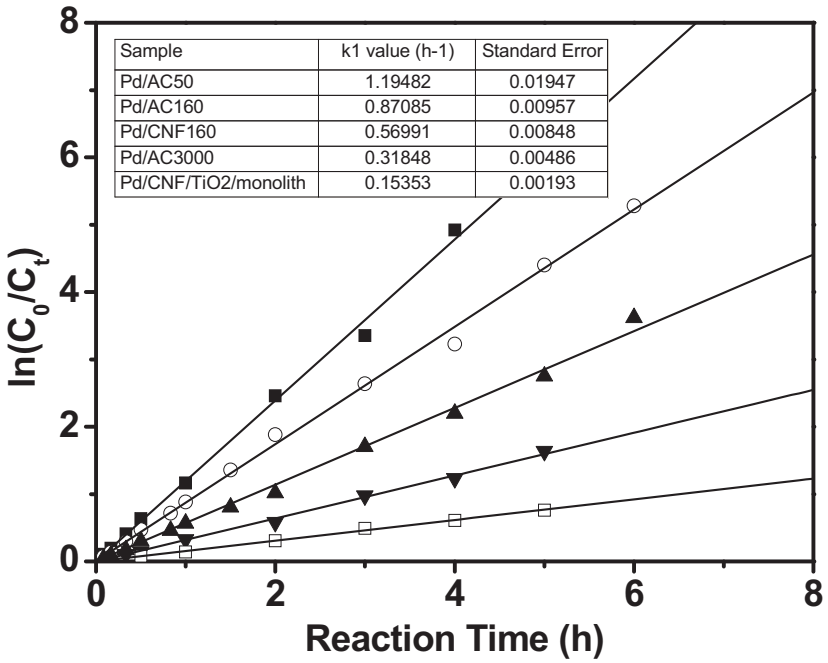

Figure 5.6: Reaction constants for 4-CBA hydrogenation to 4-HMBA over □Pd/CNF/TiO_2/monolith; ▼Pd/AC3000; ▲Pd/CNF160; ○ Pd/AC160; ■ Pd/AC50.

Figure 5.6 shows that Pd/AC50 possessed the highest reaction rate constant (approximately 1.19 h^{-1}) whereas the Pd/CNF/TiO_2/monolith had the lowest observed activity (0.15 h^{-1}), in line with the discussion above. Therefore the initial reaction rate per mole of surface-Pd, which is equivalent to an initial TOF, was calculated, based on Equation 5.5 to estimate the amount of Pd surface sites available.

$$N_{Pd} = \frac{m_{cat} \cdot Lo_{Pd} \cdot Dis_{Pd}}{106.4} \qquad 5.5$$

N_{Pd} is the total molar amount of surface Pd sites, m_{cat} is the amount of the employed catalyst in the reaction, Lo_{Pd} and Dis_{Pd} are Pd loading and dispersion, respectively. The values of the resulting initial reaction rate in TOF are presented in Table 5.3; clearly the values for Pd/AC3000 are much lower, and for Pd/AC160 are somewhat lower as compared to the three other catalysts. Table 5.3 also shows estimated values of Weisz-Prater numbers ($N_{W\text{-}P}$), Thiele

modulus (ϕ) and internal diffusion effectiveness factor (η), as detailed in the SI. The calculated Weisz-Prater numbers ($N_{W\text{-}P}$) and internal effectiveness factors (η) of H_2 and 4-CBA all indicate insignificant internal diffusion limitations for Pd/AC50, Pd/CNF160 and Pd/CNF/TiO_2/monolith. The data indicate a minor influence of diffusion on the performance of Pd/AC160, whereas the performance of Pd/AC3000 is clearly strongly affected by diffusion limitation. This is in line with the differences in the initial TOF, discussed above.

Table 5.3 Internal diffusion limitations for 4-CBA hydrogenation over Pd catalysts

Sample	Initial rate in TOF (min^{-1})	H_2			4-CBA		
		W-P number (N_{WP})	Thiele modulus (ϕ)	Effectiveness factor (η)	W-P number (N_{WP})	Thiele modulus (ϕ)	Effectiveness factor (η)
Pd/AC3000	1.3	12.2	5.1	0.5	238	80	0.04
Pd/AC160	3.8	0.1	0.3	~1.0	1.4	1.2	0.91
Pd/AC50	5.2	0.01	0.1	~1.0	0.2	0.5	0.98
Pd/CNF160	4.8	0.07	0.3	~1.0	1.1	1.1	0.93
Pd/CNF/TiO_2/ monolith	4.7	0.02	0.1	~1.0	0.3	0.6	0.98

Furthermore, considering absence of any diffusion limitation for Pd/AC50, Pd/CNF160 and the Pd/CNF/TiO_2/monolith, it is evident that the intrinsic TOF values are constant, despite the large variation in Pd dispersion and particle size, but constant numbers of active surface sites (2.8, 5.6 and 19.2 nm, respectively, Table 5.2 and Figure 5.3). Thus, hydrogenation of 4-CBA over Pd catalyst is clearly structure-insensitive.

Figure 5.7 shows the product selectivity and the 4-HMBA yield as function of conversion of 4-CBA for all five catalysts. Clearly, Pd/AC3000 exhibited much lower selectivity to 4-HMBA as compared to all other catalysts; differences between these four catalyst are not easily detected. The relationship between instant yield of 4-HMBA and intrinsic rate constant k_1, k_2 (Figure 5.1) and instant conversion of 4-CBA, assuming first order consecutive reaction, can be written as Equation 5.6, assuming absence of any transport limitations [37].

$$Y_{HMBA} = \frac{k_1/k_2}{k_1/k_2 - 1}(1 - X_{CBA})[(1 - X_{CBA})^{\frac{1}{k_1/k_2} - 1} - 1] \quad 5.6$$

If significant diffusion limitation occurs (i.e. Thiele modus of 4-HMBA ϕ_{HMBA}>3),

Equation 5.7 should be used [37].

$$Y_{HMBA} = \frac{k_1/k_2}{k_1/k_2 - 1}(1 - X_{CBA})[(1 - X_{CBA})^{\frac{1}{\sqrt{k_1/k_2}}-1} - 1] \quad 5.7$$

In Equations (5.6) and (5.7), X_{CBA} and Y_{HMBA} are the instant conversion of 4-CBA and the instant yield of 4-HMBA in the reaction, k_1 and k_2 are the intrinsic rate constants of the reaction of 4-CBA to 4-HMBA and the reaction of 4-HMBA to *p*-TA, respectively.

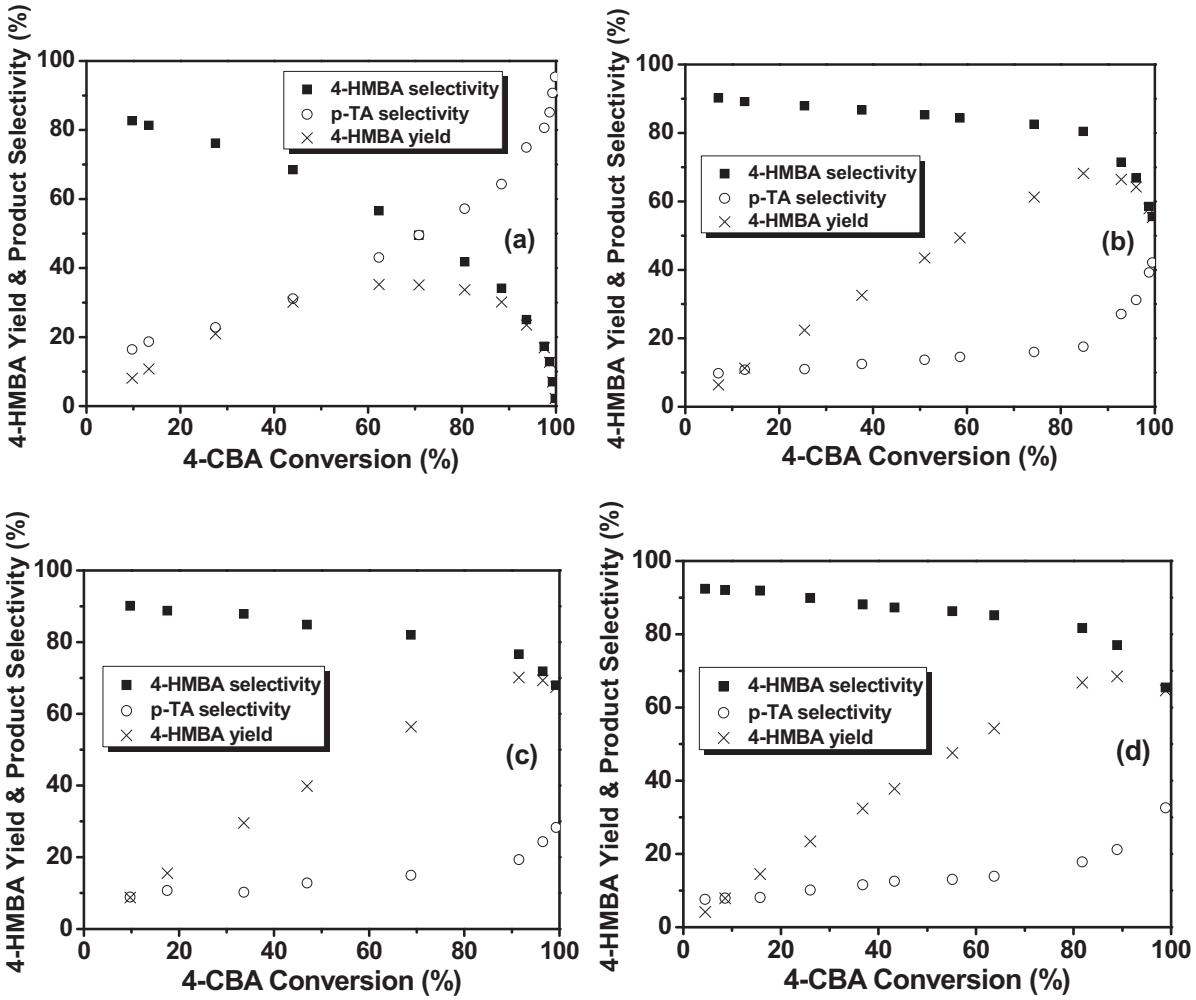

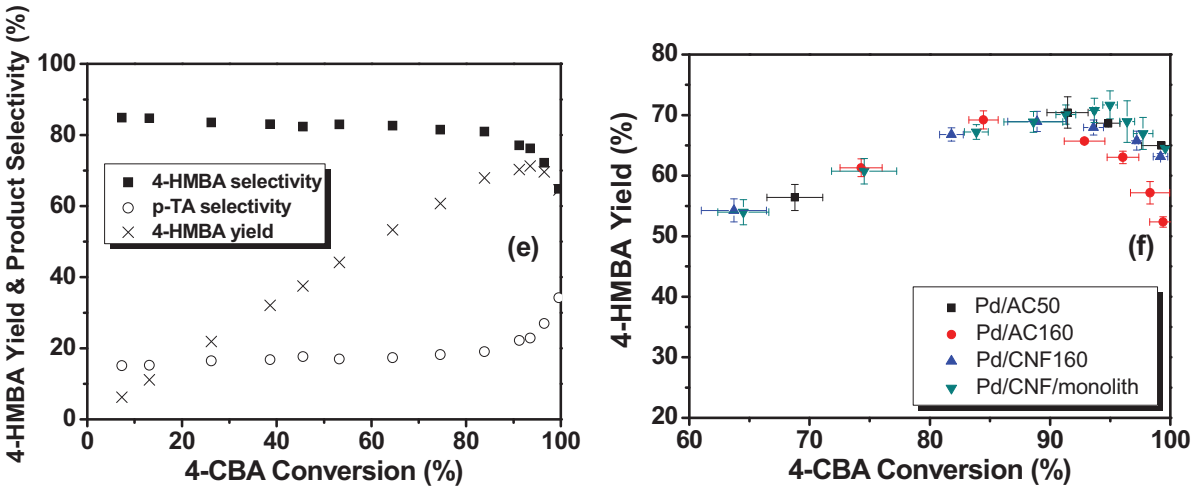

Figure 5.7: The 4-HMBA yield & product selectivity versus conversion in 4-CBA hydrogenation over 0.5 wt% Pd/AC3000 (a), Pd/AC160 (b), Pd/AC50 (c), Pd/CNF160 (d), Pd/CNF/TiO_2/monolith (e) and a comparison of the yield curves for the last four catalysts (f): ■ 4-HMBA; ○ *p*-TA .

Table 5.4 Ratio of k_1 to k_2 and max yield of 4-HMBA for 4-CBA hydrogenation on Pd catalysts

Pd catalyst	k_1/k_2	Max yield of 4-HMBA (%) [c]	4-CBA conversion at max 4-HMBA yield (%) [c]
Pd/AC3000	4.0 [a] (1.2 [b])	35 ± 1	63 ± 1
Pd/AC160	6.2	69 ± 2	85 ± 2
Pd/AC50	7.4	70 ± 3	92 ± 1
Pd/CNF160	6.8	69 ± 2	89 ± 1
Pd/CNF/TiO_2/monolith	7.6	72 ± 2	95 ± 1

Note: (a) Calculation using Equation 5.7;

(b) Calculation using Equation 5.6;

(c) Mean value of 3 repeated tests, ± the standard deviation

Table 5.4 shows the results of calculation of the intrinsic selectivity factor (k_1/k_2) for Pd/AC50, Pd/AC160, Pd/CNF160 and Pd/CNF/TiO_2/monolith using Equation 5.6. Rather similar values around 7 are obtained, confirming mass transfer limitation has a minor influence. In contrast, application of Equation 5.6 on the data of Pd/AC3000 results in a much lower value of 1.2. The fact that the selectivity factor (k_1/k_2) estimated using Equation 5.7 results in about 4, significantly closer to the intrinsic value observed for the other catalysts, confirms the effect of mass transfer limitation on the selectivity of Pd/AC3000. The details of the calculation procedure can be found in the supporting information (Figure S5.3).

Table 5.4 also shows the maximum yield to 4-HMBA as well as the 4-CBA conversion at which this maximum yield is realized for all catalyst without major diffusion issues, based on Equation 5.6. It can be seen that the differences in maximum yield are not significant as the error margin is too large. In contrast, significant differences are observed when comparing the conversion level where the maximum yield is obtained. The Pd/CNF/TiO_2/monolith maintains high selectivity for conversions up to 95%, which we attribute to minimization of concentration gradients. This effect is observed in increasing extent in the order: Pd/AC3000 <<< Pd/AC160 < Pd/CNF160 < Pd/AC50 < Pd/CNF/TiO_2/monolith. In fact, this trend can also be observed in Figure 5.7f.

In other words, Pd/CNF/TiO_2/monolith performs at least similar to slurry catalyst with the smallest particle size, without the disadvantage of the need for a filtration section. Pd/CNF/TiO_2/monolith clearly outperforms the other catalyst that can be used in fixed bed (Pd/AC3000), despite the fact that the concentration of active sites is similar.

5.4 Conclusions

The structured Pd/CNF/TiO_2/monolith performs similar to Pd supported on AC with particles as small as 50 micron. This is based on both the reaction rates observed, as well as on the effect of selectivity to the intermediate product (4-HMBA) in hydrogenation of 4-CBA, limiting the formation of *p*-TA (deep hydrogenation). This is explained in terms of preventing internal mass transfer limitation, which was achieved thanks to high porosity and low tortuosity of CNF aggregates and thin layers, but also thanks to the short diffusion length in the CNF layer on the monolith, similar to the diffusion length in the smallest slurry phase catalyst. However, the CNF/TiO_2/monolith can be used in a fixed-bed, which would abandon the need of a filtration section.

Appendix: Supplementary data

S5.1 Pd particle size distribution

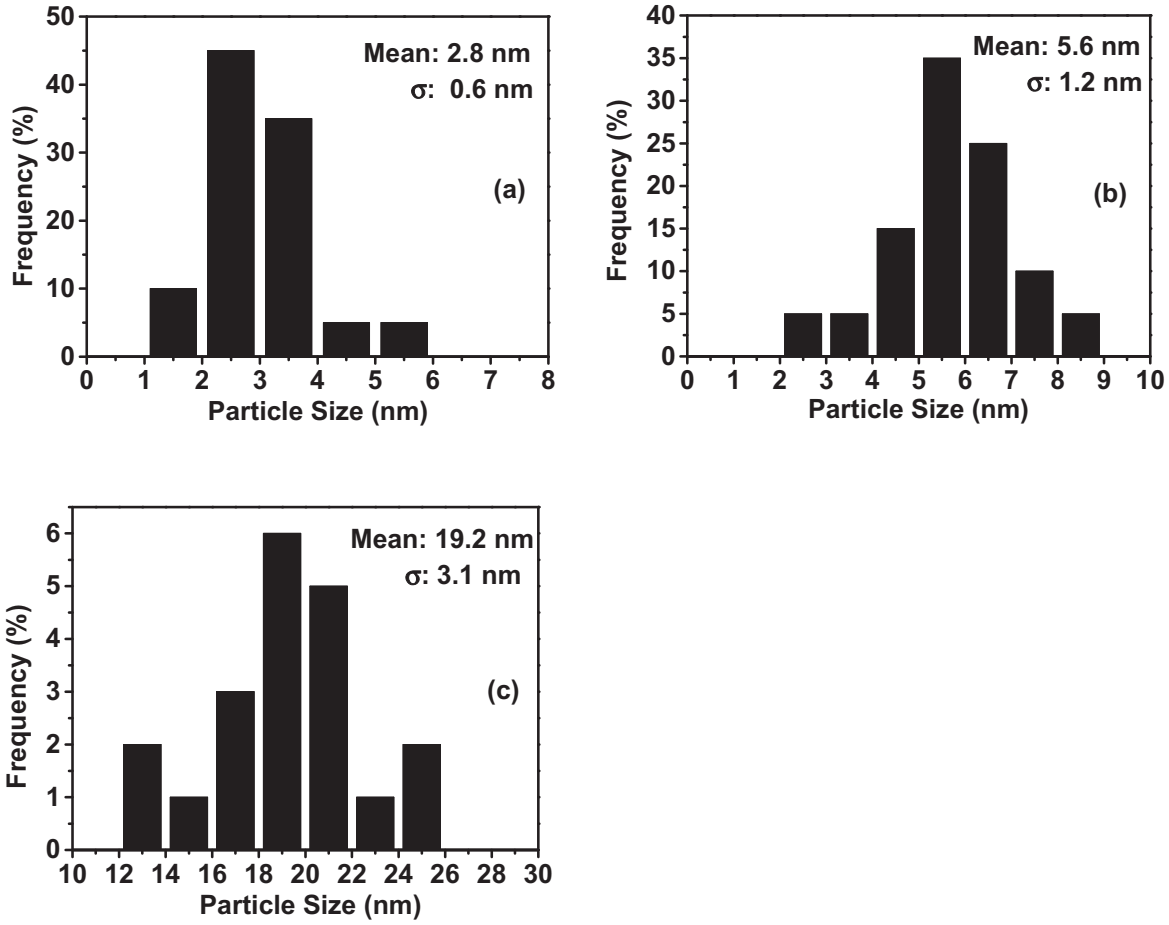

Figure S5.1:. Pd particle distribution of Pd/AC3000 (a), Pd/CNF160 (b) and Pd/CNF/monolith (c)

S5.2 Elimination of external diffusion limitation

Figure S5.2 described the apparent reaction rate constants (k_1) of 4-CBA hydrogenation to 4-HMBA (Figure 5.1) under stirring speed at 200-1000 rpm over Pd/AC3000 and Pd/CNF/monolith. It was clear that, with the increase of stirring speed, the reaction rate rose up over both catalysts. Specifically, reaction rate constant over Pd/AC3000 under stirring speed at 200 rpm was equal to 0.13 h^{-1}, while it ascended to 0.32 h^{-1} at 800 rpm, about 2.5 times of the former; but at 1000 rpm, k_1 had no obvious increase, which indicated the elimination of external diffusion limitation under this stirring speed over Pd/AC3000. The reaction over Pd/CNF/monolith possessed the same conclusion. So, stirring speed of 800 rpm could be employed in the reaction to remove the effects of external diffusion limitations on the reaction.

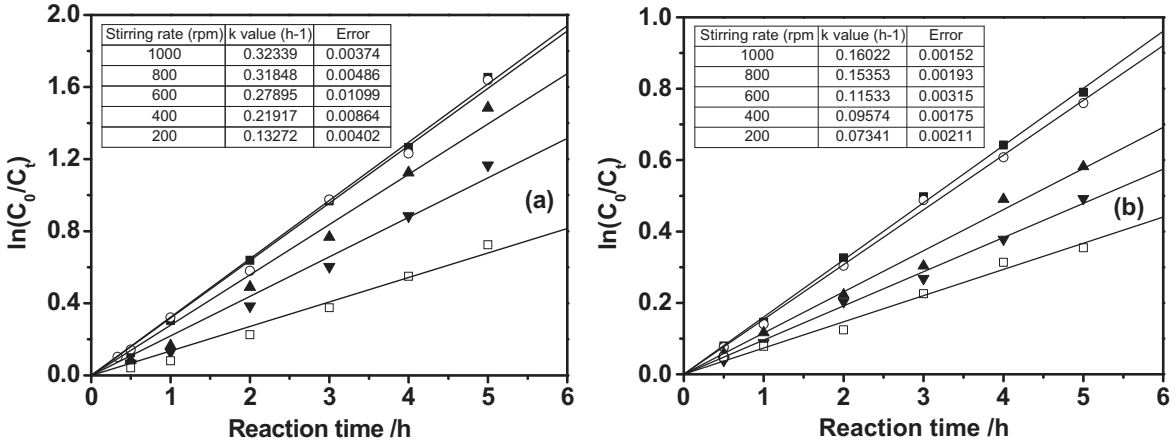

Figure S5.2: Reaction constants for 4-CBA hydrogenation with different stirring rates over Pd/AC3000 (a) and Pd/CNF/monolith (b): □ 200 rpm; ▼ 400 rpm; ▲ 600 rpm; ○ 800 rpm; ■ 1000 rpm.

S5.3 Calculation method of apparent turnover frequency (TOF), Thiele modulus (ϕ_1) and Weisz-Prater numbers ($N_{W\text{-}P}$) over catalysts

Initial reaction rate in TOFs over different catalysts including a series of Pd/AC, Pd/CNF and Pd/CNF/monolith were calculated using Equation S5.1 and S5.2.

$$TOF = k_1 \times n^0_{CBA} \times (N_{Pd})^{-1} \quad \text{S5.1}$$

where k_1 is reaction rate constant, n^0_{CBA} is initial mole amount of 4-CBA and N_{Pd} is the molar number of surface Pd sites, respectively.

In a first order reaction, the effect of internal diffusion behavior of the reactants could be estimated using Thiele modulus (ϕ_1) or Weisz-Prater criterion (W-P criterion, N_{WP}), expressed in Equation S5.2.

$$N_{WP} = \frac{r_A \cdot R_p^2}{C_{s,A} \cdot D_{eff}} = \eta\phi_1^2 = 3(\phi_1 coth\phi_1 - 1) \quad \text{S5.2}$$

Where r_A is the observed initial reaction rate per catalyst volume; R_P is the catalyst particle radius, $Cs_{,A}$ is the substrate concentration on catalyst surface and D_{eff} is the effective diffusivity of the substrate in the pores of the catalyst.

W-P criterion asserted that if N_{WP}<0.3, rates for all reactions with an order of 2 or less should have negligible mass transfer limitations, while a value for N_{WP}>6 indicates the definite diffusion control [38, 39]. The calculation methods of $N_{W\text{-}P}$ derived from some handbooks [40-42] and Table S5.1 gave some values, which were needed in determining a W-P number.

Table S5.1 Physicochemical properties of the reactants and solvent in the reaction system

Reactants and solvent	r（nm）	M (g·mol^{-1})	V_b (m^3·kmol^{-1})	χ	η (Pa·s×10^{-4})	C^0 (mol/cm^3)
H_2	0.12	2	0.0286	-	-	8.5×10^{-5} [a]
4-CBA	0.4	150.13	0.147	-	-	1.332×10^{-5} [b]
H_2O	0.14	18	-	2.6	3.15	-

Note: (a) Calculated based on Henry's law under the pressure of 2.0 MPa.

(b) Calculated based on the data of m_{H2O} and m_{CBA} in Table 4.2.

Bulk diffusivity of a dilute gas solute in a liquid solvent (D_{12}) and a dilute solid solute (<10 mol%) in water (D'_{12}) can be estimated using Equation S5.3 and S5.4 [43].

$$D_{12} = 1.1728 \times 10^{-16} \frac{T\sqrt{\chi \cdot M_2}}{\eta_2 \cdot V_1^{0.6}} \quad \text{S5.3}$$

$$D'_{12} = \frac{8.621\times10^{-14}}{\eta_2^{1.14} \cdot V_1^{0.589}} \quad \text{S5.4}$$

where T is the reaction temperature (T); χ is the solvent association parameter; M_2 is the molecular weight of solvent (g/mol); η_2 is the viscosity of the solvent under the reaction temperature (Pa·s); and V_1 is the molar volume of the gas solute at normal boiling point (m^3/kmol).

Effective diffusivity (D_e) of a substrate can be calculated using Equation S5.5 as demonstrated by Satterfield [44].

$$D_e = \frac{D_b\theta}{\tau} \quad \text{S5.5}$$

where D_b is the bulk diffusivity (cm^2/s), θ is the internal void fraction of the solid particle, τ is the tortuosity factor of the pores.

S5.4 Calculation for the prediction of k_2 over Pd catalysts.

The Equation S5.6 was used in Pd/AC50, Pd/AC160, Pd/AC3000, Pd/CNF160 and Pd/CNF/TiO_2/monolith; Equation S5.7 was used in Pd/AC3000.

$$Y_{HMBA} = \frac{\Delta k}{\Delta k-1}(1-X)[(1-X)^{\frac{1}{\Delta k}-1} - 1] \quad \text{S5.6}$$

$$Y_{HMBA} = \frac{\Delta k}{\Delta k-1}(1-X)[(1-X)^{\frac{1}{\sqrt{\Delta k}}-1} - 1] \quad \text{S5.7}$$

The equations were solved by trial and error method and the fitting curve were as follows:

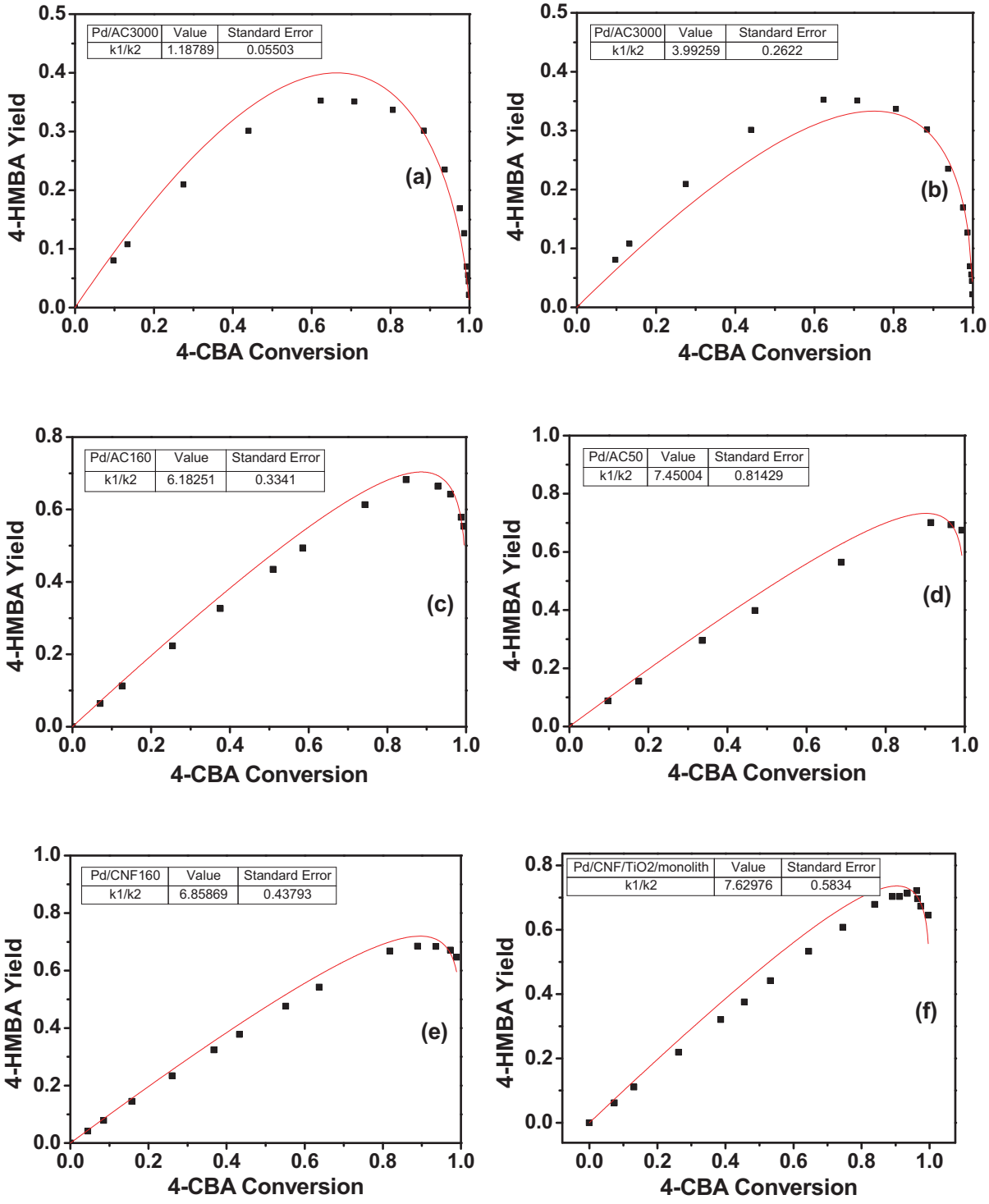

Figure S5.3: Fitting curve of 4-CBA conversion vs. 4-HMBA yield over Pd/AC3000 with Equation S5.6 (a), Pd/AC3000 with Equation S5.7 (b), Pd/AC160 with Equation S5.6 (c), Pd/AC50 with Equation S5.6 (d), Pd/CNF160 with Equation S5.6 (e) and Pd/CNF/TiO_2/monolith with Equation S5.6 (f).

References

[1] Y. Zhou, X. Li, X. Pan, X. Bao, J. Mater. Chem. 22 (2012) 14155-14159.

[2] J. H. Bitter, J. Mater. Chem. 20 (2010) 7312-7321.

[3] F. B. Su, L. Lv, F. Y. Lee, T. Liu, A. I. Cooper and X. S. Zhao, J. Am. Chem. Soc. 129 (2007) 14213-14223.

[4] L. Kiwi-Minsker, I. Yuranov, V. Höller, A. Renken, Chem. Eng. Sci. 54 (1999) 4785-4790.

[5] J. K. Chinthaginjala, K. Seshan, and L. Lefferts, Ind. Eng. Chem. Res. 46 (2007) 3968-3978.

[6] A. Holmen, H. J. Venvik, R. Myrstad, J. Zhu, D. Chen, Catal. Today 216 (2013) 150-157.

[7] X. Zhang, Y. C. Guo, Z. C. Zhang, J. S. Gao, C. M. Xu, J. Catal. 292 (2012) 213-226.

[8] J. K. Chinthaginjala, L. Lefferts, Appl. Catal. B Environ. 101 (2010) 144-149.

[9] S. Pacheco Benito, L. Lefferts, Carbon 48 (2010) 2862-2872.

[10] L. Z. Gao, L. Kiwi-Minsker, A. Renken, Surf. Coat. Tech. 202 (2008) 3029-3042.

[11] A. E. Palomares, C. Franch, T. Yuranova, L. Kiwi-Minsker, E. García-Bordeje, S. Derrouiche, Appl. Catal. B Environ. 146 (2014) 186-191.

[12] S. Celebi, T. A. Nijhuis, J. van der Schaaf, F. A. de Bruijn, J. C. Schouten, Carbon 49 (2011) 501-507.

[13] Q. Liu, Z. Liu, W. Wu, Catal Today 147 (2009) S285-S289.

[14] C. Hung, J. Hazard. Mater. 180 (2010) 561-565.

[15] L. E. Gómez, I. S. Tiscornia, A. V. Boix, E. E. Miró, Appl. Catal. A Gen, 401 (2011) 124-133.

[16] M. T. Kreutzer, P. Du, J. J. Heiszwolf, F. Kapteijn, J. A. Moulijn, Chem. Eng. Sci. 56 (2001) 6015-6023.

[17] J. Zhu, Y. Jia, M. S. Li, M. H. Lu, J. J. Zhu, Ind. Eng. Chem. Res. 52 (2013) 1224-1233.

[18] E. García-Bordejé, F. Kapteijn, J. A. Moulijn, Carbon 40 (2002) 1079-1088.

[19] M. T. Kreutzer, F. Kapteijn, J. A. Moulijn, Catal. Today 105 (2005) 421-428.

[20] N. Jarrah, J. G. Ommen, L. Lefferts, Catal. Today 79-80 (2003) 29-33.

[21] C. M. Park, Encyclopedia of Chemical Technology, Vol 18. New York: Wiley, 1996, pp. 991.

[22] Y. Chen, J. L. Fulton, W. Partenheimer, J. Am. Chem. Soc. 127 (2005) 14085-14093.

[23] W. Partenheimer, Catal. Today 23 (1995) 69-158.

[24] R. W. Fischer, F. Rohrscheid, Applied Homogeneous Catalysis with Organometallic Compounds, Vol 1. Weinheim: Wiley-VCH, 2002, pp. 443.

[25] S. H. Jhung, A. V. Romanenko, K. H. Lee, Y. S. Park, E. M. Moroz, V. A. Likholobov, Appl. Catal. A Gen. 225 (2002) 131-139.

[26] K. T. Li, M. H. Hsu, I. Wang, Catal. Commun. 9 (2008) 2257-2260.

[27] James D E. US 4782181. 1988.

[28] F. Menegazzo, T. Fantinel, M. Signoretto, F. Pinna, Catal. Commun. 8 (2007) 876-879.

[29] Y. Kan, K. Li, J. Y. Wang, L. Lin, C. Y. Zeng, Adv. Mater. Res. 361-363 (2011) 584-592.

[30] J. C. Gao, J. Y Wang, W. B. Du, L. Lin, C. Y. Zeng, Adv. Mater. Res. 634-638 (2013) 587-594.

[31] L. D. Lillwitz. US 4448987. 1984.

[32] S. X. Xia, Z. L. Yuan, L. N. Wang, P. Chen, Z. Y. Hou, Appl. Catal. A Gen. 403 (2011) 173-182.

[33] R. Ocampo-Pérez, M. M. Abdel daiem, J. Rivera-Utrilla, J. D. Méndez-Díaz, M. Sánchez-Polo, J. colloid interf. Sci. 385 (2012) 174-182.

[34] X. Li, X. Pan, Y. Zhou, X. Bao, Carbon 57 (2013) 34-41.

[35] P. B. Weisz, Z. Phys. Chem. 11 (1957) 1-15.

[36] P. B. Weisz, C.D. Prater, Adv. Catal. Relat. Subj. 6 (1954) 143-196.

[37] G. Ertl, H. Knözinger, F. Schüth, J. Weitkamp, Handbook of heterogeneous catalysis, second ed., Wiley-VCT Verlag GmbH & Co. KGaA, Hoboken, New Jersey, 2008, pp. 1759-1760.

[38] J. Zhu, M. S. Li, M. H. Lu, J. J. Zhu, Catal. Sci. Technol. 3 (2013) 737-744.

[39] B. E. Poling, J. M. Prausnitz, J. P. O'Connell, The properties of gases and liquids, fifth ed., Chem. Ind. Press, Beijing, 2005.

[40] S. Mukherjee, M. A. Vannice, J. Catal. 243 (2006) 108-130.

[41] N. L. Chen, Solvents Handbook, third ed., Chem. Ind. Press, Beijing, 2002.

[42] G. Q. Liu, L. X. Ma, J. Liu, Handbook of physical properties in chemistry & chemical engineering (Organic volume), Chem. Ind. Press, Beijing, 2002.

[43] C. N. Satterfield, Mass Transfer in Heterogeneous Catalysis, Cambridge, Mass.: MIT Press, 1970.

[44] A. K. Prashar, S. Mayadevi, R. N. Devi, Catal. Commun. 28 (2012) 42-46.

Chapter 6

Concluding remarks and recommendations

The work in this thesis aimed at developing macro-structured carbon nanofiber (CNF) materials that can be used as catalyst supports for selective hydrogenation in three-phase reactors. The first part of the thesis is focused on the preparation of stable CNF layers deposited on the surface of titania extrudate (CNF/TiO_2) and cordierite monolith (CNF/TiO_2/monolith), which were employed as the catalyst supports later. The second part of the thesis is dedicated to evaluating the catalytic performance of palladium catalysts supported on CNF/TiO_2 and CNF/monolith, i.e., Pd/CNF/TiO_2 and Pd/CNF/TiO_2/monolith, in comparison to palladium catalysts supported on activated carbon (Pd/AC).

6.1 Preparation of stable CNF layers on titania extrudate and cordierite monolith

The support CNF/TiO_2 was synthesized by methane decomposition over TiO_2 extrudate using Ni-Cu as a catalyst at 873 K for 5 h. Addition of a little Cu promoter in the composite synthesis helped to improve the textural and structural properties of CNF/TiO_2. The suitable mole ratio of Ni to Cu in Ni-Cu/TiO_2 employed in the carbon deposit was found to be 8:1. During preparation, a CNF surface layer with the thickness of 1.5-2.0 μm was deposited, which consisted of numerous fibers with a diameter in a range of 50-80 nm. It had a BET surface area of 60 m^2 per gram catalyst, but 160 m^2 per gram carbon. 97% of the pore volme is caused by mesopores. The composite contained 38% carbon by weight, composed of 90% carbon nanofibers and 10% amorphous carbon.

Another macro-structured CNF support, CNF/TiO_2/monolith, was prepared through TiO_2 coating on the surface of the monolith by sol-gel method, followed by CNF growth on the titania coating by methane decomposition at 873 K for 4 h. The total BET surface area of the composite was 31 m^2 per gram catalyst, but 160 m^2 per gram carbon, similar to the surface area of CNF/TiO_2. The macro- and mesopore structure dominated the pore volume of the material (about 93%), very similar to CNFs deposited on the surface of titania only. In short, the two macro-structured CNF supports prepared in this thesis have properties suggesting advantages for three-phase catalytic reactions.

In addition, two supports exhibited good attachment of CNFs to the support as well as excellent resistance to acids. For example, CNF/TiO_2/monolith lost only 1.4 % weight during 60 minutes ultrasonic treatment. This confirmed the strong anchoring of the CNFs to the monolith. The weight loss was small (only 1.9 wt. %) after refluxing in boiling HNO_3 solution (20 wt. %) for 180 min, much less as compared to weight loss during the same treatment of

the bare monolith (9.2 wt. %). The structures of CNFs after HNO_3 treatment were partly corroded but kept mainly its integrity. The strong acid resistance of CNF/TiO_2/monolith was attributed to the TiO_2 and CNF coating on the surface of the monolith, protecting it for acid corrosion.

6.2 Application of maco-structured CNF materials

Selective hydrogenations of citral, cinnamaldehyde (CAL) and 4-carboxybenzaldehyde (4-CBA) were used in the thesis as the model reactions to evaluate the catalytic performance of CNF/TiO_2 and CNF/TiO_2/monolith supported palladium catalysts, i.e., Pd/CNF/TiO_2 and Pd/CNF/TiO_2/monolith. The results are compared to those of Pd/AC. Three molecules mentioned above were selected because the double bonds can be consecutively hydrogenated. Three intermediate products, citronellal, hydrocinnamic aldehyde (HCAL) and 4-(hydroxymethyl) benzoic acid (4-HMBA) were the desired intermediate products in the study. However, a large amount of their deep hydrogenated products, such as 3,7-dimethyloctanol, hydrocinnamic alcohol (HCOL) and *p*-toluic acid (*p*-TA), were expected to be produced if internal mass transport of the molecules is seriously limiting the reaction in the calalyst.

Results indicated that, compared with Pd/AC catalyst with large particle size, macro-structured Pd/CNF/TiO_2 and Pd/CNF/TiO_2/monolith exhibited improved catalytic performance on selective hydrogenation of citral, CAL and 4-CBA, as similar to the slurry Pd/CNF catalyst with the particle size of micron scale. Their intermediates, citronellal, HCAL and 4-HMBA, were dominant products in the reactions; However, 3,7-dimethyloctanol, hydrocinnamic alcohol and *p*-toluic acid, the deep hydrogenation products were the main products on Pd/AC with large particle size. Calculationof the Weisz-Prater number and Thiele modulus proved the absence of internal diffusion limitations in Pd/CNF/TiO_2 and Pd/CNF/TiO_2/monolith. Their high catalytic performance was attributed to both high porosity and low tortuosity of CNF aggregates, and the short diffusion length in the thin CNF layer. In contrast, the occurrence of serious diffusion limitations in Pd/AC with large particle size was caused by its predominant microporous structures and long diffusion length.

In summary, two prepared macro-structured CNF supports, CNF/TiO_2 and CNF/TiO_2/monolith, exhibited improved structural properties over activated carbon support, which led to improved catalytic performance in selective hydrogenation reactions as

compared to fixed bed Pd/AC catalysts with large particle size. The Pd/CNF/TiO_2/monolith perform similar to slurry catalysts with small support particle size; however, Pd/CNF/TiO_2/monolith can be easily used in a fixed-bed reactor, which makes the filtration section unnecessary.

6.3 Recommendations

In preparation of macro-structured CNF supports, we deposited CNFs on TiO_2 extrudates and monoliths by methane decomposition using monometallic Ni or bimetallic Ni-Cu catalyst. The effects of Cu in Ni particles on the formation of CNF were also investigated. In the study, addition of small amounts of Cu in Ni particles significantly improved the textural properties of CNF/TiO_2. Actually, CNF can be formed on iron group metal particles (Fe, Co and Ni), using CO, C_2H_2 or C_2H_4 as carbon source [1, 2]. Therefore, further study of addition of Cu promoter in Fe or Co particles for the growth of CNF on TiO_2 extrudate and monolith is recommended. The resulting properties, meso-porosity and low tortuosity should be compared to the CNFs prepared by a Ni-Cu catalyst.

Regarding the study of catalytic performance over Pd/CNF/TiO_2 and Pd/CNF/TiO_2/monolith, we observed that the product distribution in selective hydrogenation is importantly affected by mass transfer of intermediate products inside the catalyst support. The differences in structural properties of catalysts became the main focus in the thesis. The improved catalytic performance of Pd/CNF/TiO_2 and Pd/CNF/TiO_2/monolith as compared to Pd/AC is due to their dominant mesoporous structures and short diffusion length in the thin CNF layer. However, besides structural properties of the catalyst, diffusion coefficients of the molecules also affect its mass transfers in catalyst. It is recommended to estimate the catalytic performance over one catalyst, using reactant molecules with different diffusion coefficients. Based on equations for estimating the diffusion coefficient of a dilute solid solute (<10 mol%) in organic solvent (Equation 1) [3], the molecule with both smaller molar volume (V_b) and lower enthalpy of vaporization (L^{vap}) at normal boiling point possesses the larger diffusion coefficient.

$$D'_{12} = 4.4\times10^{-15}\frac{T}{\eta_2}\left(\frac{V_2}{V_1}\right)^{1/6}\left(\frac{L_2^{vap}}{L_1^{vap}}\right)^{1/2} \quad (1)$$

where T is the reaction temperature; η_2 is the viscosity of the solvent under the reaction temperature; V_1 is the molar volume of a solute at normal boiling point; L_1^{vap} is the enthalpy

of vaporization of a solute at normal boiling point.

Crotonaldehyde, another α,β-unsaturated aldehyde, has the larger diffusion coefficient than citral and CAL under the same reaction system due to its smaller molar volume and lower enthalpy of vaporization at normal boiling point. Three molecules can be used in selective hydrogenation over Pd/CNF/TiO_2 or Pd/CNF/TiO_2/monolith, for estimating the effects of diffusion coefficient on its catalytic performance.

In addition, we prepared macro-structured CNF supported Pd catalysts, and compared their catalytic performance to Pd/AC, using selective hydrogenation of α,β-unsaturated aldehyde (citral and CAL) as the model reaction in the thesis. The catalytic performance of supported group VIII metal was studied systematically [4, 5] and results indicated that Rh, Ni and Pd favor C=C bond hydrogenation, while Os, Ru, Co and Pt were more selective for C=O bond hydrogenation. The differences among Group VIII metals have been explained based on the width of the metal d-band. In particular, the narrower the width of the metal d-band, the greater the interaction of the metal surface with the conjugated C=C bond compared to C=O bond [6].

Since Pd catalyst is more active for hydrogenation of the C=C bond than the C=O bond, citronellal and HCAL are reasonably dominant intermediate products in the reaction [6]. Thermodynamically and kinetically, a C=C bond is more easily hydrogenated than a C=O bond, and so the selective hydrogenation of unsaturated aldehydes to unsaturated alcohols is still a challenging task at present [7]. Actually, unsaturated alcohols such as geraniol, nerol and COL, are important intermediates in the synthesis of fine chemicals like flavor, fragrance and pharmaceutical compounds as well. Therefore, it is worthwhile to further study Pt and Ru catalysts supported on CNF/TiO_2 and CNF/TiO_2/monolith to obtain unsaturated alcohols in citral or CAL hydrogenation. Meanwhile, some literatures reported that addition of a second metal can drastically improve the activity and selectivity to the desired products. Compared to monometallic platinum, Pt-Sn catalysts have shown a much higher rate of hydrogenation of α,β-unsaturated aldehydes and furthermore a very high selectivity towards the formation of the corresponding unsaturated alcohols [8, 9]. The improved performance has been explained in terms of an interaction of ionic tin species with the organic substrate which increases the polarization of the carbonyl group. The higher polarization of the C=O group favor the attack of the hydrogen atoms chemisorbed on the platinum sites. Performing experiments with these improved catalysts on supports with less internal diffusion limitation, can result in increased selectivity to the unsaturated alcohols, which are important intermediates used in fine

chemical industries.

In the thesis, as-prepared macro-structured carbon nano fiber catalysts were employed in selective hydrogenations because the product distributions of those reactions are seriously affected by internal diffusion limitations, and the selectivity to the intermediate products can be improved due to the removal of internal diffusion limitation in them. Actually, those catalysts are interesting for all reactions with internal diffusion limitation as an activity or selectivity problem. Catalytic dehydrogenation, another important process in chemical industry for instance the higher paraffin's (C_{10}-C_{14}) dehydrogenation to the corresponding mono olefins in the manufacture of bio-degradable detergents, is also restricted by internal diffusion limitation. In the paraffin dehydrogenation process, γ-Al_2O_3 supported Pt-Sn catalyst had been studied extensively. Amounts of di-olefins and aromatics are formed by subsequent secondary dehydrogenation reactions. All these side products can lead to the formation of light paraffin's by cracking. Furthermore, coking in the reaction deactivates the catalyst and should be periodically burnt in oxygen-diluent mixture to regenerate the catalyst [10, 11]. These disadvantages caused by internal diffusion limitations are unfavorable to the production of mono olefins. Therefore, the decrease of internal diffusion limitation in catalyst is expected to improve the dehydrogenation activity and selectivity, slow down the coking process, and extend the life-span of the catalyst. Thus, macro-structured CNF supported catalysts are recommended to be employed in selective dehydrogenation of n-dodecane to mono olefins, for the purpose of exploring the effects of catalyst structures to selective dehydrogenation.

Finally, the tests of Pd/CNF/TiO_2 and Pd/CNF/TiO_2/monolith in this thesis were carried out in a stirred slurry reactor, and results proved their good catalytic performance in selective hydrogenation reactions. But generally, macro-structured catalysts are more suitable for fixed-bed reactor due to avoiding catalyst separation and high pressure drop [12]. So, packed-bed reactor is recommended for investigating the catalytic performance of Pd/CNF/TiO_2 and Pd/CNF/TiO_2/monolith, in comparison to that in stirred slurry reactor.

References

[1] K. P. de Jong, J. W. Geus, Catal. Rev. Sci. Eng. 42 (2000) 481-510.

[2] Y. Yamada, Y. Hosono, N. Murakoshi, N. Higashi, H. Ichi-oka, T. Miyake, N. Ikenaga, T. Suzuki, Diam. Relat. Mater. 15 (2006) 1080-1084.

[3] C. N. Satterfield, Mass Transfer in Heterogeneous Catalysis, Cambridge, Mass.: MIT Press, 1970.

[4] U. K. Singh, M. A. Vannice, J. Catal. 199 (2001) 73-84.

[5] U. K. Singh, M. N. Sysak, M. A. Vannice, J. Catal. 191 (2000) 181-191.

[6] F. Delbecq, P. Sautet, J. Catal. 152 (1995) 217-236.

[7] M. Tamura, K. Tokonami, Y. Nakagawa, K. Tomishige, Chem. Commun. 49 (2013) 7034-7036.

[8] I. M. J. Vilella, S. R. de Miguel, C. Salinas-Martínez de Lecea, Ángel Linares-Solano, O. A. Scelza, Appl. Catal. A: Gen. 281 (2005) 247-258.

[9] G. Neri, C. Milone, S. Galvagno, A. P. J. Pijpers, J. Schwank, Appl. Catal. A: Gen. 227 (2002) 105-115.

[10] G. Padmavathi, K. K. Chaudhuri, D. Rajeshwer, G. Sreenivasa Rao, K. R. Krishnamurthy, P. C. Trivedi, K. K. Hathi, N. Subramanyam, Chem. Eng. Sci. 60 (2005) 4119-4129.

[11] Y. Lai, S. He, X. Li, C. Sun, K. Seshan, Appl. Catal. A: Gen. 469 (2014) 74-80.

[12] K. Pangarkar, T. J. Schildhauer, J. R. van Ommen, J. Nijenhuis, F. Kapteijn, J. A. Moulijn, Ind. Eng. Chem. Res. 47 (2008) 3720-3751.

List of Publications

Journal Papers

- Jie Zhu, Fan Wu, Mingshi Li, Jianjun Zhu, Jan G. van Ommen, Leon Lefferts, Influence of Internal Diffusion on Selective Hydrogenation of 4-carboxybenzaldehyde over Palladium Catalysts Supported on Carbon Nanofiber Coated Monolith, ***Appl. Catal. A: Gen.*** 498 (2015) 222-229.

- Jie Zhu, Yong Jia, Mingshi Li, Mohong Lu, and Jianjun Zhu, Carbon nanofibers grown on anatase washcoated cordierite monolith and its supported palladium catalyst for cinnamaldehyde hydrogenation, ***Ind. Eng. Chem. Res.*** 52 (2013) 1224-1233.

- Jie Zhu, Mohong Lu, Mingshi Li, Jianjun Zhu, Effect of structural properties on catalytic performance in citral selective hydrogenation over carbon-titania composite supported Pd catalyst, ***Catal. Sci. Technol.*** 3 (2013) 737-744.

- Jie Zhu, Mohong Lu, Mingshi Li, Jianjun Zhu, Yuhua Shan, Synthesis of carbon–titania composite and its application as catalyst support, ***Mater. Chem. Phys***. 132 (2012) 316-323.

Presentations

Poster:

- Nitrite Hydrogenation using Pd on a Novel Carbon Nanofiber Support in a Structured Reactor, ***NCCC XV***, The Netherlands, 2014.

Summary

In the past few years, significant attention has been drawn to the carbon nanofiber (CNF) due to its exceptional mechanical and electronic properties. CNF has been shown to be important in the field of catalysis. Compared to traditional catalyst supports (alumina, silica and activated carbons), metals supported onto CNF can exhibit unusually high catalytic activity and selectivity due to its high surface area and pore volume without micro porosity. However, CNF suffer from some drawbacks for slurry phase operation. The agglomeration of the nanofibers and the difficulty of filtration can adversely impact catalytic processes. In addition, CNF agglomerates are difficult to use directly in fixed-bed reactors due to a high pressure drop. Therefore, many studies on macro-structured CNF(T) and their prepared catalysts have been launched, for the purpose of resolving the disadvantages of the powdered catalysts employed in catalytic reactors, especially in fixed-bed ones. This thesis describes the preparation of stable CNF layers depositing on the surface of titania extrudate (CNF/TiO_2) and cordierite monolith (CNF/TiO_2/monolith) and their application as catalyst supports for selective hydrogenation of citral, cinnamaldehyde (CAL) and 4-carboxybenzaldehyde (4-CBA).

Chapter 2 focuses on the synthesis of a promising carbon-titania composite material, CNF/TiO_2. It was prepared through methane decomposition over the TiO_2 extrudates. The suitable mole ratio of Ni to Cu in Ni-Cu/TiO_2 employed in carbon deposit was found to be 8:1. The synthesized CNF/TiO_2 had the good textural and structural properties: the BET surface area was 60 m^2/g and the mesopore structure dominated the pore space of the material, which is beneficial for eliminating mass transfer limitations. Meanwhile, the dominant ingredient of carbon deposit over the composite was CNFs (90%).

The preparation of palladium catalysts supported over CNF/TiO_2 (Pd/CNF/TiO_2) was described in **Chapter 3**, and the catalytic properties over macro-structured Pd/CNF/TiO_2 and Pd/AC for citral hydrogenation were estimated using Weisz-Prater criterion. The calculating results of Weisz-Prater numbers (less than 0.3 of each reactant) inferred the absence of internal diffusion limitations in Pd/CNF/TiO_2. It is in accordance with the high citronellal selectivity in citral hydrogenation over it. Meso- and macro-pores, the dominant structures in Pd/CNF/TiO_2, resulted in the elimination of internal diffusion limitation in the catalyst. These results showed that CNF/TiO_2, an effective catalyst support, has a potential application in three phase catalytic reactions, especially those controlled by internal diffusion.

In **Chapter 4**, another macro-structured CNF support, CNF/TiO_2/monolith, was synthesized by TiO_2 coating on the surface of the cordierite monolith and followed by CNF growth on it. The total BET surface area of the composite was 31 m^2/g and the macro- and mesopore structure dominated the pore space of the material (about 93%). Meanwhile, 94% of the carbon deposit on the surface of the composite was CNF. TiO_2 film and CNF coating was deemed to increase the textural and acid-resistant properties of the composite. Synthesized CNF/TiO_2/monolith was subsequently employed to prepare its supported palladium catalysts, Pd/CNF/TiO_2/monolith. The catalytic performance was determined by the selective hydrogenation of cinnamaldehyde (CAL) to hydrocinnamic aldehyde (HCAL). The selectivity to HCAL was high (about 90%) over Pd/CNF/TiO_2/monolith at 95% CAL conversion, the same as that over powdered Pd/CNF (about 93%), being much higher than that over Pd/AC (about 45%). The high selectivity was attributed to the removal of acidic oxygen-containing surface groups and the elimination of internal diffusion limitation on Pd/CNF/TiO_2/monolith.

In addition, Pd/CNF/TiO_2/monolith was employed in **Chapter 5** for another model reaction, selective hydrogenation of 4-CBA. The effect of mass transfer on catalyst performance was studied experimentally and the results are described using simple kinetic models. The results were compared to Pd catalysts supported on activated carbon (Pd/AC) and carbon nanofibers aggregates (Pd/CNF). Catalytic performance of Pd/CNF/TiO_2/monolith is similar to Pd/CNF and Pd/AC with particles as small as 50 micron (Pd/AC50), whereas Pd/AC with larger support particles revealed lower activity due to internal mass transfer limitation. Also selectivity to the intermediate hydrogenation product, 4-(hydroxymethyl) benzoic acid (4-HMBA), versus deep hydrogenation to *p*-toluic acid (*p*-TA), is clearly affected by internal mass transfer. Pd/AC with large particles (3000 μm) achieves a maximum yield to the intermediate product of only 35%, whereas all other catalysts achieve typically 70%. Remarkably, the conversion level at which the maximum yield of intermediate product is achieved is highest for Pd/CNF/TiO_2/monolith. This advantage is assigned to superior internal mass transfer properties, thanks to high porosity, low tortuosity and short diffusion length of the CNF layer. Clearly, Pd/CNF/TiO_2/monolith applied as a fixed bed outperforms slurry catalysts, abandoning the need of a filtration section.

An outlook with a discussion on future developments of the work presented in this thesis is described in **Chapter 6**. It includes 5 aspects. First of all, bimetallic Co-Cu or Fe-Cu catalyst will be employed to grow CNF on TiO_2 extrudate and monolith, and resulting

properties be compared to the CNFs prepared by a Ni-Cu catalyst. Next, crotonaldehyde, as well as citral and CAL in this thesis, will be used to estimate the effects of the molecular diffusion coefficient on catalytic performance. Then, Pt and Ru catalysts supported on CNF/TiO_2 and CNF/TiO_2/monolith, rather than Pd one, will be studied to improve the yield of unsaturated alcohols in citral or CAL hydrogenation. In addition, Pd/CNF/TiO_2 and Pd/CNF/TiO_2/monolith catalyst like in this thesis will also be tested in selective dehydrogenation of n-dodecane to mono olefins, for the purpose of exploring the effects of catalyst structures to selective dehydrogenation. Finally, packed-bed reactor will be used for investigating the catalytic performance of Pd/CNF/TiO_2 and Pd/CNF/TiO_2/monolith, in comparison to that in stirred slurry reactor, during citral or CAL hydrogenation.

Samenvatting

In de laatste jaren is er veel aandacht voor koolstof nano draden (carbon nano fibers (CNF)), vanwege hub bijzondere mechanische en elektronische eigenschappen. De CNF's zijn ook aangetoond belangrijk in het veld van de katalyse. Vergeleken met de traditionele katalysator dragers (alumina, silica en geactiveerde koolstof) tonen metalen op CNF ongebruikelijke hoge katalytisch activiteit en selectiviteit, als gevolg van het hoge oppervlak en het grote poriën volume zonder microporositeit. Jammer genoeg de CNF's hebben ook enige nadelen voor het gebruik in slurry fase operaties. De agglomeratie van de CNF's en het moeilijke filtreren, hebben een negatieve invloed op de katalytische processen. Daar komt bij dat CNF's moeilijk direct te gebruiken zijn in gepakt bed reactors als gevolg van de daar door CNF's gecreëerde hoge drukval. Daarom zijn er veel studies gedaan naar de macro-gestructureerde CNF(T) en de daarmee bereide katalysatoren, met de bedoeling het oplossen van de nadelen van poeder katalysatoren, speciaal gebruikt in gepakt bed reactoren. Dit proefschrift beschrijft de bereiding van stabiele CNF lagen afgezet op het oppervlak van titania extrudaten (CNF/TiO_2) en corderiet monolieten (CNF/TiO_2/monoliet) en hun toepassing als katalysator drager voor de selectieve hydrogenering van citral, cinnamaldehyde (CAL) en 4-carboxybenzaldehyde (4-CBA).

Hoofdstuk 2 focust op de synthese van veel belovend koolstof-titania composiet materiaal (CNF/TiO_2). Het werd bereid, door methaan ontleding over TiO_2 extrudaten. De meest bruikbare molaire verhouding van Ni tot Cu in Ni-Cu/TiO_2 gebruikt voor de koolafzetting was 8:1. De gesynthetiseerde CNF/TiO_2 had de goede texturele en structurele eigenschappen: Het BET oppervlak was 60 m^2/g en de mesoporiën domineerden het porievolume, wat goed is voor het elimineren van massa transport limitaties. Het dominante deel van de afgezette koolstof op het composiet waren CNF's (90%).

De bereiding van Palladium katalysatoren op CNF/TiO_2 (Pd/CNF/TiO_2) worden beschreven in **Hoofdstuk 3** en de katalytische eigenschappen van de macrostructuur Pd/CNF/TiO_2 en Pd/AC voor citral hydrogenering werden geschat met het Weisz-Prater criterium. De berekende resultaten geven aan dat er geen interne diffussie limitering is in Pd/CNF/TiO_2. Het resulteert in een hoge citronellal selectiviteit. De meso en macro-poriën de dominante structuur in Pd/CNF/TiO_2 resulteert in de eliminatie van de interne diffusie limitering in de katalysator. Dit resultaat toont aan dat CNF/TiO_2 een effectieve katalysator drager is en een potentieel heeft in drie fase katalytische reacties, met name die gecontroleerd

worden door interne diffusie.

In **Hoofdstuk 4** een ander macro-gestructureerde CNF, CNF/TiO_2/monoliet, werd gesynthetiseerd door een TiO_2 coating aan te brengen op het oppervlak van een cordieriet monoliet, gevolgd door CNF groei daarop. Het totale BET oppervlak van de composiet was 31 m^2/g en macro- en meso-poriën-structuur domineerde het porie volume van het materiaal (ongeveer 93%). 94% van de koolafzetting op het oppervlak van de composiet waren CNF's. De TiO_2 film en CNF coating was bedoeld om texturele- en zuur-resistentie eigenschappen van de composiet te verbeteren. De gesynthetiseerde CNF/TiO_2/monoliet werd vervolgens gebruikt om om een gedragen PD katalysator te bereiden Pd/CNF/TiO_2/monoliet. De katalytische prestaties werden bepaald aan de hand van de selectieve reductie van cinnamaldehyde (CAL) naar hydrocinnamicaldehyde (HCAL). De selectiviteit naar HCAL was hoog (ongeveer 90%) over Pd/CNF/TiO_2/monoliet bij 95% CAL conversie, hetzelfde als over gepoederde PD/CNF (93%), maar veel hoger dan die over Pd/AC (45%). De hoge selectiviteit wordt toe gewezen aan de verwijdering van zure groepen en de eliminatie van interne diffusie limitering op Pd/CNF/TiO_2/monoliet.

De Pd/CNF/TiO_2/monoliet werd in **Hoofdstuk 5** ook nog gebruikt voor een andere model reactie, selectieve hydrogenering van 4-CBA. Het effect van massa transport op de katalytische prestaties werd experimenteel bestudeerd en de resultaten beschreven met een simpel kinetisch model. De resultaten werden vergeleken met Pd katalystor op een actieve kool drager (Pd/AC) en op aggregaten van nano-kooldraden (Pd/CNF). De katalytische prestaties van Pd/CNF/TiO_2/monoliet is gelijk aan Pd/CNF en Pd/AC met deeltjes van 50 micron (Pd/AC50), terwijl Pd/AC met grotere drager deeltjes een lagere activiteit vertonen ten gevolge van interne massatransport limitering. Ook de selectiviteit naar het intermediair hydrogeneringsproduct, 4-(hydroxymethyl) benzoëzuur (4H-HMBA), versus diepe hydrogenering naar *p*-tolueenzuur (*p*-TA) is duidelijk beïnvloed door het interne massa transport. Pd/AC met grote deeltjes (3000um) bereikt alleen een maximum opbrengst van het intermediaire product van 35%, terwijl alle andere katalysatoren 70% halen. Opmerkelijk is dat het conversie niveau, waarbij de maximum opbrengst wordt bereikt het hoogste is voor Pd/CNF/TiO_2/monoliet. Dit voordeel wordt toegeschreven aan een superior intern massa transport, ten gevolge van de hoge porositeit, lage tortuositeit en de korte diffusie lengtes van CNF laag. Pd/CNF/TiO_2/monoliet toegepast in een vast bed overtreft de slurryfase katalysator, omdat de filtratie sectie overbodig wordt.

Een toekomstvisie met discussie over potentiele ontwikkelingen van het werk in dit

proefschrift is beschreven in **Hoofdstuk 6.** Er worden 5 aspecten genoemd. Allereerst het gebruik van bimetallische Co-Cu of Fe-Cu katalysatoren voor de groei van CNF's op TiO_2 extrudaten en monolieten. De resulterende eigenschappen zullen vergeleken worden met CNF's gemaakt met een Ni-Cu katalysator. Vervolgens zullen citral en CAL net als in dit proefschrift worden gebruikt om het effect van diffusie op de katalytische prestaties af te schatten. Ook zullen Pt en Ru katalysatoren gedragen op CNF/TiO_2 en CNF/TiO_2/monoliet worden bestudeerd, om de opbrengst van onverzadigde alcoholen te vergroten bij de citral een de Cal hydrogenering. Daarnaast zullen Pd/CNF/TiO_2 en Pd/CNF/TiO_2/Monoliet katalysatoren, dezelfde als in dit proefschrift, worden getest gedurende de selektieve dehydrogenering van n-Dodecaan naar mono olefinen, met als doel de invloed van de katalysator structuur op de selectieve dehydrogenering te onderzoeken. Tenslotte zal een vast bed reactor kunnen worden vergeleken met een slurry fase reactor, wat betreft de prestaties van Pd/CNF/TiO_2 en Pd/CNF/TiO_2/Monoliet katalysatoren voor de hydrogenering van Citral of CAL.

Acknowledgements

A muggy weather came, as usual, in this May to Changzhou, my hometown, a middle city in east China. It reminded me the rainy but comfortable weather in the Netherlands. No doubt that my life in the University of Twente would become a memorable journey I experienced. At the end of this dissertation, I will acknowledge many people I met during this memorable PhD journey.

First of all, I would like to express my sincerest gratitude to my professor, Leon Lefferts, for giving me the opportunity to pursue research in CPM group. Leon, thank you for your guidance and patience. I remember you taught me the "critical approach" in the experiments, which assisted me in making my research valuable and relevant; I remember your great patience on improving my writing, which coached me how to capture the key problems and then organize the structure and words in the paper; I also remember your great patience on repeatedly correcting my spoken English due to my poor listening comprehension and Chinese English.

Prof. Mingshi Li, I am very grateful to you for your keen insight, fruitful discussions and unflagging support. You are more than a supervisor to me. You are my good friend. I remember that you asked me "what's the monolith?" in our first meeting. I said that it was probably a plate with a single layer. Actually, I have not heard this word before at that time, not to speak of its applications. But now, I am sure that I can tell you the answer. ☺ You always gave me enthusiasm when I was puzzled in my research. Your useful advices and scientific inputs helped me to improve myself and my research. It would have been very difficult without your support.

Prof. Jianjun Zhu, I would like to thank you for introducing me the great opportunity to study in the University of Twente. I never forgot your call from the Netherlands several years ago to ask me the idea on study further in CPM group. I cannot catch this opportunity without your call. I am also very grateful to you for your continuous guidance during my research.

I would like to thank Dr. Jan van Ommen. I always felt enjoyable in our talks. You not only gave me your scientific advices and insightful discussions in the research, but share me your lives and interests. I am impressed for you diving in the sea at the age of 70, which urged me to make a decision to do some exercises every day, as you do.

Many thanks to the scientific staff in CPM group: Seshan, Barbara and Arie, I enjoyed and learned a lot from the discussion with you in group seminars, coffee breaks and Friday

borrels.

I also thank our technicians, Karin and Tom for your technical support during my experiments in the lab. Karin and Tom, from the bottom of my heart, I wish that you both fully regain your health and wish to see you both always happy.

Special thanks to our group's secretary, Maaike. I promise that you are the kindest secretary I met till now. You gave me so many helps in my lives in the Netherlands. I never forgot your warm dinner invitation to your house on 28 Dec, 2013. It was my first time to taste the real dutch dinner, and it absolutely delicious. I wish you happy and energetic forever, and wish your granddaughter more and more beautiful when she grows up.

Bert, your thick mustache and big belly impressed me. I feel you are the busiest man in CPM group and have to manage many things. Despite your heavy work, every time I met the problem in the lab, you would solve it for me. You are the real fan of the borrel, and always drunk one cart of beers. I like to listen to your comments on new technology, culture and focus events. I learned a lot from your words. Thank you!

Joline, you are a typical dutch girl, tall and beautiful, and so kind to me. We collaborated each other in one project. I would like to acknowledge you for your helps in the experiments and lives. You taught me how to use the apparatus to prepare the samples. You explained what Leon said to me after the progress meeting in patience because of my poor listening comprehension. You guided me how to watch Carnival Festival in Oldenzaal. You also gave me a farewell gift, one calendar book with beautiful scenery all over the Netherlands. I like it very much. Thank you very much!

I would also like to acknowledge my office mates, Kamila, Roger and Chau. Kamila and Roger, it's my pleasure to have you as my paranymphs. Kamila, you are a very beautiful and nice girl. You gave me many useful suggestions in lives and studies at UT. I never forget, in my final period, it's you to help me revise the format of the thesis, which need to suit the requirements of the publisher. Thank you very much! Roger, you are a humorous but scrupulous Spanish boy. We often joke our names due to the similar pronunciations. I always seek your helps in the experiments because you were in charge of IC. I also never forget one accident, in which I closed the H_2 valve for a few minutes during your catalyst reduction. Believe me, I did not mean it at that time. Chau, you are a small lady but powerful. You are good at cooking, and the cake you cooked taste delicious. I enjoyed a lot with you, my dear office mates, and wish you all the best in all aspects of your lives.

Yingnan and Songbo, it is my pleasure to meet you both in the Netherlands. Yingnan, I

never forgot that you pick me up in Enschede railway station in the early morning when I came to the Netherlands. You gave me many valuable suggestions in lives and research. Wish you and your wife Yin happiness in lives, and have your children in the near future. Songbo, we are the schoolmates at Changzhou University, China. Thank you for your helps in my lives. Your wife, Jiajia, is good at cooking. Till now, I am still recollect the tastes of dumplings and other foods which she cooked. Wish you happiness in your lives and success in your works.

Rao, your Indian English is difficult to understand, and I can only guess few words in one sentence you said. But you are a very kind and warm-hearted man. I remember you helped me to replace the bicycle tire. I feel that you are good enough to open a bicycle shop. You also taught me how to use IC to measure the samples in the experiments. Thank you very much for your helps.

I would also like to thank my sincere friends Cristina, Masoud, Shilpa, Arturo, Kaisa, Heikki, Guido, Pramod for your friendships. I miss the pleasant time with you in the borrels, group trip, and NCCC conference.

The Chinese community in UT has bought me lots of happiness and relaxation. My wholehearted thanks to my good friends, Lijie, Shanqiu, Yanbo, Yunlong, Weiyu, Yi, Aijie, Qingqian, Xiumei, Hairong and Xiaohua. Many wonderful memories and jolly experiences, such as weekend dinner party, Saturday open market shopping and travel to Keukenhof, Giethoorn and Paris, to remember. Special thanks for your constant support.

Lijie, you are the first Chinese student I met in Netherlands. You are expert in house decoration. “Hong Shao Rou” you cooked impressed me. Yanbo, we call you mathematician due to your solid mathematics knowledge. You always say some humorous stories in the party, especially “the young street” in your hometown, which caused us laugh for a whole day. Shanqiu, you are an optimist in nature. Every time you met the difficulty, you could always found the solutions. Special thanks for your room sharing to me for half a month before my last days in Netherlands.

Aijie, you are a beautiful and smart girl. You proposed so many creative and novel ideas in the research. Wish you publish your paper in Nature in the near future. Qingqian, you are a small but serious girl. Also wish you success in the field of politics.

Finally, I would like to thank my family, whom I love so much in these years. My parents, you gave me all your love, encouragement, trust and sacrifices. I remember someone said, the researcher is destined to be lonely in the road of the research. Exactly, I cannot walk

ahead in this road without your supports. My special gratitude to Xiao, my wife, for your understanding and supports during the final and stressful moments of my PhD. You are my greatest happiness in my life. Haohao, my lovely son, you are the gift of the god to me. I hope you will grow up healthily and happily.

Thank you all.

Changzhou, June - 2015
Jie Zhu

Biography

Jie Zhu (朱劼) was born in 1977, in Changzhou, Jiangsu Province, China. He graduated from Beijing Institute of Technology with the bachelor degree on Chemical Engineering, and then received his master degree on Applied Chemistry at the same university. After his graduation, he started his works in Changzhou University as a lecturer. In 2011, he got *Jiangsu Government Scholarship for Overseas Studies* to pursue PhD programme on the topic of macro-structured carbon nanofibers catalyst and its application on selective hydrogenation, in collaboration with Catalytic Processes and Materials group (CPM) in University of Twente. The results of the research are presented in this book.

UNIVERSITY OF TWENTE.

9 789036 539425